Neutron Scattering Measurements of Low-Dimensional Quantum Systems

Neutron Scattering Measurements of Low-Dimensional Quantum Systems

by

SARA HARAVIFARD, B.Sc., M.Sc.

A Thesis

Submitted to the School of Graduate Studies

in Partial Fulfillment of the Requirements

for the Degree

Doctor of Philosophy

McMaster University

DOCTOR OF PHILOSOPHY (2010) McMaster University

(Physics) Hamilton, Ontario

TITLE: Neutron Scattering Measurements of Low-Dimensional Quantum Systems

AUTHOR: Sara Haravifard

SUPERVISOR: Professor Bruce D. Gaulin

NUMBER OF PAGES: xv, 148

Abstract

Low dimensional quantum magnets which display a collective singlet ground state and a gap in their magnetic excitation spectrum provide a framework for much exotic phase behavior in new materials, with high temperature superconductivity being the best appreciated example. Neutron scattering techniques can be applied to study a wide variety of problems in condensed matter physics. These techniques are particularly useful as applied to understanding the magnetic properties of quantum magnets that display exotic phases.

$SrCu_2(BO_3)_2$, is a rare example of a two-dimensional quantum magnet for which an exact theoretical solution describing its ground state is known to be a collective singlet. Previous high resolution neutron scattering measurements identified the most prominent features of the spin excitation spectrum in $SrCu_2(BO_3)_2$, including the presence of one and two triplet excitations and weak dispersion characteristic of subleading terms in the spin Hamiltonian.

The resemblance between the spin gap behavior in the Mott insulator $SrCu_2(BO_3)_2$ and that associated with high temperature superconductors motivated the consideration of the significance of doping in order to understand the properties of this quantum magnetic system. For this reason, a series of neutron scattering studies on doped $SrCu_2(BO_3)_2$ were initiated.

These series of investigations began with the performance of neutron scattering measurements on a $SrCu_{(2-x)}Mg_x(BO_3)_2$ single crystal in order to introduce magnetic vacancies to the system. These results revealed the presence of new spin excitations within the singlet-triplet gap of this system. Application of a magnetic field induces Zeeman-split states associated with un-paired spins which exist as a consequence of doping with quenched non-magnetic impurities. Additional substantial broadening of both the one and two triplet excitations is observed in the doped system as compared to the pure system. Theoretical calculations are shown to qualitatively account for these features.

These studies were extended to neutron scattering measurements on $Sr_{(1-x)}La_xCu_2(BO_3)_2$, with an aim of introducing charged carriers into this system. The broadening of the one and two triplet excitations is observed and compared to the thermally induced finite lifetime of the pure system. The temperature dependence of this broadening in $Sr_{(1-x)}La_xCu_2(BO_3)_2$ is different compared to that observed in both $SrCu_2(BO_3)_2$ and $SrCu_{(2-x)}Mg_x(BO_3)_2$.

It has also been suggested that there is a relation between the spin-lattice interaction in $SrCu_2(BO_3)_2$ and the magnetic dynamics at low temperatures and high magnetic fields. For this reason there has been increased interest in the study of the crystalline structure and vibrational modes of $SrCu_2(BO_3)_2$. In order to investigate the role of the lattice in the formation of the singlet ground state in $SrCu_2(BO_3)_2$, a series of low and high energy neutron scattering measurements were carried out on this system to study both the crystalline structure as well as the normal modes of vibration of the lattice,

the transverse acoustic and optical phonons. Transverse acoustic phonons with energies comparable to and higher than the onset of the two triplet continuum show substantially increased lifetimes on entering the singlet ground state below ~ 10 K. This may indicate the removal of the decay channel for the phonons due to the gapping of the spin excitation spectrum in $SrCu_2(BO_3)_2$ at low temperatures. In high energy inelastic neutron scattering we observe broadening of optic phonons in the ~ 52 to 65 meV region on entering the low temperature singlet ground state.

Additionally, the magnetic properties of $CuMoO_4$, which is a triclinic quantum magnet system based on S=1/2 moments at the Cu^{2+} site, were studied using elastic and inelastic neutron scattering experiments. This material exhibits a first order structural phase transition at ~ 190 K as well as a magnetic phase transition at ~ 1.75 K. We were primarily interested in the low temperature magnetic properties of this material. Magnetization and heat capacity measurements as well as elastic and inelastic neutron scattering measurements were conducted on this system within the low temperature ordered phase. These studies confirm that this material has a magnetic phase transition at ~ 1.7 K. Neutron scattering results indicate that this magnetically ordered phase is characterized by a doubling of the *a* axis. Inelastic neutron scattering measurements revealed a gapped magnetic excitation spectrum in zero magnetic field, which could be filled in by the application of magnetic fields approaching 7 T.

Acknowledgements

I would like to express my sincere appreciation to my supervisor, Professor Bruce Gaulin for his unlimited support and continuous guidance during the course of this research. This work could not have been accomplished without his efforts. Sincere thanks are owed to the other members of my supervisory committee Professor John Greedan and Professor Graeme Luke for their collaboration and assistance throughout my study at McMaster University.

I would like to express my gratitude toward the management and staff of Chalk River Laboratories, ON and ISIS Laboratories, UK for their hospitality and assistance. Particularly, I offer my appreciations to M. Telling and T. Perring of ISIS, as well as Z. Yamani, W. Buyers, Z. Tun and I. Swainson of Chalk River for their assistance on conducting the experiments. I should also thank my colleagues at McMaster University in particular H. Dabkowska and S. Dunsiger, and our collaborator T. Asano from Kyushu University. I would also like to thank all the faculty, staff and graduate students at the Department of Physics and Astronomy for their help and support throughout these years, especially my dear friend Rosemary McNeice who has always been there for me when I needed her the most. I would also like to acknowledge the generous financial support by McMaster University and NSERC of Canada.

I would like to extend my appreciation to my parents for their encouragement and support. Finally, I would like to express my deep gratitude to my beloved husband, Farzin, for his consistent support and sacrifices that made completion of this thesis possible.

Preface

The main part of the original work in this thesis is included in Chapters 4, 5, 6 and 7. The results presented in these chapters reproduce a series of one journal paper and three manuscripts intended for submission to journals. One paper has been peer-reviewed and published in Physical Review Letters. Two of the papers will be submitted to Physical Review B for publication and one will be submitted to Journal of Physics: Condensed Matter for publication. I am the primary author in this paper and manuscripts, which are co-authored by my supervisor, B. Gaulin, and our collaborators in each project. The neutron scattering experiments and subsequent analysis of the data presented in this thesis have been conducted by myself under the supervision of B. D. Gaulin.

I was heavily involved in the sample preparation and single crystal growth of the $SrCu_2(BO_3)_2$ sample that was employed in the experiments described in chapters 4, 5 and 6 under the guidance of H. A. Dabkowska. The other two samples, $SrCu_{(1-x)}Mg_x(BO_3)_2$ and $Sr_{(1-x)}La_xCu_2(BO_3)_2$, were grown by H.A. Dabkowska. S.R. Dunsiger and I performed the sample characterization and quality assessment measurements on $SrCu_2(BO_3)_2$, $SrCu_{(1-x)}Mg_x(BO_3)_2$ and $Sr_{(1-x)}La_xCu_2(BO_3)_2$. While conducting neutron scattering experiments on the $SrCu_{(1-x)}Mg_x(BO_3)_2$ and $Sr_{(1-x)}La_xCu_2(BO_3)_2$ samples (please see chapters 4 and 5) I benefited from the assistance of S.R. Dunsiger and M. Telling at the ISIS facilities of the Rutherford Appleton Laboratory. The results presented in Chapter 6 arose from several neutron scattering experiments which I carried out in collaboration with Z. Yamani at the Chalk River Laboratories and T. Perring at the ISIS

facilities. I have prepared the $CuMoO_4$ sample for scattering experiments (see Chapter 7) with the assistance of T. Asano, our collaborator from Kyushu University in Japan. The neutron scattering measurements were conducted by myself in collaboration with T. Asano, Z. Yamani and I. Swainson at the Chalk River Laboratories.

I analysed all the experimental data presented in this thesis and wrote the computer programs needed for that purpose. I carried out the resolution convolution calculations using the FORTRAN program I wrote myself and ResLib, which is part of the ORNL libraries. Fits to the data were performed using MatLab and the non-square fitting library, MINUIT, which is part of the CERNLIB libraries. I used MSLICE, HOMER and TobyPlot which are parts of the ISIS libraries for single crystal neutron scattering visualisation as well as GSAS, which is part of LANL library, for powder neutron diffraction analysis.

Contents

List of Figures

Chapter 1

Quantum Magnetism

1.1. Phase Transitions and Order Parameters

The degree of ordering in a system is the outcome of competition between interactions that enforce order to minimize energy and thermal motion that increases disorder to maximize entropy; the result of which for many systems is formation of different macroscopic phases. The transformation of a thermodynamic system from one of its phases to another is referred to as a phase transition. A phase transitions happen when the free energy of system is non-analytic for some thermodynamic variables; in other word there is a discontinuity in the free energy of the system or one of its derivatives. The distinguishing characteristic of a phase transition is a sudden change in one or more physical properties. The transitions between solid, liquid, and gaseous phases of water or the transition between the ferromagnetic and paramagnetic phases of

magnetic materials at the Curie point are examples of such changes. According to the modern classification scheme, phase transitions are divided into two broad categories: first-order or discontinuous transitions and second-order or continuous transition.

If there is a finite discontinuity in one or more of the first derivatives of the appropriate thermodynamic potential, the transition is first-order or discontinuous. For example in a magnetic system this can be a discontinuity in the magnetization and for a fluid the discontinuity can be in the volume. One of the characteristics of first-order phase transitions is the existence of a latent heat. This means that during such a transition, the system either absorbs or releases a fixed amount of energy and since energy cannot be instantaneously transferred between the system and its environment, first-order transitions are associated with "mixed-phase regimes" in which some parts of the system have completed the transition and others have not, a good example of which is boiling water.

The second class of phase transitions is the second-order or continuous phase transitions. If the first derivatives of thermodynamic potential are continuous but the second derivatives are discontinuous or infinite, the transition will be described as higher order, continuous, or critical. The key feature of a continuous phase transition is the presence of fluctuating micro regions of both phases near the critical point. The characteristic size of these fluctuating regions, called the correlation length ξ, tends to infinity at the critical point. (Collins 1989).

A magnetic system involves a set of interacting magnetic moments which are located at lattice points of a crystal. These magnetic moments arise from the spin angular momenta of the unpaired electrons residing on the atoms in a crystalline solid. In a ferromagnetic system nearest neighbors interact in such a way that makes it favorable to have spins pointing in the same direction below a temperature referred to as the critical temperature T_c. Thermal fluctuations may drive a region of the system into a state at which the spins are in opposite directions and consequently there will be an increase in the free energy of the system (Kadanoff 1976).

If the energy required in the formation of such "droplet" regions is significantly greater than the thermal energy present in the system (i.e. k_BT) then such a process will be unlikely to happen, otherwise, as the temperature rises increasing the thermal energy of the system, a larger number of these droplets are formed; however, the net magnetization (i.e. number of spins in one direction minus number of spins in the opposite direction) approaches zero. Therefore, the energy for formation of a droplet decreases as temperature approaches T_c, and consequently, size of the droplets increases rapidly. The size of the largest such droplet, defined as correlation length ξ, diverges with $T \rightarrow T_c$ (Stanley 1971).

The existence of a quantity, which is non-zero below a finite temperature T_c and zero above it, is an important feature associated with the critical points of a wide variety of physical systems and is referred to as the order parameter.

1.2. The Shastry-Sutherland Model

According to classical electromagnetic theory, magnetic fields are produced by electric currents or changing electric fields and far from the electric currents producing them can be described by magnetic dipoles; therefore, it would be expected that magnetic effects in materials are produced by microscopic current loops created by the motion of electrons in atoms. However, Neils Bohr in 1911 showed that the phenomenon of diamagnetism does not exist in classical physics; thus, the source of magnetism should be explained by quantum mechanics through the existence of an intrinsic magnetic moment, which in turn is proportional to the intrinsic spin.

In certain magnetic materials the electrons responsible for magnetic behavior are localized near the atoms of a regular lattice. Each electron has a spin 1/2 which can point either up or down along the axis specified by the applied magnetic field. The electrons interact with each other and with the nearby atoms and are described in part by the spatial wavefunction $\psi(r_1, r_2)$. This wavefunction must be multiplied by the spin eigenstates to obtain the actual state of the system. For a two electron system, we denote the basis for these states as:

$$|\uparrow\uparrow\rangle, |\downarrow\downarrow\rangle, |\uparrow\downarrow\rangle, |\downarrow\uparrow\rangle \tag{1.1}$$

where the arrows corresponds to the spin of the electrons (Sakurai 1985)

These states are eigenstates of the z-component of the total spin angular momentum, S_z, such that S_z operating on any of these states has an eigenvalue equal to the sum of the spins in the z direction. For example:

$$S_z|\uparrow\uparrow\rangle = 1|\uparrow\uparrow\rangle \tag{1.2}$$

and

$$S_z|\uparrow\downarrow\rangle = 0|\uparrow\downarrow\rangle \tag{1.3}$$

Since electrons are fermions, the basic states in Equation 1.1 are not physically meaningful, because if two electrons are interchanged, the new wavefunction must either be the same or differ by only a minus sign. The simplest normalized linear combinations of the states in Equation 1.1 that satisfy this condition are:

$$\frac{1}{\sqrt{2}}\left(|\uparrow\downarrow\rangle - |\downarrow\uparrow\rangle\right) \tag{1.4}$$

$$|\uparrow\uparrow\rangle \tag{1.5}$$

$$\frac{1}{\sqrt{2}}\left(|\uparrow\downarrow\rangle + |\downarrow\uparrow\rangle\right) \tag{1.6}$$

$$|\downarrow\downarrow\rangle \tag{1.7}$$

The state in Equation 1.4 is antisymmetric, because interchanging the two electrons leads to minus the original state. This state has a total spin, $S = 0$, and is called the singlet state. The collection of the last three states (i.e. Equations 1.5 to 1.7) is called the triplet state and has $S = 1$. According to the Pauli principle the states of fermions must be antisymmetric, thus the spin state is antisymmetric when the spatial part of the wavefunction ψ (r_1, r_2) is symmetric and vice versa. That is, if the spin state is

symmetric, then $\psi(r_1, r_2) = -\psi(r_2, r_1)$. Similarly, if the spin state is antisymmetric, then $\psi(r_1, r_2) = +\psi(r_2, r_1)$. Hence, when $r_1 = r_2$, ψ is zero for symmetric spin states and is nonzero for antisymmetric spin states. This means that if the spins are parallel, the separation between the two electrons will rarely be small and their average electrostatic energy will be less than it is for antiparallel spins. This is referred to as the second Hund's rule.

A general model (and probably the most common one) for describing the total magnetic energy of magnetism for the spin-spin interaction is expressed as:

$$\mathrm{H} = -\sum_{i,j=1}^{N} J_{ij} S_i S_j - g\mu_0 H \cdot \sum_{i=1}^{N} S_i \tag{1.8}$$

where H is the Hamiltonian operator, H is the external magnetic field, $g\mu_0$ is the magnetic moment of the electron and J_{ij} is the *exchange interaction* which can be positive or negative (Aschroft and Mermin 1976).

In 1981, Shastry and Sutherland introduced a two-dimensional model for which geometrical frustration was essential. In this model, the spins are configured in such a way that each spin is coupled to pairs of spins. With the experimental realization of the Shastry-Sutherland model in Strontium copper borate, $SrCu_2(BO_3)_2$ (Kageyama *et al.* 1999) synthesized by Smith and Kezler in 1991, the model attracted a lot of attention, as it became possible to compare the theoretical findings and experimental data directly.

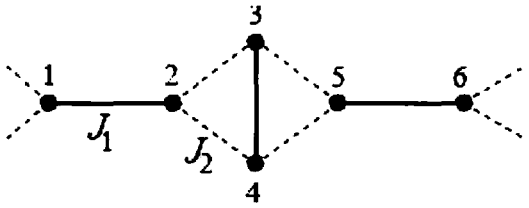

Figure 1.1: Illustration of a dimer solid. Spins are denoted by circles. Two spins interacting via J_1 couple to a dimer. The dimers interact via J_2. The singlet-on-dimers state is always an eigenstate.

The Hamilton operator describing the Shastry-Sutherland model, with spins of size $S = ½$ on the vertices is given by:

$$H = J_1 \sum_{\substack{\text{intra dimers} \\ i,j}} S_i S_j + J_2 \sum_{\substack{\text{inter dimers} \\ k,l}} S_k S_l \tag{1.9}$$

in which, the sums run over all couplings between the sites connecting diagonal bonds (J_1), and between sites on different dimers (J_2), respectively. It can also be shown that for certain values of J_1 and J_2 the state in which all dimers are singlet is always an eigenstate (Shastry and Sutherland 1981).

Figure 1.2 shows the Shastry-Sutherland model for the Hamiltonian described in Equation 1.9. In the limit $J_1 = 0$ a simple square lattice is obtained. For other cases, the model can be seen as a square lattice with additional (frustrating) diagonal bonds. The ratio $x = J_2/J_1$ is introduced as the inverse frustration. Because of the particular geometry of the system, it is sometimes called orthogonal dimer model (Miyahara and Ueda 1999).

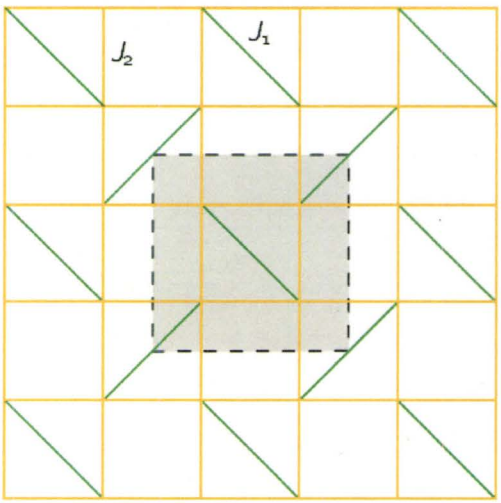

Figure 1.2: Shastry-Sutherland model with spins on the vertices. The couplings on the square lattice are parameterized by J_2 and the diagonal couplings (dimers) are parameterized by J_1. The grey shaded region depicts the unit cell of the system. (shastry and Sutherland 1981)

In their original work in 1981 Shastry and Sutherland designed this model in an effort to create a two- (and three-) dimensional system exhibiting an exact ground state made from a product of singlets. Shastry and Sutherland showed, that the singlet state is the exact ground state for $x = J_2/J_1 < 1/2$ (for spin $S = 1/2$). Consequently, the elementary excitations above the singlet ground state are given by promoting one of the singlets to a triplet.

The left part of Figure 1.3 shows the classical phase diagram (i.e. large S) of the Shastry-Sutherland model. It can be shown that there is a long range ordered anti-ferromagnetic phase (i.e. Néel phase) for large $J_2 > 0$ and a ferromagnetic ordering for large $J_2 < 0$ (Löw and Müller-Hartmann 2002).

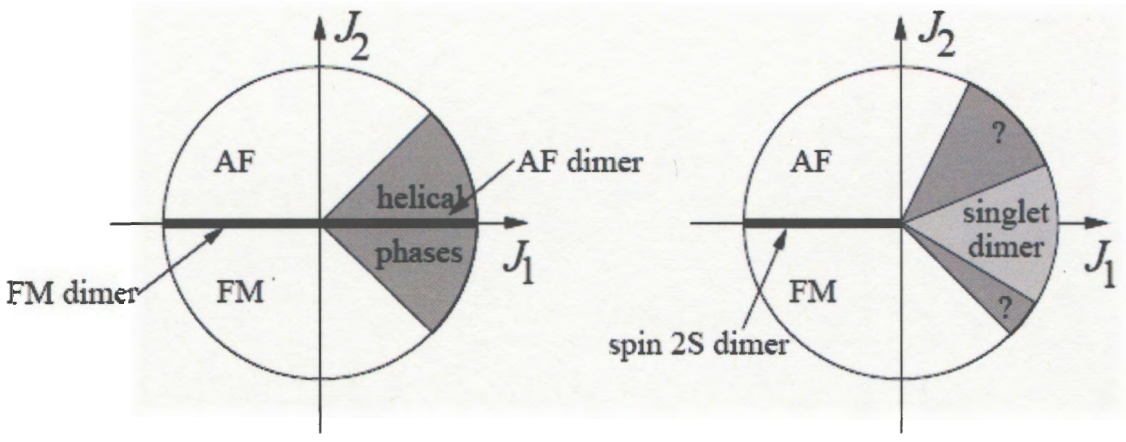

Figure 1.3: The left part shows the classical phase diagram of the two-dimensional Shastry-Sutherland model. The phase transition lines can be calculated exactly. The right part depicts the phase diagram in the quantum mechanical case (small *S*). The singlet dimer phase covers a finite region. The nature of the adjacent phases is not understood yet (Löw and Müller-Hartmann 2002).

In the quantum mechanical regime (i.e. small S), the dimer-singlet product state becomes the exact ground state for $J_1 > 0$ and J_2 not too large. The phase diagram on the $J_1 < 0$ side is similar to the classical phase diagram. This is sketched in the right part of Figure 1.3. In 1999, Miyahara and Ueda found that this dimer to Néel transition occurs at $x_c = J_2/J_1 \approx 0.7$, which is a broadly accepted value. Recently, there has been discussion suggesting the existence of an intermediate phase between the singlet collective ground state and long range antiferromagnetic state. The existence and nature of this intermediate phase is still an open question (Miyahara and Ueda 2003).

Chapter 2

Neutron Scattering

2.1. Introduction

In order to resolve details of condensed matter structures, a scattering experiment can be conducted. When the atomic positions are arranged in a crystal lattice, the well known idea of Bragg (1913) can be used to understand the scattering intensity distribution. The incoming waves are *reflected* by parallel lattice planes defined by the periodically aligned atoms. Diffraction maxima are visible if the path difference is an integer multiple of the wavelength,

$$2d \sin\theta = n\lambda_i \tag{2.1}$$

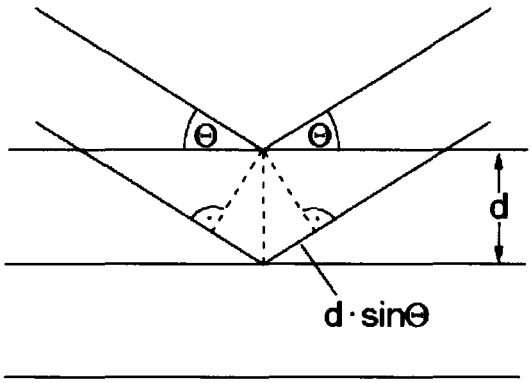

Figure 2.1: Diffraction geometry with path difference of waves scattered at a crystal lattice (Aschroft and Mermin 1976).

2.2. Scattering from crystals

In general, the nucleus in an atom is surrounded by a spatial distribution of electrons, which can be described by a local electron density $n_e(r)$ within the atomic volume V. The summation of scattering amplitudes of all electrons, using correct phase shifts leads to the atomic structure factor $f_j(Q)$:

$$f_j(Q) = \int_V dV n_e(r) e^{iQ \cdot r} \tag{2.2}$$

Due to this spatial distribution of the shell electrons, there is always a Q-dependence of x-ray scattering. This Q-dependence is absent for nuclear neutron scattering experiments, since the nucleus appears as a *point source* on the scale of the thermal neutron wavelengths. However, for neutron scattering, a Q-dependence occurs for the magnetic scattering where the magnetic moment caused by unpaired electrons

couples to the magnetic moment of the neutron. Normally, only a few electrons orbiting in the outer shell of the atom will contribute to the magnetic moment. Therefore, the magnetic scattering form factor for neutrons is not identical to the electronic form factor for x-rays.

Let's consider a Bravais lattice with N atoms described by their position vectors $r_n = n_1a + n_2b + n_3c$ where a, b and c are basis vectors in real space. For simplicity, only one type of atom is assumed to be present, thus $f_n = f$. The scattered amplitude of such a lattice is then given by the phase-correct addition of all separate scattering contributions:

$$\begin{aligned} F'(Q) &= \sum_{n}^{N} f_n e^{iQ\cdot r_n} \\ &= f(Q) \sum_{n_1,n_2,n_3}^{N} e^{iQ\cdot(n_1a+n_2b+n_3c)} \\ &= f(Q)\left(\sum_{n_1}^{N_1} e^{in_1Q\cdot a}\right)\left(\sum_{n_2}^{N_2} e^{in_2Q\cdot b}\right)\left(\sum_{n_3}^{N_3} e^{in_3Q\cdot c}\right) \end{aligned} \tag{2.3}$$

where the lattice sum over N atoms in the crystal is separated into three partial sums over N_1, N_2 and N_3.

The condition for constructive interference with sharp maxima requires that each of the three factors has to be non-zero, individually. This means that Q has to satisfy three equations simultaneously:

$$Q\cdot a = 2\pi h \quad Q\cdot b = 2\pi k \quad Q\cdot c = 2\pi l \tag{2.4}$$

where h, k and l are any set of integers. These conditions are known as *Laue conditions*.

In order to identify the solutions of the scattering vector Q that fulfill these conditions $Q = hA + kB + lC$ with a new set of basis vectors A, B and C is made, where:

$$A = \frac{2\pi}{V_c}(b \times c) \quad B = \frac{2\pi}{V_c}(c \times a) \quad C = \frac{2\pi}{V_c}(a \times b) \tag{2.5}$$

and $V_c = a \cdot (b \times c)$ is the volume of a unit cell. The vectors A, B and C have the dimension of a reciprocal length; therefore the lattice they span is called the reciprocal lattice. In this way, each crystal has two associated lattices, the real lattice with its points $r = n_1a + n_2b + n_3c$ and the reciprocal lattice with its points $G = hA + kB + lC$.

The role of the reciprocal lattice can be illustrated further with the discussion of the momentum transfers during the scattering process. Figure 2.2 shows the scattering triangle made up by Q, k_i and k_f together with the reciprocal lattice points. The constructive interference occurs when the scattering vector Q coincides with the lattice vector G:

$$Q = k_i - k_f = G \tag{2.6}$$

Multiplying this equation by $\hbar$ delivers:

$$\hbar Q = \hbar k_f - \hbar k_i = \hbar G \tag{2.7}$$

with $\hbar k = 2\pi\hbar/\lambda = h/\lambda = p$ being the momentum. Hence, Equation 2.7 stands for the momentum conservation in the scattering process.

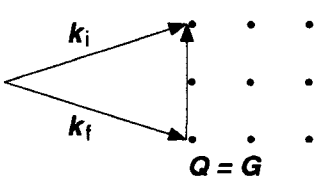

Figure 2.2: Diffraction geometry with path difference of scattered waves.

This fact was used by P. P. Ewald for an instructive geometric interpretation of the Bragg's law and the prediction of allowed scattering maxima, as illustrated in Fig. 2.3. In the figure, k_i shows that the direction of the incoming beam may end at any point of the reciprocal lattice. A sphere of radius $|k_i| = 2\pi/\lambda_i$ around the origin of k_i gives the length of k_i of the scattered beam. Now, any point of the reciprocal lattice on the surface of the sphere defines a diffracted beam, $k_f = k_i - G$.

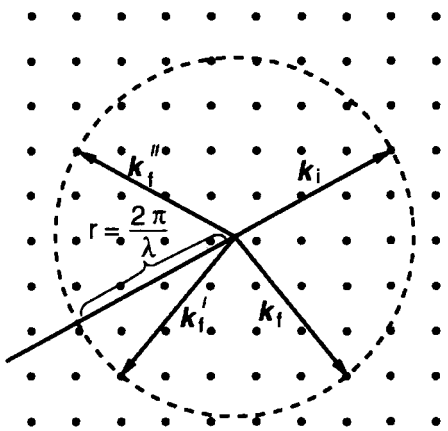

Figure 2.3: Allowed k_f leading to scattering maxima according to the Ewald construction (Aschroft and Mermin 1976).

2.3. Neutron Scattering

Neutron scattering is a powerful tool to probe dynamic and static properties of condensed matter at microscopic levels. The energies of cold and thermal neutrons are of the order of microscopic excitations in condensed matter and the wavelengths of cold and thermal neutrons are comparable to the intermolecular distances. Since neutrons have no

electrical charge, there is no Coulomb interaction between them and the nuclei of the sample, and therefore they can easily and deeply penetrate the material.

Neutron scattering events are described by means of energy and momentum transfer. The kinematics of a neutron scattering event is shown in Figure 2.4. A neutron with incident momentum p_0 and incident wave-vector k_0 has incident energy of:

$$E_0 = \frac{p_0^{\,2}}{2m} = \frac{\hbar^2 k_0^{\,2}}{2m} \tag{2.8}$$

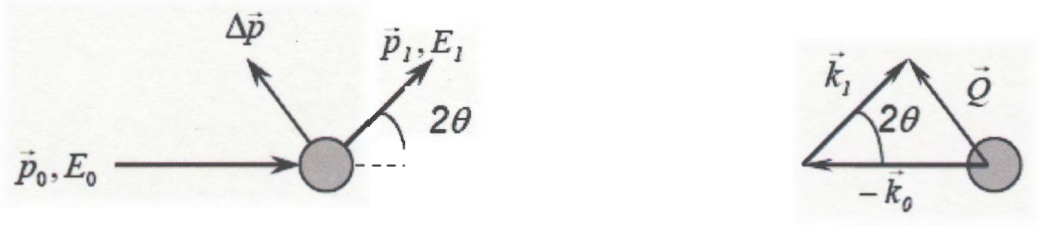

Figure 2.4: Neutron scattering kinematics in real space (left) and in reciprocal space (right) (Squires 1986).

After interactions with the sample, the neutron scatters to the direction 2θ, with a momentum p_1, a wave-vector k_1 and energy E_1. As with any particle scattering technique, the energy and the momentum conservation are the two basic principles of neutron scattering. The energy conservation allows defining the energy transfer of the incident and scattered neutrons:

$$\hbar\omega = E_1 - E_0 = \frac{\hbar^2}{2m}\left(k_1^{\,2} - k_0^{\,2}\right) \tag{2.9}$$

Eventually, momentum conservation makes it possible to define the scattering vector Q:

$$\hbar Q = p_1 - p_0 = \hbar k_1 - \hbar k_0 \tag{2.10}$$

The magnitude of Q is related to the incident and scattered neutron energies and to the scattering angle 2θ as follows:

$$Q^2 = \frac{2m}{\hbar^2}\left(E_0 + E_1 - 2\sqrt{E_0 E_1}\cos 2\theta\right) \tag{2.11}$$

Both the sign and the magnitude of the energy transfer are used to classify the neutron scattering event, as shown in Figure 2.5.

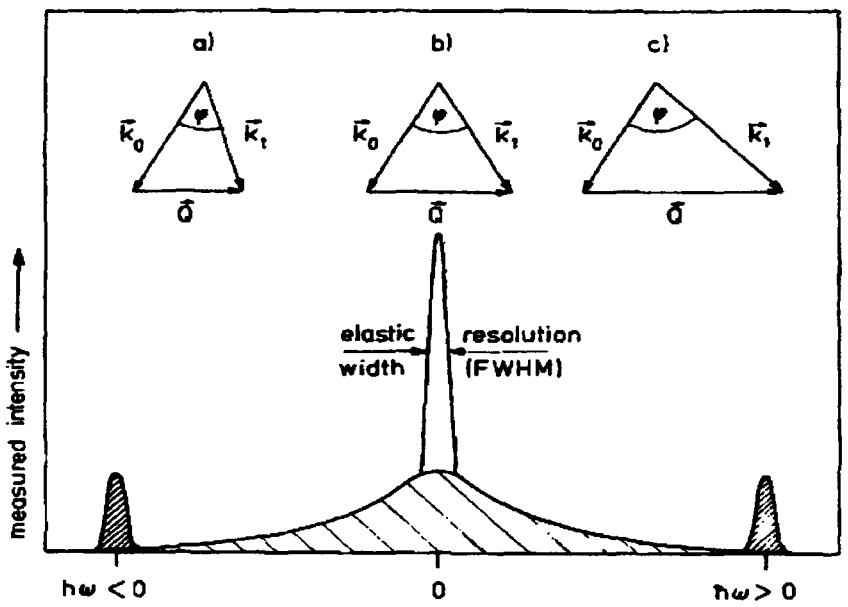

Figure 2.5: Neutron scattering spectrum as a function of energy transfer. The momentum conservation triangles are shown for processes of (a) neutron energy loss, (b) elastic scattering and (c) neutron energy gain (Squires 1986).

Neutron scattering is considered elastic, when $\hbar\omega = E_1 - E_0 = 0$, i.e. the neutrons do not change their energy in the scattering process. If neutrons either gain (i.e. $\hbar\omega > 0$), or lose energy (i.e. $\hbar\omega < 0$) in the scattering process, the scattering is called inelastic.

2.3.1. Neutron scattering cross-section

The quantity measured in a neutron scattering experiment is the double differential cross-section, $\partial^2\sigma/\partial\Omega\partial E_1$, which gives the proportion of neutrons with an incident energy E_0 scattered into a solid angle element $d\Omega$ with an energy between E_1 and E_1+dE_1. The geometry of the scattering experiment is shown in Figure 2.6.

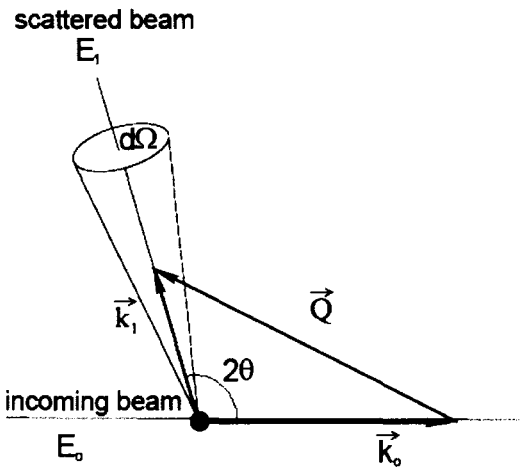

Figure 2.6: Scattering geometry from a single core (Squires 1986).

An incident neutron with a wave vector k_0 is scattered into a state with wave vector k_1. Before and after the interaction with the neutron, the sample can be described by the quantum states λ_0 and λ_1, respectively. The probability that the combined state of the neutron and the sample makes the transition from the initial state $|k_0\lambda_0\rangle$, to the final state $|k_1\lambda_1\rangle$ is given by Fermi's Golden Rule:

$$\sum_{k_1 \text{ in } d\Omega} W_{k_0,\lambda_0\to k_1,\lambda_1} = \frac{2\pi}{\hbar}\rho_{k_1}\left|\langle k_1\lambda_1|V|k_0\lambda_0\rangle\right|^2 \qquad (2.12)$$

Where ρ_{k_1} is the density of the final states of the neutrons described by k_1 in $d\Omega$ and V is the interaction potential between the nuclei in the sample and the neutron. Using the Born approximation for the cross-section, the double differential cross section is given by:

$$\frac{\partial^2\sigma}{\partial\Omega\partial E_1} = \frac{k_1}{k_0}\sum_{\lambda_0\lambda_1} p_{\lambda_0} \left|\langle k_1\lambda_1 | V | k_0\lambda_0\rangle\right|^2 \delta(\hbar\omega + E_{\lambda_0} - E_{\lambda_1}) \tag{2.13}$$

where the δ-function is included to ensure the energy conservation with the neutron energy transfer $\hbar\omega$, the initial sample energy E_{λ_0} and the final sample energy E_{λ_1}. In this equation, p_{λ_0} is the probability that the initial state of the sample is λ_0. This probability is given by Boltzmann distribution:

$$p_{\lambda_0} = \frac{1}{Z} e^{-E_{\lambda_0}/k_B T} \text{ , and } Z = \sum_{\lambda_0} e^{-E_{\lambda_0}/k_B T} \tag{2.14}$$

k_B is the Boltzmann constant, Z the partition function of the sample and T the sample temperature. After further manipulations, the double differential scattering cross-section can be written as:

$$\frac{\partial^2\sigma}{\partial\Omega\partial E_1} = \frac{1}{2\pi\hbar}\frac{k_1}{k_0}\sum_{j,i}\overline{b_j b_i}\int\left\langle e^{-iQR_i(0)} e^{-iQR_j(t)}\right\rangle e^{-i\omega t} dt \tag{2.15}$$

where b_j and b_i are the scattering lengths of the j^{th} and i^{th} nuclei, $R_i(0)$ is the position operator of the i^{th} nucleus at time zero, $R_j(t)$ is the position operator of the j^{th} nucleus at time t, and $\langle\ \rangle$ denotes a thermal average.

The average $\overline{b_j b_i}$ for cases $j = i$ and $j \neq i$ is given as $\overline{b_j b_i}^{\,j=i} = \overline{b^2}$, and $\overline{b_j b_i}^{\,j\neq i} = \overline{b}^{\,2}$; therefore Equation 2.15 can be written as a sum of two components, due to the different mean values for cases $j = i$ and $j \neq i$ as follows:

$$\begin{aligned}\frac{\partial^2\sigma}{\partial\Omega\partial E_1} &= \frac{1}{2\pi\hbar}\frac{k_1}{k_0}\overline{b}^{\,2}\sum_{j,i}^{j\neq i}\int\left\langle e^{-iQR_i(0)}e^{-iQR_j(t)}\right\rangle e^{-i\omega t}dt \\ &+\frac{1}{2\pi\hbar}\frac{k_1}{k_0}\overline{b^2}\sum_{j}^{j=i}\int\left\langle e^{-iQRj(0)}e^{-iQR_j(t)}\right\rangle e^{-i\omega t}dt\end{aligned} \tag{2.16}$$

This leads to the introduction of *coherent* and *incoherent* scattering, related to the terms of the sum in Equation 2.16 respectively. The coherent scattering arises from interference effects and would be the scattering if all the nuclei of any element had the same scattering length b. The incoherent scattering, on the other hand, does not arise from interference effects and is related to the distribution or deviation of scattering length from the mean value $\overline{b}$ and therefore is proportional to $\overline{b^2} - \overline{b}^{\,2}$. The coherent and the incoherent scattering cross section into all directions can be defined as follows:

$$\begin{aligned}\sigma_{coh} &= 4\pi\overline{b}^{\,2} \\ \sigma_{inc} &= 4\pi\left(\overline{b^2} - \overline{b}^{\,2}\right)\end{aligned} \tag{2.17}$$

Subsequently, the double differential cross section can be re-written as:

$$\begin{aligned}\frac{\partial^2\sigma}{\partial\Omega\partial\omega} &= \frac{1}{8\pi^2\hbar}\frac{k_1}{k_0}\sigma_{coh}\sum_{j,i}\int\left\langle e^{-iQR_i(0)}e^{-iQR_j(t)}\right\rangle e^{-i\omega t}dt \\ &+\frac{1}{8\pi^2\hbar}\frac{k_1}{k_0}\sigma_{inc}\sum_{j}\int\left\langle e^{-iQRj(0)}e^{-iQR_j(t)}\right\rangle e^{-i\omega t}dt \\ &= \left(\frac{\partial^2\sigma}{\partial\Omega\partial\omega}\right)_{coh} + \left(\frac{\partial^2\sigma}{\partial\Omega\partial\omega}\right)_{inc}\end{aligned} \tag{2.18}$$

The coherent scattering contains information about the correlation between the positions of different nuclei and the collective excitations in a sample. The incoherent scattering component can provide information about the individual nuclei and single particle excitations in the sample.

2.3.2. Scattering functions

The pair-correlation function describes the position of nuclei in space and time, and is given for N nuclei as:

$$G(R,t)=\frac{1}{N}\sum_{i,j}^{N}\left\langle \delta\left\{R+R_i(0)-R_j(t)\right\}\right\rangle \tag{2.19}$$

The space Fourier transformation of the pair-correlation function $G(Q,t)$ is called intermediate scattering function:

$$I(Q,t)=\int_{-\infty}^{\infty}G(R,t)e^{iQ.R}dR=\frac{1}{N}\sum_{i,j}\left\langle e^{-iQ.R_i(0)}e^{-iQ.R_j(t)}\right\rangle \tag{2.20}$$

A time Fourier transform of the intermediate scattering functions leads to the scattering function (also called as the dynamic structure factor), which provides information on the sample states as a function of energy and momentum:

$$S(Q,\omega)=\frac{1}{2\pi\hbar}\int_{-\infty}^{\infty}I(Q,t)e^{-i\omega t}dt \tag{2.21}$$

Both $I(Q,t)$ and $S(Q,t)$ can be divided into a coherent and an incoherent part. The relationship between the coherent and incoherent scattering functions and the double differential scattering cross section can be written as:

$$\frac{\partial^2\sigma}{\partial\Omega\partial E} = \frac{\sigma_{inc}}{4\pi\hbar}\frac{k_1}{k_0}NS_{inc}(Q,\omega) + \frac{\sigma_{coh}}{4\pi\hbar}\frac{k_1}{k_0}NS_{coh}(Q,\omega) \qquad (2.22)$$

2.3.3. Magnetic cross-section

The interaction between the magnetic moment of a neutron μ_n, and the electrons inside the scattering system originates from the Zeeman interaction of the neutron with the magnetic field distribution inside the sample arising from the spin and orbital angular momenta of unpaired electrons. The magnetic moment of a neutron is given by $\mu_n = -\gamma\mu_N\sigma_n$ where $\gamma = 1.913$ is the gyromagnetic ratio of the neutron, and $\mu_N = 5.051 \times 10^{-27}$ J/T is the nuclear magneton. If p denotes the electron momentum operator and R the distance vector measured from this electron, then by introducing the unit vector $\hat{R} = R/|R|$, the total Zeeman interaction with the field produced by this electron can be derived from electromagnetic theory:

$$V_{mag}(r) = \frac{\mu_0}{2\pi}\gamma\mu_N\mu_B\sigma_n \cdot \left(\nabla\times\left(\frac{s\times R}{|R|^2}\right) + \frac{1}{\hbar}\frac{p\times\hat{R}}{|R|^2}\right) \qquad (2.23)$$

where $\sigma_n = 2s_n$ is the Pauli spin operator and s is the operator for the electron spin.

The first term originates from the field created by the magnetic moment associated with the electronic spin angular momentum. The second term comes from the orbital angular momentum of electronic charges. The motion of these charges may be

viewed as current elements and hence contributes to the field distributions as described by the law of Biot and Savart.

Substituting this electromagnetic potential into double partial differential cross section one can come up with the equation for magnetic scattering differential cross section. This was first pointed out by Van Hove (1954):

$$\left(\frac{\partial^2\sigma}{\partial\Omega\partial E_1}\right)_{mag} = \frac{1}{\hbar}\frac{k_1}{k_0}(\gamma r_0 g/2)^2 |F(Q)|^2 \exp(-2W)\sum_{\alpha\beta}\left(\delta_{\alpha\beta}-\hat{Q}_\alpha\hat{Q}_\beta\right)S^{\alpha\beta}(Q,\omega) \quad (2.24)$$

The scattering function $S^{\alpha\beta}(Q,\omega)$ is then given by:

$$S^{\alpha\beta}(Q,\omega) = \frac{1}{2\pi}\sum_{R,R'}\exp\left(-iQ\cdot(R-R')\right)\int_{-\infty}^{\infty}dt\,\exp(-i\omega t)\left\langle S_R^{\alpha}(0)S_{R'}^{\beta}(t)\right\rangle \quad (2.25)$$

A useful property of $S(Q,\omega)$ is that it is connected to the imaginary part of the generalized magnetic susceptibility $\chi(Q,\omega) = \chi'(Q,\omega) + i\,\chi''(Q,\omega)$ through the fluctuation-dissipation theorem (Furrer 1995):

$$S(Q,\omega) = [n(\omega)+1]\chi''(Q,\omega) = \frac{\chi''(Q,\omega)}{1-\exp(-\hbar\omega/k_BT)} \quad (2.26)$$

in which the exponential term is called the Bose factor. The imaginary part of the susceptibility $\chi''(Q,\omega)$ is a very important property of the system and describes how the system responds to external forces. For instance, the magnetic susceptibility of a system characterizes the magnetic response of that system to the magnetic field:

$$M(Q,\omega) = \chi''(Q,\omega)\,H(Q,\omega) \quad (2.27)$$

The probability that a neutron gains an energy ω is different from the probability that a neutron loses an energy ω in the scattering process. This is due to the fact that it is $\exp(-\hbar\omega/k_BT)$ times less probable for the system to be in a higher initial state. Hence, the scattering function has to be corrected for this factor when calculating the susceptibility at different temperatures and energy transfers and this is exactly what the Bose factor does in Equation 2.26.

2.4. Instruments

2.4.1. Triple-Axis Spectrometers

A triple-axis spectrometer is a conceptually simple machine. It is based only on the Bragg's law and simple geometry in reciprocal space. In a triple-axis experiment a beam of neutrons traverses a path through the instrument determined by the settings of three angles θ_S, θ_M and θ_A. Figure 2.7 shows a triple-axis spectrometer with a monochromator crystal, located in the beam path from source to sample position, and an analyzer crystal, located in the path from sample to detector. Monochromators and analyzers are either perfect crystals or crystals that have been deformed in a controlled manner to obtain certain characteristic properties. Typical monochromator and analyzer materials are pyrolytic graphite (PG), silicon and germanium.

At the monochromator and analyzer positions, neutrons are reflected according to Bragg's law:

$$n\lambda = 2d \sin\theta_i \tag{2.28}$$

where n is an integer and $i = M, A$ for monochromator and analyzer respectively. The setting of the angle θ_i causes a family of crystal planes, characterized by their distance d, to diffract exactly those neutrons with wavelengths $\lambda = 2\pi/k$ determined by Equation 2.28. Hence, a monochromator transforms a polychromatic beam of neutrons to a beam of neutrons with wavenumbers k, $2k$, etc. When this beam hits the sample, the scattered neutrons leave the sample along a distribution of directions and with a distribution of energies and spin directions which are determined by the spin-dependent partial differential scattering cross-sections.

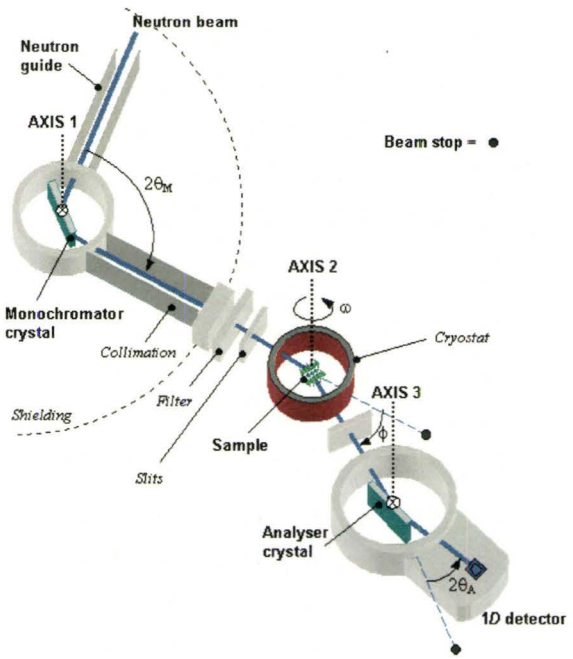

Figure 2.7: The layout of a triple-axis spectrometer (Connolly 2003).

By varying the scattering angle θ_S between k_i and k_f, the angular distribution can be explored. At the same time, the energy distribution in each given direction can be studied by varying the analyzer angle θ_A. Additional information may be collected by considering not only the change in momentum and energy of the neutron in the scattering process, but also possible changes in its spin state.

2.4.2. Time-of-Flight Spectrometers

The time-of-flight method complements the triple-axis spectrometer technique. The triple-axis spectrometer is ideally suited to the study of excitations in oriented samples at specific points in (Q,ω) phase space. Time-of-flight instruments, on the other hand, may be used to explore rather large regions of phase space since many detectors simultaneously collect neutrons over a wide range of values of the scattered energy.

Figure 2.8 illustrates a simple time-of-flight spectrometer. A neutron beam from the reactor reflects from a monochromator crystal. The monochromatic beam, characterized by its energy E_0 and wave vector k_0, is then pulsed by a chopper placed at a known distance, L_{CS}, from the sample. An array of detectors is arranged at a known fixed distance, L_{SD}, from the sample, and scattered neutrons arrive at the detectors at times determined by their scattered energies, E. The time of flight of a neutron from the chopper is given by:

$$t_{CD} = t_{CS} + t_{SD} = \tau_0 L_{CS} + \tau L_{SD} \tag{2.29}$$

where t_{CS} and t_{SD} are the times of flight of the neutron from chopper to sample and from sample to detector, respectively, and τ_0 and τ are the reciprocal velocities of the neutron before and after scattering. If the initial energy E_0, is known, then using t_{CD} and the final energy E, the energy transfer (i.e. $\hbar\omega = E_0 - E$) may be determined. Given the angle between the incident and scattered neutron wave-vectors, the wave-vector transfer (i.e. $Q = k_0 - k$) can also be calculated.

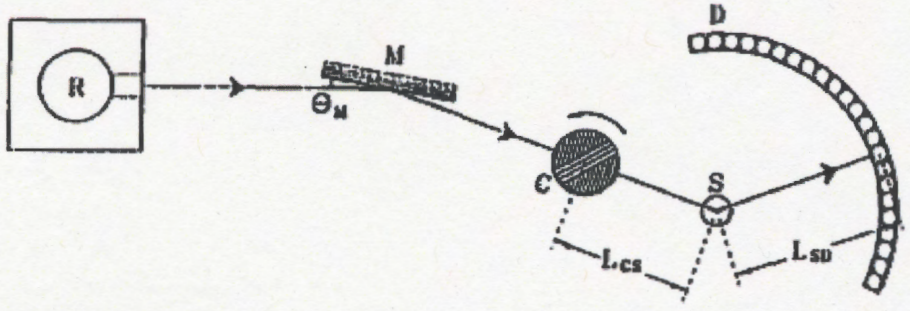

Figure 2.8: Schematic plan view of a simple time-of-flight spectrometer. The letters *R*, *M*, *C*, *S*, and *D* denote the reactor, monochromator, chopper, sample and detectors, respectively (Copley and Udovic 1993).

2.4.3. Powder Diffractometers

In a polycrystallines or powders there will be a great number of crystallites in all possible orientations. When a powder with randomly oriented crystallites is placed in an incident beam, the beam will see all possible interatomic planes. This can be explained using the Ewald sphere:

- There is a d^*_{hkl} vector associated with each point in the reciprocal lattice with its origin on the Ewald sphere at the point where the direct incident beam exists.

- Each crystallite located in the center of the Ewald sphere has its own reciprocal lattice with its orientation determined by the orientation of the crystallite with respect to the beam.

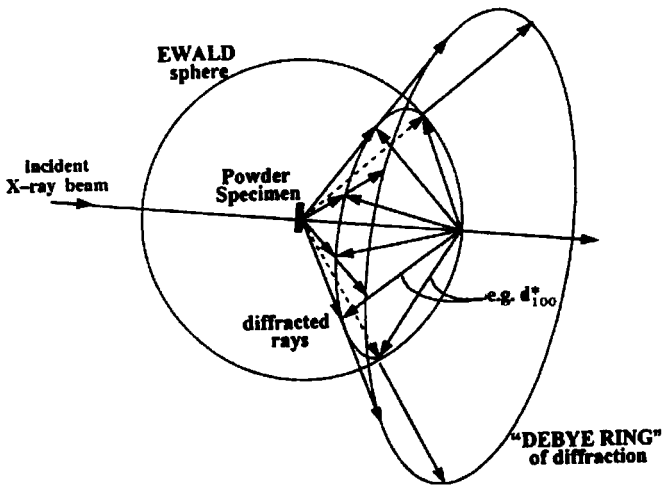

Figure 2.9: The intersection of d^*_{100} vectors from a powder with the Ewald sphere (Connolly 2003).

Figure 2.9 shows this geometry from the d^*_{100} reflection, which forms a sphere of vectors originating from the point of interaction with the beam. The number of vectors will be equal to the number of crystallites interacting with the beam. The angle between the beam and the cone of diffraction is 2θ.

Chapter 3

Neutron Scattering from $SrCu_2(BO_3)_2$

3.1. Introduction

Layered quantum magnets have been at the forefront of condensed matter physics research in large part due to their relevance to high temperature superconductivity. Two-dimensional copper-oxides, in which conducting holes are introduced, provide the framework for much exotic behavior, with high temperature superconductivity being the best appreciated example. More broadly, quantum antiferromagnets are of interest because the pattern for their behavior is not the orderly, antiparallel arrangement of magnetic moments in a Néel state, but is the formation of singlets in which the magnetic moments lose their spin-up or spin-down identity and reside in a quantum mechanical superposition of both spin-up and spin-down.

Kageyama *et al.* (1999a) discovered a new two-dimensional spin gap system $SrCu_2(BO_3)_2$. A remarkable feature of $SrCu_2(BO_3)_2$ is that the theoretical model for interacting spin 1/2 dimers, which was considered and solved exactly by Shastry and Sutherland in 1981, is appropriate for this system (Miyahara and Ueda 1999).

In this chapter, I will summarize and discuss the pre-existing neutron scattering studies of pure $SrCu_2(BO_3)_2$. These high-resolution inelastic neutron scattering measurements, probe both the energy and Q dependencies of the previously identified bands of excitations with new precision. These measurements were performed on two different high-resolution cold neutron instruments, allowing both high energy resolution to resolve the three n = 1 triplet excitations in $SrCu_2(BO_3)_2$, and high Q resolution to detect different Q dependencies among the n-triplet excitations, where n = 1, 2, and 3.

3.2. Structure of $SrCu_2(BO3)_2$

$SrCu_2(BO_3)_2$ crystallizes (Smith and Keszler 1991) into the tetragonal space group $I\bar{4}2m$ with lattice parameters a =8.995 Å, c = 6.649 Å. The schematic crystal structure is represented in Fig. 3.1. As shown on this figure, $SrCu_2(BO_3)_2$ is a layered compound consisting of slightly buckled $Cu(BO_3)$-planes separated by Sr Atoms. Figure 3.2 gives a top-view onto an isolated $Cu(BO_3)$-plane.

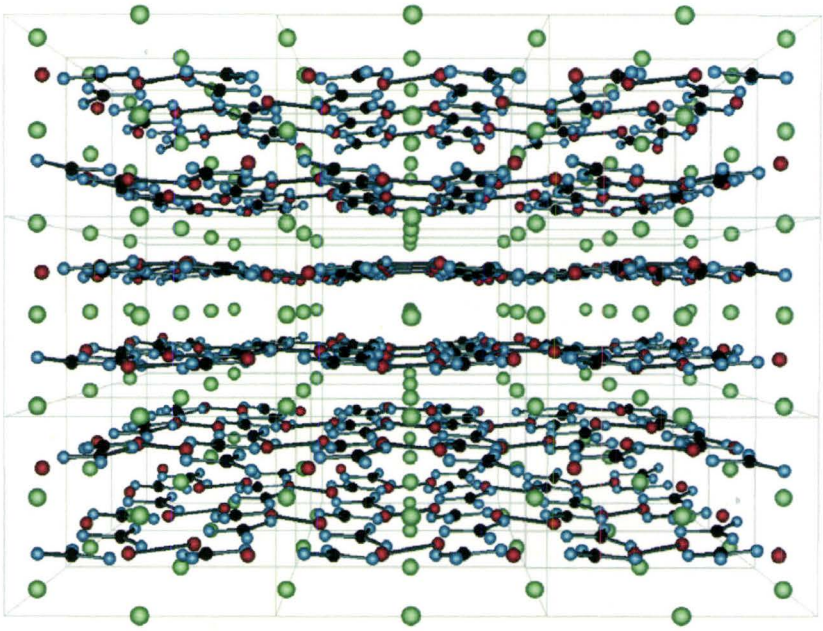

Figure 3.1: Crystal structure of $SrCu_2(BO_3)_2$, which is a layered compound with slightly buckled $Cu(BO_3)$-planes separated by Sr-atoms: green spheres; Cu: red, B: black, O: blue (Knetter *et al.* 2000).

The magnetic properties of the crystal are determined by the $S = 1/2$ spins which are considered to be situated on the Cu^{2+} sites. By geometry we find two Cu^{2+} ions close to each other and we connect them by lines as shown in Figure 3.2. It can be seen that the Cu^{2+}sites are arranged in dimers at right angles to each other forming a square lattice.

The leading terms, in the Hamiltonian which describe how the spin 1/2 magnetic moments interact are given by an intra-dimer antiferromagnetic exchange interaction, J, as well as an inter-dimer exchange interaction, J'. J = 85K and J' = 54K are anti-ferromagnetic interactions estimated from the susceptibility and the gap measurements (Miyahara and Ueda 1999). It was first observed by Miyahara and Ueda that a single $Cu(BO_3)$-plane can be mapped onto the Shastry-Sutherland model.

One should also note that every second $Cu(BO_3)$-plane is rotated by $\pi/2$ about one of the dimer centers, so that each dimer has a rotated dimer above and below. Thus the inter-plane exchange interactions are frustrated by the geometry. Since fits to the susceptibility measurements result in weaker inter-plane interactions (Miyahara and Ueda 1999), we will mostly concentrate on the in-plane physics.

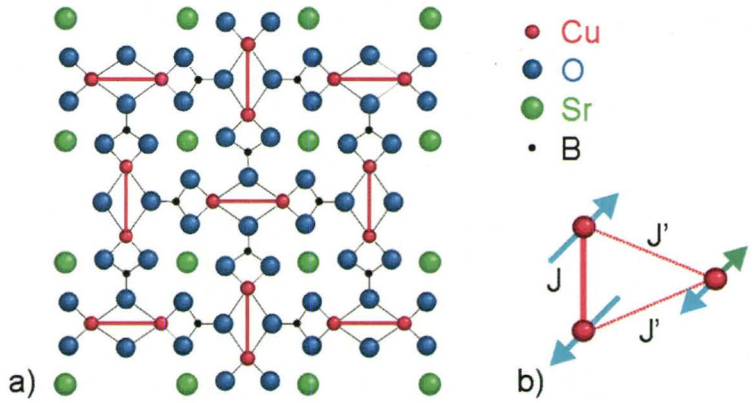

Figure 3.2: (a) A schematic drawing of the basal plane structure of $SrCu_2(BO_3)_2$ is shown. Red atoms joined by red bars highlight the Cu^{2+} dimers. (b) The leading order exchange interactions which shows the nearest-neighbor (*nn*) intra-dimer (J) and next-nearest neighbor (*nnn*) inter-dimer (J') antiferromagnetic interactions (Kageyama *et al.* 1999a).

3.3. Theoretical model for $SrCu_2(BO_3)_2$

In 1999, Miyahara and Ueda introduced the frustrated Shastry-Sutherland model for $SrCu_2(BO_3)_2$ with $S = 1/2$ as shown in Equation 3.1 where *nn* stands for nearest neighbor and *nnn* for next nearest neighbor:

$$H = J\sum_{nn} S_i \cdot S_j + J'\sum_{nnn} S_i \cdot S_j \qquad (3.1)$$

It is known that both interactions, J and J', are antiferromagnetic and similar in strength, such that the system is not far from the critical value of $x = J'/J$ for a quantum phase transition to a four sublattice Néel state (Miyahara and Ueda 1999). In their original work, Shastry-Sutherland (1981) argued that the direct product of the singlet states on J bonds, described by Equation 4.2, is always an eigenstate of the Hamiltonian.

$$|\psi\rangle = \prod_a |s\rangle_a = \prod_a \frac{1}{\sqrt{2}}\left(|\uparrow\downarrow\rangle_a - |\downarrow\uparrow\rangle_a\right) \tag{3.2}$$

In this equation, a denotes a nearest-neighbor bond.

They also showed that, this eigenstate (Equation 3.2) is the exact ground-state of the Hamiltonian for $J'/J \leq 0.5$. For $J'/J \geq 0.5$, there is no exact solution for this model. Therefore, one can conclude that there is a quantum phase transition at $(J'/J)_c$ greater than 0.5. For small J'/J the collective singlet state shown in Equation 3.2 is the ground-state, which has a spin gap and does not exhibit long range ordering.

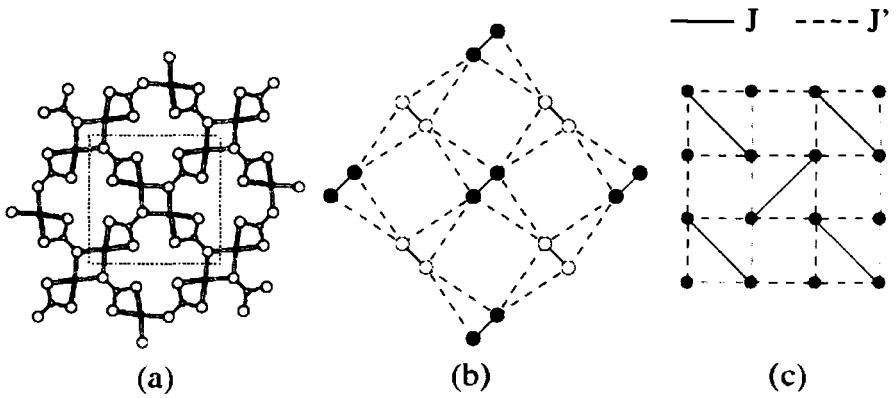

Figure 3.3: (a) Schematic view of the crystal structure of a $CuBO_3$ layer. Full circles represent Cu sites. Big open circles are O sites and small open circles are B sites. The dotted line shows the unit cell (Kageyama *et al.* 1999). (b) Two-dimensional orthogonal dimer model, which is equivalent to (c) the Shastry–Sutherland model (Miyahara and Ueda 2003).

Assuming $J = 0$ and $J' \neq 0$, the model is equivalent to a two-dimensional Heisenberg model. Manousaki (1991) reported that there is a general agreement that the two-dimensional Heisenberg model has antiferromagnetic long-range order ground-state and no spin gap. Therefore, in the limit $J'/J >> 1$, the antiferromagnetically ordered state must be the ground state. Series expansion calculations by Koga and Kawakami (2000) give the phase transition point $(J'/J)_c = 0.68$ associated with this quantum phase transition.

Initially, a direct phase transition from the dimer singlet state to the AF ordered state was proposed (Shastry and Sutherland 1981, Miyahara and Ueda 1999). However, recent works favor the possibility of an intermediate phase and therefore, in addition to these two states, it is possible that other states also exist between them (Albercht *et al.* 1996, Chung *et al.* 2001, Takushima *et al.* 2001, Läuchli *et al.* 2002). At present, our picture of the ground state of this orthogonal dimer model is that there may be three phases. The theoretical existence of the dimer singlet state for $J'/J < 1$ and an AF ordered state for $J'/J >> 1$ is established and the nature of the intermediate state in this model remains an open question.

One of the unique features of $SrCu_2(BO_3)_2$ are the very localized triplet excitations which have a tendency to crystallize at high magnetic fields. Recent experiments showed that the triplet excited states split in the presence of a magnetic field. Experiments also revealed that the spin triplet excitation energy decreases linearly with increasing magnetic field, which extrapolates to zero at about 20T magnetic field (Cépas *et al.* 2001, Cépas and Ziman 2001, Nojiri *et al.* 2003). However, the experimental data

deviates from this linear extrapolation at a finite magnetic field (Jorge *et al.* 2005). This indicates that the magnetic field causes the lowest energy triplet state to cross the ground-state. (Jorge *et al.* 2005).

It has also been shown, both by theory and experiment, that the lowest branch of magnetic excitations in $SrCu_2(BO_3)_2$ has a relatively small bandwidth (Kageyama *et al.* 2000, Weihong *et al.* 1999, Gaulin *et al.* 2004). The experiments previously conducted in this study, which will be discussed later in this chapter, showed a large bandwidth for the higher energy excitations.

The inelastic neutron scattering experiments show that the excitations are not purely localized and that the triplet states split in zero magnetic field. Cépas *et al.* (2001) argued that the corrections to the Hamiltonian, although small, are necessary to describe the dispersion and this splitting of the excited states in zero field can be accounted for by considering the Dzyaloshinsky-Moria (DM) interaction, which occurs in low-symmetry crystals, in the Hamiltonian. The contribution from DM interaction term to the Hamiltonian is given by:

$$H_{DM} = \sum_{\langle i \to j \rangle} D \cdot \left(S_i \times S_j \right) + \sum_{\langle i \to j \rangle'} D' \cdot \left(S_i \times S_j \right) \tag{3.3}$$

Here, $\langle i, j \rangle$ and $\langle i, j \rangle'$ indicate that i and j are nearest neighbor and next-nearest neighbor, respectively. The arrows indicate that the corresponding bonds have a particular orientation.

Assuming that the $CuBO_3$ in $SrCu_2(BO_3)_2$ is a mirror plane, there is a center of inversion at the middle of the dimer bond which forbids the DM interaction between

nearest neighbors. However, each dimer is separated from the neighboring dimer by a BO_3 triangle for which there is no center of inversion at the middle of the bond. This allows the DM interaction to exist between the next nearest neighbors. It also indicates that the main components of D must be perpendicular to the copper plane (Cépas *et al.* 2001). However since there is a buckling in the copper plane, in the real material at temperatures below 395K the mirror symmetry in this plane is lost (Sparta *et al.* 2001). This, in-plane components of the Dzyaloshinsky–Moriya interaction may also exist.

3.4. Previous Experiments on $SrCu_2(BO_3)_2$

Kageyama *et al.* (1999b) were the first to publish data on the magnetic response of $SrCu_2(BO_3)_2$. The magnetic susceptibility measured on powder samples shows a maximum at around 20K and a rapid drop towards zero with decreasing temperature, indicating an energy gap in the magnetic spectrum. The temperature dependence of the magnetic susceptibility is shown in Fig 3.4. Kageyama *et al.* (1999b) estimates the value of the spin gap to be $\Delta = 34K \pm 1K$ based on the fit to the isolated dimer model. Various experiments also showed evidence that $SrCu_2(BO_3)_2$ has the spin gap $\Delta \sim 35K$ (Kageyama *et al.* 1999b, Nojiri *et al.* 1999, Kageyama *et al.* 2000a, Lemmens *et al.* 2000). Therefore it is experimentally confirmed that the ground state of this material is nonmagnetic.

Kageyama *et al.* (2000b) later published relatively low resolution inelastic neutron scattering (INS) data obtained from a large single crystal. These measurements revealed three bands of excitations corresponding to single (n = 1) triplet excitations, as well as to two (n = 2), and to three (n = 3) triplet excitations. These measurements directly showed the appearance of an energy gap in the spectrum of excitations with decreasing temperature, as well as the dispersion of these excitations in an applied magnetic field. Electron spin resonance (Nojiri *et al.* 1999), far infrared studies (Rõõm *et al.* 2000) and nuclear magnetic resonance (Kodama *et al.* 2002) give further evidence for a singlet ground state above which a triplet excitation with gap 2.9 meV can be found.

More recent studies (Cépas *et al.* 2001, Kakurai 2002) have been able to investigate subleading terms in the spin Hamiltonian. Terms such as the Dzyaloshinski-Moriya (DM) interaction, which is allowed by symmetry between spins on neighboring dimers, can account for both the dispersion of these excitations and the removal of the threefold degeneracy which would otherwise characterize the n = 1 triplet excitation spectrum in $SrCu_2(BO_3)_2$. The presence of such small terms in the spin Hamiltonian has also been investigated through high field specific heat measurements (Jorge *et al.* 2005).

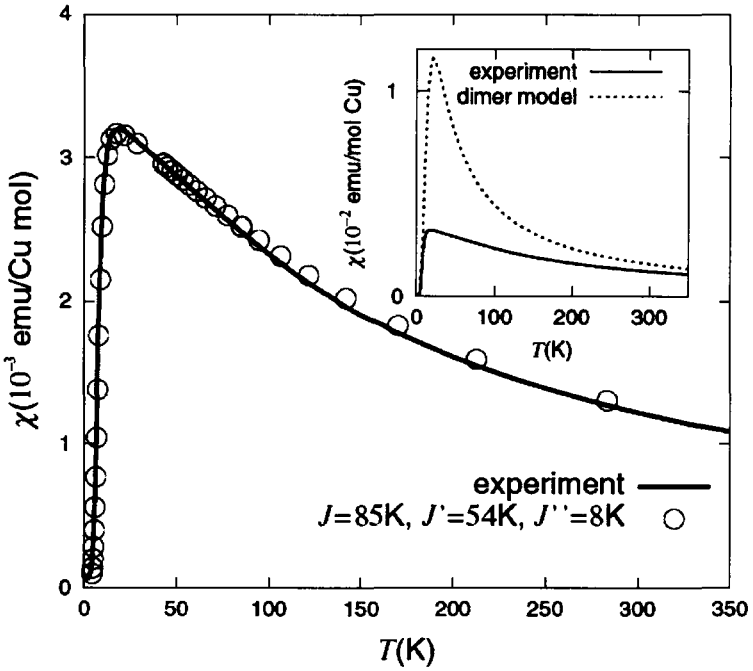

Figure 3.4: The temperature dependence of the magnetic susceptibility (solid curve). Circles are the result of numerical calculation with the optimal parameter set. The inset is the result of fitting by an isolated dimer model (Kageyama *et al.* 1999b , Miyahara and Ueda 1999).

The estimated values of J and J' have evolved over time as both theory and experiment have improved. One can find various fits of the model parameters to the experimental data. The earliest fit by Miyahara and Ueda (1999) gives $x = 0.68$ and $J =$ 100K = 8.617meV. In a later and improved calculation, they found $x = 0.635$ and $J =$ 85K= 7.325meV (Totsuka *et al.* 2001). Other values in this range are for instance $x =$ 0.664 and $J = 83$K = 7.15meV (Zheng *et al.* 1999) or $x = 0.65$ and $J = 87$K= 7.50meV (T. Munehisa and Y. Munehisa 2003). The range of given x values is rather close to the critical value of $x_c \approx 0.69$. There are experimental possibilities which may push

$SrCu_2(BO_3)_2$ towards the critical value by means of pressure or chemical substitutions. A direct observation of a real substance at or close to a quantum critical point would indeed be very interesting, but has so far not been realized.

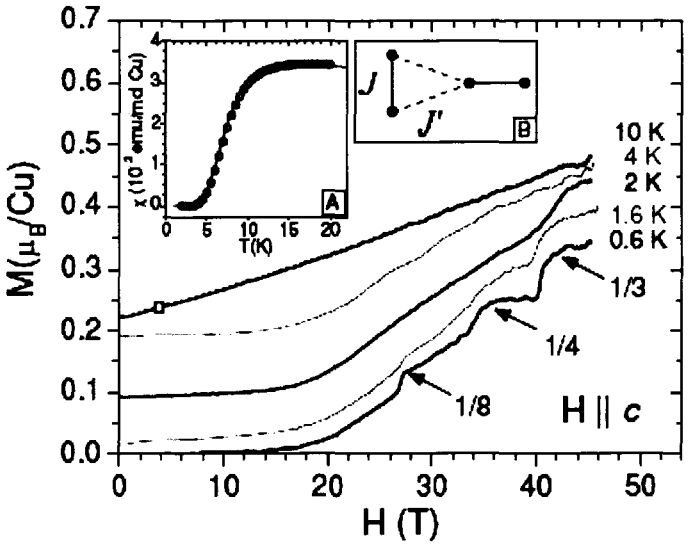

Figure 3.5: Magnetization vs field for $SrCu_2(BO_3)_2$ at different temperatures between 0.6K and 10K. Inset A: Magnetic susceptibility measured at H = 4T in a SQUID magnetometer and the calculated susceptibility. Inset B: Two copper dimers in the $CuBO_3$ plane where the coupling constants J (*nn*) and J' (*nnn*) are indicated. (Jorge *et al.* 2005)

Much interest has also focused on magnetization plateaus which appear beyond 20T in $SrCu_2(BO_3)_2$ (Kodama *et al.* 2002). Magnetic fields generate triplets, within a background of singlets, which can undergo Bose-Einstein condensation (BEC) at densities determined by the applied magnetic field, which takes on the role of a chemical potential. Figure 3.5 shows the high field magnetization measurements which have been performed by Jorge *et al.* (2005).

3.5. Experimental Details

Sample Preparation

The single crystal of $SrCu_2(^{11}BO_3)_2$ was grown by floating zone image furnace techniques. Stoichiometric amounts of CuO, $SrCO_3$ and B_2O_3 were mixed, preannealed, and then annealed at 870 °C. Finally, the powder was reground, pelletized and annealed in O_2 several times. Rods were formed by hydrostatic pressing and the growth was performed in a Crystal System Optical Furnace at a growth speed of 0.25 mm/h in O_2. No additional flux was applied.

The crystal is cylindrical in shape, with approximate dimensions of 0.6 cm in diameter by 10 cm long. Small pieces of the crystal were used for bulk characterization and the characteristic falloff of the dc susceptibility near 10K. Well-defined plateaus in the magnetization versus applied magnetic field were observed, which is shown in Fig 3.5 (Jorge *et al.* 2005). Neutron diffraction measurements performed at Chalk River Laboratories, enabled by the use of ^{11}B isotope, revealed a high quality single crystal throughout the volume of the sample with a mosaic spread of less than 0.2 degree. Figure 3.7 illustrates the dc susceptibility measurements performed on the sample using SQUID magnetometer.

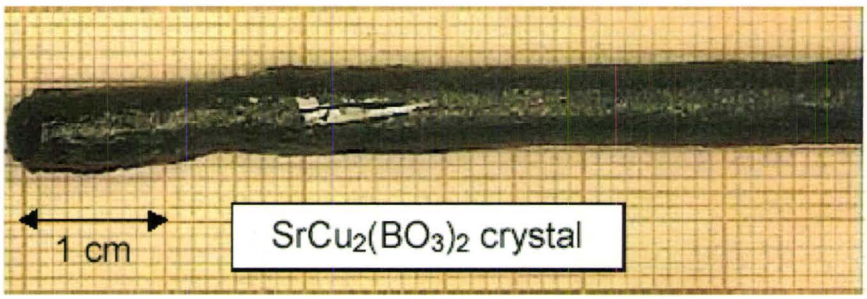

Figure 3.6: Single crystal of $SrCu_2(BO_3)_2$ grown using optical floating zone technique.

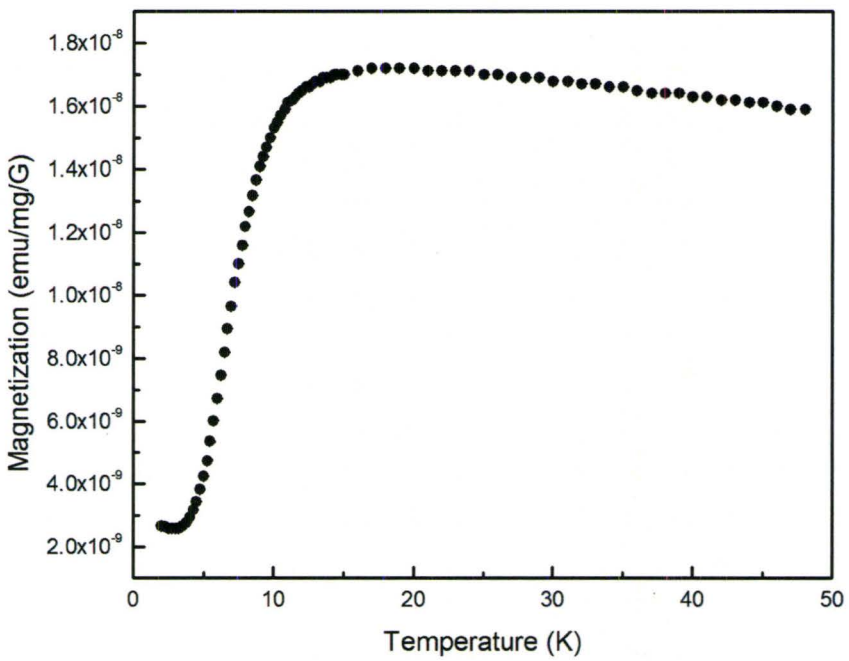

Figure 3.7: SQUID measurements performed on the grown $SrCu_2(BO_3)_2$ single crystal showing the same dc-susceptibility behavior as observed previously by Kageyama *et al.* in 1999b.

3.6. Neutron Scattering Studies

In this section I describe the results of the neutron scattering studies on pure $SrCu_2(BO_3)_2$ that was previously conducted.

Spin Polarized Inelastic Neutron Spectrometer (SPINS) measurements

In this study, a series of constant-**Q** measurements with the triple axis spectrometer were performed across the (H, 0, L) plane of $SrCu_2(BO_3)_2$ at 1.4 K. The summary of such scans with intervals of $\Delta H = 0.2$ is shown in the color contour map in top panel of Fig. 3.9, which displays the data within the($\hbar\omega$, H) plane at K = 0 and L = 0. The bottom panel of the figure shows typical scans making up this map. The top panel of the Fig. 3.9 clearly identifies both the $n = 1$ triplet excitation near $\hbar\omega = 3.0$ meV and the $n = 2$ triplet excitation near $\hbar\omega \sim 4.9$ meV. It can also be seen that there is a continuous component of the $n = 2$ triplet excitation extending to at least 8 meV.

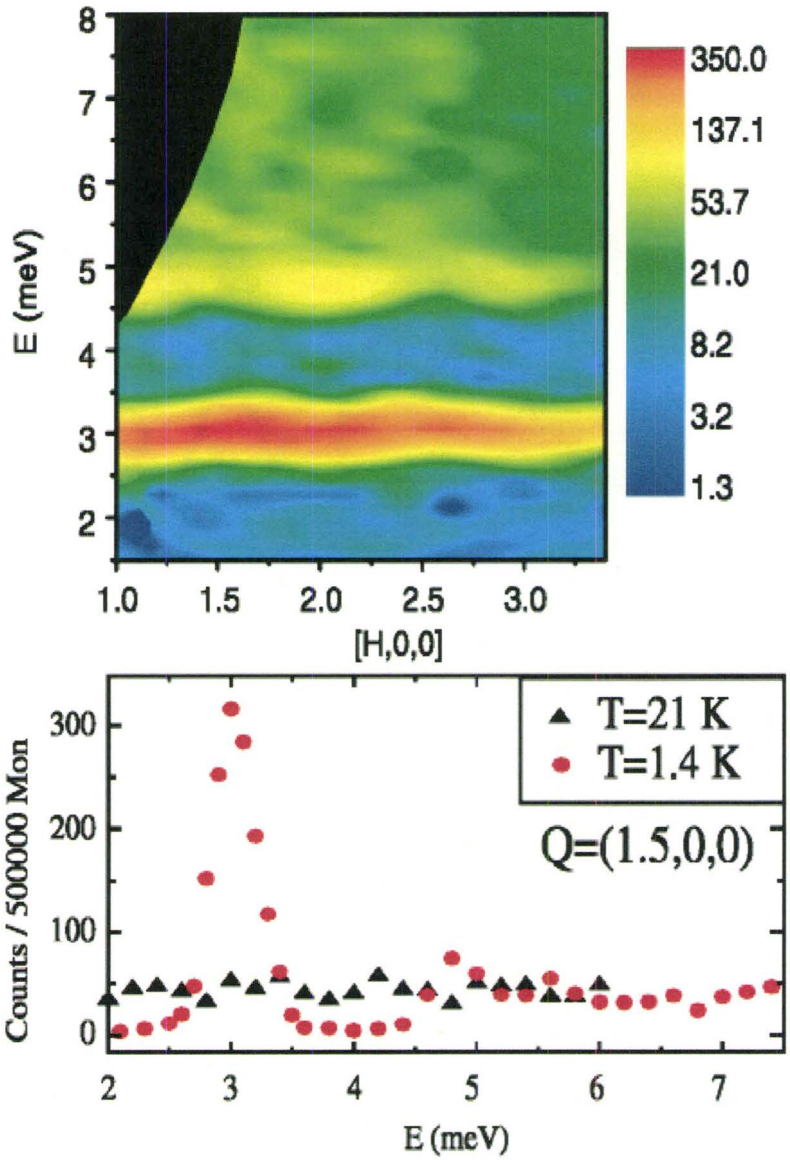

Figure 3.8: Top panel: A map of the measured dynamic structure factor for $SrCu_2(BO_3)_2$ at $T = 1.4$K along the (H, 0, 0) direction. Bottom panel: Constant-**Q** scans for **Q**=(1.5,0,0) (Gaulin *et al.* 2004).

These measurements are qualitatively similar to the low resolution results reported by Kageyama *et al.* (2000a) within the (H, K, 0) plane of $SrCu_2(BO_3)_2$.

However, there are important differences. As can be seen in Fig. 3.8, there is no substantial dispersion of the maximum of the spectral weight of the n = 2 triplet excitation in contrast to a bandwidth of 1.5 meV reported in the Kageyama *et al.*'s measurements. Also it can be seen that the **Q**-dependence of these excitations is different from that reported by Kageyama *et al* (2000a).

Figure 3.9 illustrates the results of constant energy scans conducted at $\hbar\omega$ = 3, 4.8, and 9 meV. The energies correspond to the n-triplet excitations with n = 1, 2 and 3, respectively. These measurements show most of the weight of the n = 1 excitation at 3 meV to peak up at half integer values of H (i.e. H = 1.5 and 2.5) within the (H, 0, L) plane, and at integer value of H = 2 for the n = 2 and n = 3 excitations at 4.8 meV and 9 meV, respectively.

The results indicate distinct form factors for the n-triplet excitations, in which the n = 1 triplet is different from the multi-triplet excitations. Using perturbation techniques, Knetter and Uhrig (2004) recently calculated the n = 2 triplet contribution to the dynamic structure factor within the (H, K, 0) plane of $SrCu_2(BO_3)_2$. They specifically showed that there is a peak in the form factor at (2, 0, 0). This is consistent with the inelastic scattering measurements conducted in this study. Furthermore, there is an excellent agreement between these results for the n = 2 triplet in the (H, 0, 0) direction, as shown in Fig. 3.9, and the theory. It is also clear from this figure that the **Q**-dependence of all the excitations show little L-dependence, consistent with well isolated two-dimensional basal planes.

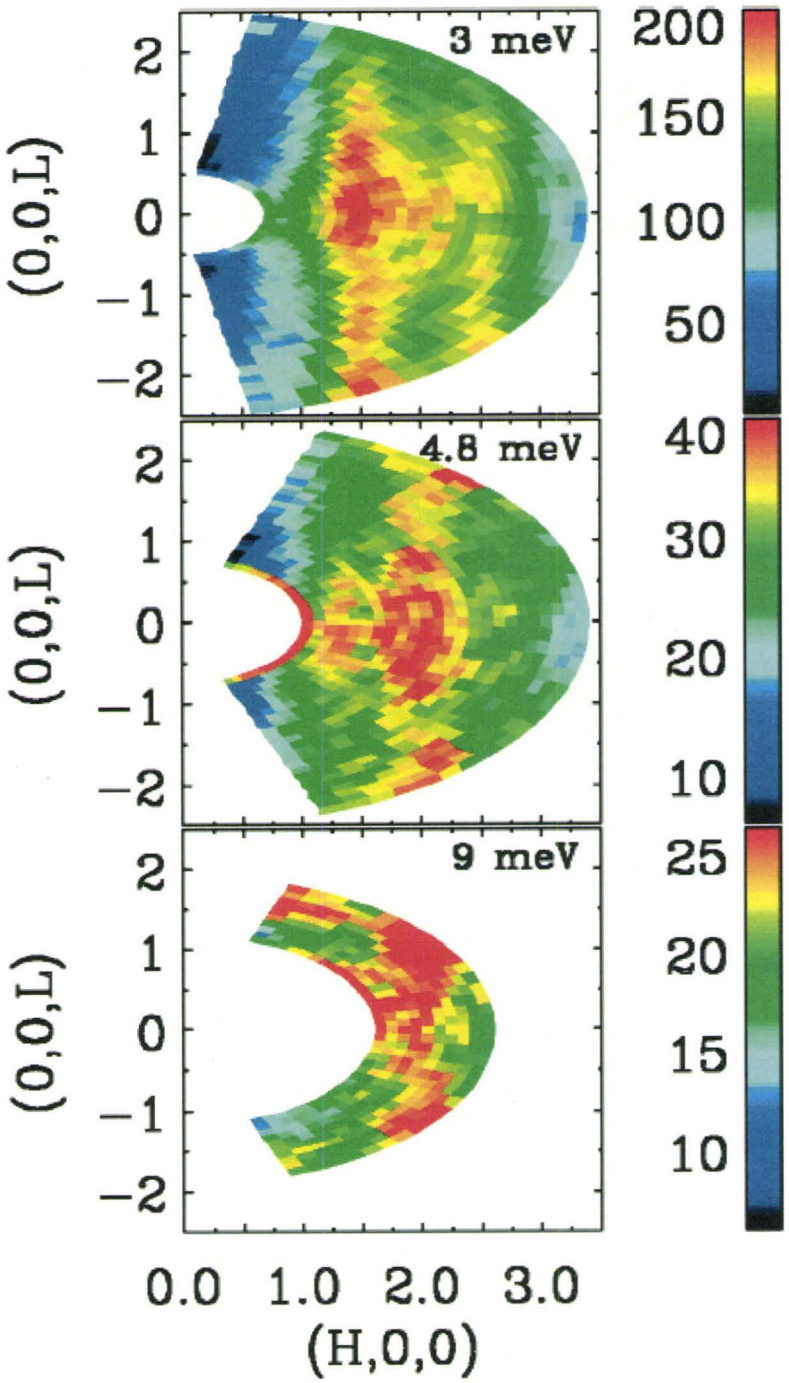

Figure 3.9: Constant energy scans at 3 (top panel), 4.8 (middle panel), and 9 meV (bottom panel) probing the **Q**-dependence of the n = 1, 2, and 3 triplet excitations in $SrCu_2(BO_3)_2$ within the (H, 0, L) plane at T = 1.4 K (Gaulin *et al.* 2004).

DCS time of flight measurements:

Since the scattering results show little L-dependence, the DCS measurements could be integrated along L. These results allow a high precision determination of the dispersion of the $n = 1$ triplet excitations in the (H, 0) direction within the tetragonal basal plane. This is illustrated in Fig. 3.10. The top panel shows a color contour map of the inelastic scattering. The bottom panel shows cuts through this map, for constant-**Q** scans at (-1, 0), (-1.5, 0), and (-2, 0), respectively from top to bottom. These inelastic measurements clearly resolve three branches of triplet excitation. Earlier work (Cépas *et al.* 2004, Kakurai 2002, Jorge *et al.* 2005, Zorko *et al.* 2004, Nojiri *et al.* 2003) suggests that the dispersion of these branches is a result of DM interaction. The energies of the top and bottom modes at **Q** = (-2, 0) and (-1, 0) are in excellent agreement with the ESR results of Nojiri *et al.* (1999) who found states at 2.81 meV (679 ± 2 GHz) and 3.16 meV (764 ± 2 GHz) for **Q** = 0. This splitting arises from the out-of-plane DM interaction, D_{OP}. To the lowest order in J'/J (i.e., ignoring quantum fluctuations), this splitting has the value of $4D_{OP}$ (Gaulin *et al.* 2004). However, the spectrum and its bandwidth are renormalized due to quantum fluctuations. Cépas *et al.* (2001) estimated that this renormalization reduces the bandwidth by a factor of about 2.

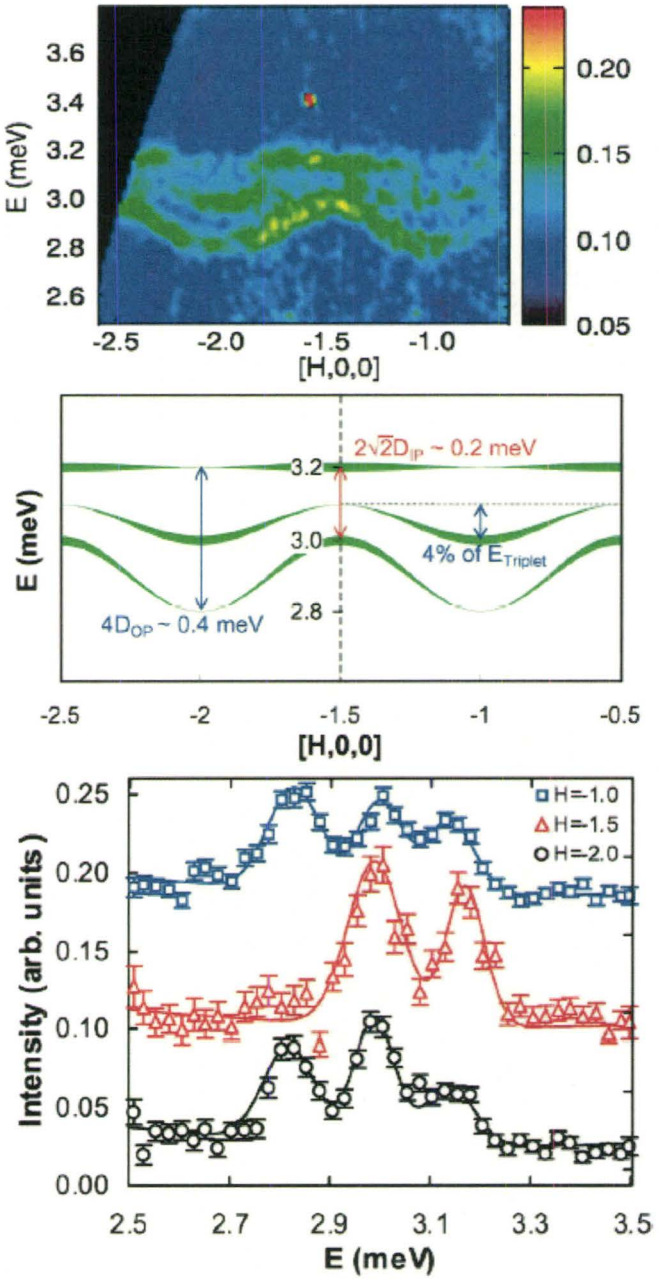

Figure 3.10: Top panel: Color contour map of the dynamic structure factor for the $n = 1$ triplet excitations along the (H, 0) direction within the basal plane of $SrCu_2(BO_3)_2$ measured with the DCS spectrometer at $T = 1.4$K and integrated along L. Middle panel: A cartoon of the dispersion and form factors appropriate to the S^z and $S^{\pm}$ for the $n = 1$ triplet excitations. Bottom panel: Cuts through the map of the top panel, which approximate constant-**Q** scans and clearly resolve the three branches to the $n = 1$ triplet excitation.

The gap between the $S^z = \pm 1$ modes at $\mathbf{Q} = (-1.5, 0)$ has been attributed (Karkurai 2002) to the in-plane DM interaction, D_{IP}, which is a result of the buckling of the planes. This splitting, which has the theoretical value of $2\sqrt{2}\,D_{IP}$ (Gaulin *et al.* 2004), is observed to be about 0.18 meV for these measurements. Details of the renormalization of the value of this gap due to quantum fluctuations are at present unknown. However, if the renormalization for in and out-of-plane DM interactions were similar, then D_{IP} would be about $0.7D_{OP}$, which is quite large in light of the small magnitude of the buckling of the layers (Cépas *et al.* 2001).

The middle panel of Fig. 3.10 shows the $S^z = 0$ mode, which is sketched along with higher and lower energy $S^{\pm}$ modes. This mode is predicted to have a zero form factor at $\mathbf{Q} = (1.5, 0)$ (Cépas *et al.* 2001) and is expected to be centered between the top and bottom $S^{\pm}$ bands, whose form factors are maximal near (1.5, 0). The bandwidth of the $S^z = 0$ mode is extremely small, roughly 0.1 meV, and it is known to be least affected by anisotropic interactions; hence it is most directly comparable to calculations of the $n = 1$ triplet excitation based on Equation 3.1. This bandwidth, which scales as x^6 ($x = J'/J$), is similar to the bandwidth found by Weihong *et al.* (1999) for $x = 0.6$ and is about 4% of the $n = 1$ triplet gap energy.

Temperature Dependence measurements:

The temperature dependence of both $n = 1$ and $n = 2$ triplet excitations and that of the $n = 1$ triplet excitations were measured using SPINS and DCS, respectively. The

SPINS measurements at **Q** = (1.5, 0, 0) and (2, 0, 0) and energy transfers of $\hbar\omega$ = 3 and 4.85 meV, for the n = 1 and n = 2 triplet excitations, respectively, are shown in Fig. 3.11. The DCS measurements integrate the inelastic scattering in data sets of the form shown in the top panel of Fig. 3.11. The DCS measurements integrate between 2.7 and 3.3 meV and across all wave vectors from H = -2.25 to H = -0.75 along (H, 0) within the basal plane.

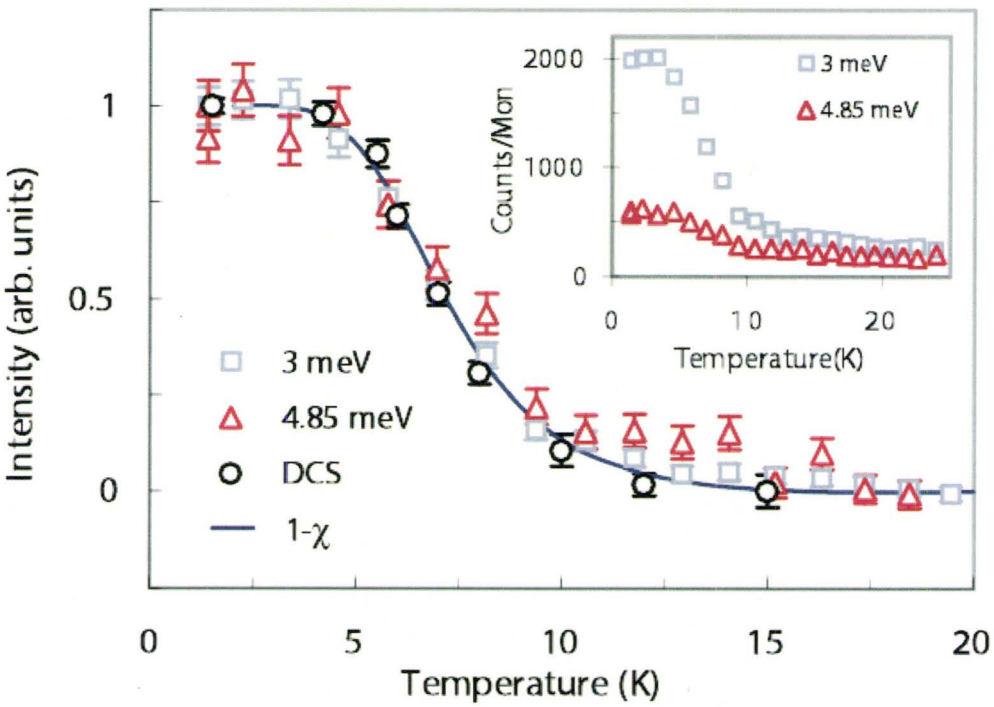

Figure 3.11: The temperature dependence of inelastic intensity at (1.5, 0, 0) and $\hbar\omega$ = 3 meV, as well as at (2, 0, 0) and $\hbar\omega$ = 4.85 meV. The inset shows the raw intensity data, while the main figure shows the normalized intensity assuming zero at 20 K and compared to the complement of the measured dc susceptibility ($1 - \chi$).

As it can be seen in Fig. 3.11, the temperature dependences of the $n = 1$ and $n = 2$ triplet excitations are identical. This could not have been concluded from earlier measurements (Kageyama *et al.* 2000). The temperature dependence of the inelastic scattering can be very well described as the complement of the dc susceptibility (Jorge *et al.* 2005). The complement of χ, referred to as $1 - \chi$ in Fig. 3.11, is given by $\chi\,(T = 20\text{K}) - \chi\,(T)$ and is scaled to compare the temperature dependence of the inelastic scattering. It can be seen from Fig. 3.11 that this provides an excellent description of the temperature dependence of the inelastic scattering.

Chapter 4

Neutron Scattering from $SrCu_{2-x}Mg_x(BO_3)_2$:

While pure $SrCu_2(BO_3)_2$ is well studied, there is little information on this quantum magnet in the presence of dopants and none on doped single crystals at the time we carried out our experiments. In this investigation high resolution neutron scattering measurements on $SrCu_2(BO_3)_2$ doped with Mg was studied revealing the presence of new spin excitations within the gap of this system. The results of these measurements are incorporated in this chapter which is reprinted from Physics Review Letters, Vol. 97, 247206, December 14, 2006.

In-Gap Spin Excitations and Finite Triplet Lifetimes in the Dilute Singlet Ground State System $SrCu_{2-x}Mg_x(BO_3)_2$

S. Haravifard,[1] S.R. Dunsiger,[1] S. El Shawish,[3] B.D. Gaulin,[1,2] H.A. Dabkowska,[1] M.T.F. Telling,[4] and J. Bonča,[3,5]

[1]*Department of Physics and Astronomy, McMaster University, Hamilton, Ontario, L8S 4M1, Canada*

[2]*Canadian Institute for Advanced Research, 180 Dundas St. W., Toronto, Ontario, M5G 1Z8, Canada*

[3]*J. Stefan Institute, SI-1000 Ljubljana, Slovenia*

[4]*Rutherford Appleton Laboratory, ISIS Pulsed Neutron Facility, Chilton, Didcot, Oxon, OX110QX, UK*

[5]*Faculty of Mathematics and Physics, University of Ljubljana, SI-1000 Ljubljana, Slovenia*

Reprinted from Physics Review Letters **97**, 247206 (2006)

Abstract

High resolution neutron scattering measurements on a single crystal of $SrCu_{2-x}Mg_x(BO_3)_2$ with x~0.05 reveal the presence of new spin excitations within the gap of this quasi-two dimensional, singlet ground state system. Application of a magnetic field induces Zeeman-split states associated with S=1/2 unpaired spins which are antiferromagnetically correlated with the bulk singlet. Substantial broadening of both the one and two-triplet excitations in the doped single crystal is observed, as compared with pure $SrCu_2(BO_3)_2$. Theoretical calculations using a variational algorithm and a single quenched magnetic vacancy on an infinite lattice are shown to qualitatively account for these effects.

In-Gap Spin Excitations and Finite Triplet Lifetimes in the Dilute Singlet Ground State System $SrCu_{2-x}Mg_x(BO_3)_2$

Quasi-two dimensional quantum magnets which display collective singlet or spin gap behavior are very topical due to the novelty of their ground states[1] and their relation to high temperature superconductivity in the copper oxides. There are relatively few such materials, and crystal growth difficulties have further limited their study in single crystal form. $SrCu_2(BO_3)_2$ is established as a realization of the two dimensional Shastry-

Sutherland model[2] for interacting S=1/2 dimers[3,4]. It is comprised of well separated layers of Cu^{2+}, S=1/2 orthogonal dimers arranged on a square lattice. The material crystallizes into the tetragonal space group I42*m* with room temperature lattice parameters of a= 8.995 Å, c= 6.649 Å[5].

$SrCu_2(BO_3)_2$ has been well studied by an array of experimental techniques, which show it to possess a non-magnetic ground state. In particular earlier neutron[6-9] and ESR spectroscopy[10,11] have established the leading terms in its microscopic Hamiltonian:

$$\mathcal{H} = J\sum_{nn} \mathbf{S_i}\cdot\mathbf{S_j} + J'\sum_{nnn} \mathbf{S_i}\cdot\mathbf{S_j} + g\mu_B\mathbf{H}\cdot\sum_{i}\mathbf{S_i} \quad (1)$$

where J is the exchange interaction within the dimers and J' is the exchange interaction between S=1/2 spins on neighboring dimers. Subleading Dzyaloshinskii-Moriya interactions weakly split the three triplet modes even in zero applied magnetic field[7-9,12].

Both the exchange interactions are antiferromagnetic and their ratio x= J'/J has been estimated between 0.68 and 0.60, with more recent refinements being smaller. Theoretically, such a quantum magnet is known to possess a singlet ground state so long as the ratio, x, of inter to intra-dimer antiferromagnetic exchange is sufficiently small[13] All of these estimates place $SrCu_2(BO_3)_2$ on the low side of the critical value of x at which a quantum phase transition occurs between a four sublattice Neel state and a collective singlet state.

In finite magnetic field, much interest has focused on a finite magnetization which develops at fields beyond ~ 20 T, wherein the lowest energy of the three triplet states has been driven to zero energy[4,14-16]. The magnetic field acts as a chemical potential for the

triplet density within the quasi-two-dimensional planes. Magnetization plateaus ensue at higher fields, corresponding to Bose condensation of the triplets at certain densities.

While pure $SrCu_2(BO_3)_2$ has been well studied, there is little information on this quantum magnet in the presence of dopants, and no reports on doped single crystals. This problem is very interesting by analogy with the remarkable properties of doped quasi-two dimensional Mott insulators and high temperature superconductivity[17]. $SrCu_2(BO_3)_2$ is itself a Mott insulator and the theory of doped Mott insulators on the Shastry-Sutherland lattice shows the possibility of several different superconducting phases as a function of doping[18-20]. Several doping studies of $SrCu_2(BO_3)_2$ have been reported on polycrystalline samples wherein Al, La, Na, and Y substitute at the Sr site and Mg substitutes at the Cu site[21].

In this Letter we report high resolution time-of-flight neutron scattering measurements on large single crystals of $SrCu_{2-x}Mg_x(^{11}BO_3)_2$and $SrCu_2(^{11}BO_3)_2$. These measurements show that doping of the magnetic Cu^{2+} site with non-magnetic, isoelectronic Mg^{2+} at the 2.5% level introduces new magnetic excitations into the singlet energy gap, and gives a finite lifetime to all three single triplet excitations, while also substantially broadening the two triplet bound state.

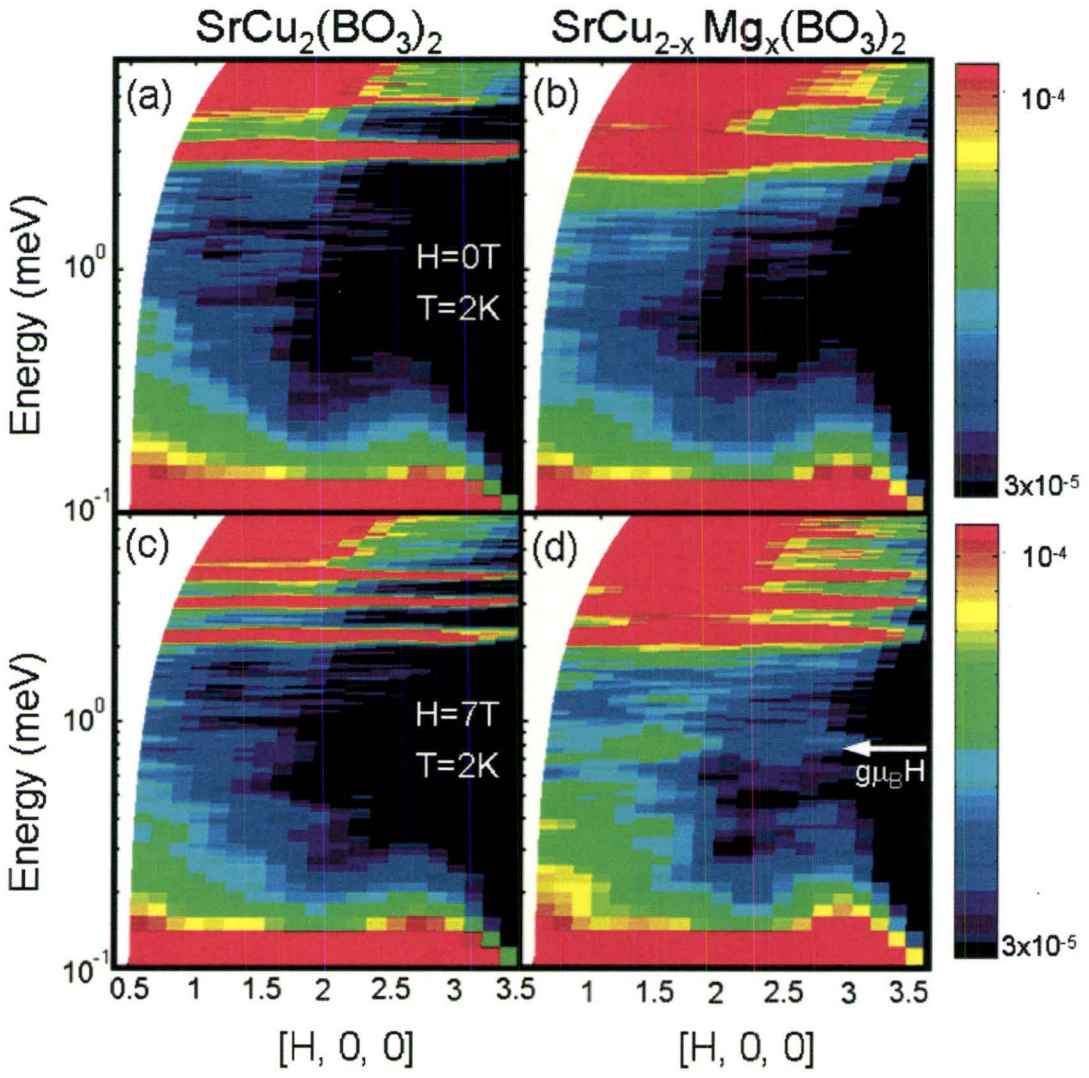

FIG. 1: (a) The two left hand panels show neutron scattering data from $SrCu_2(BO_3)_2$ at T=2 K. The scattering has been integrated along L and we show data in a magnetic field of zero and 7 T. The right hand panels show the same data for $SrCu_{2-x}Mg_x(BO_3)_2$. The energy axis is on a logarithmic scale. The Zeeman-split S=1/2 level in $SrCu_{2-x}Mg_x(BO_3)_2$ in H=7 T at g μ_BH=0.8 meV is indicated in panel (d).

Two single crystal samples, $SrCu_2(^{11}BO_3)_2$ and $SrCu_{2-x}Mg_x(^{11}BO_3)_2$, were grown by floating zone image furnace techniques at a rate of 0.2 mm/hour in an O_2 atmosphere.

The crystals were of almost identical cylindrical shape, with approximate dimensions of 4.5 cm in length by 0.6 cm in diameter. These samples were grown using ^{11}B, to avoid the high neutron absorption cross section of natural boron. The pure $SrCu_2(^{11}BO_3)_2$ single crystal was the same high quality single crystal studied previously[9]. Time-of-flight neutron scattering measurements were performed using the OSIRIS spectrometer[22] at the ISIS Pulsed Neutron Source of the Rutherford Appleton Laboratory. OSIRIS is an indirect geometry time-of-flight spectrometer which employs an array of pyrolytic graphite monochromators to energy analyse the scattered neutron beam. The data was collected with the spectrometer configured to use the 004 analysing reflection afforded by pyrolytic graphite. In this configuration, only those neutrons with a scattered energy of 7.375 meV are Bragg reflected towards the detector. The [H, 0, L] plane of both crystals was coincident with the horizontal scattering plane, and the samples were mounted in a 7 T vertical, [0, K, 0], field magnet cryostat.

Figure 1 shows representative time-of-flight neutron scattering data, taken at T=2 K and H=0 and 7 T for $SrCu_2(BO_3)_2$ (a and c) and for $SrCu_{2-x}Mg_x(BO_3)_2$ (b and d). This data was integrated along L, in which direction the spin excitations show little dispersion[9]. Note the logarithmic energy and intensity scales, chosen to draw attention to the details of the in-gap excitations seen in $SrCu_{2-x}Mg_x(BO_3)_2$. The splitting of the triplet excitations near 3 meV on application of the 7 T magnetic field is clear. In finite field, weak dispersion of the triplet excitations as a function of wavevector H is seen, and this has been attributed to subleading terms in the spin Hamiltonian - terms other than those in Eq. 1. There are several qualitative features evident on examination of this data. The

one triplet excitations show significantly greater breadth in energy in $SrCu_{2-x}Mg_x(BO_3)_2$ than in $SrCu_2(BO_3)_2$. In addition, application of a H=7 T magnetic field gives rise to an inelastic peak at $g\mu_B H$=0.8 meV in H=7 T, which is centered around [H ~ 1.4, 0, 0] in **Q**-space, but extends in wavevector H to almost [H ~ 3, 0, 0]. Both of these features are discussed at length below.

Figures 2b and 2d show the same experimental data as in Fig. 1, now integrated in wavevector along L and also in H between H=1 rlu and H=3 rlu, and plotted as a function of energy. The data in a magnetic field of 0 and 7T is shown in Figs 2b and 2d, respectively. The extra breadth in both the single triplet excitations and the two triplet bound states above it is clear. Broad inelastic peaks appear within the gap, which possess little magnetic field dependence, indicating a longitudinal nature. Sharp, field-induced inelastic scattering at $\hbar\omega$ ~ 0.8 meV is also evident.

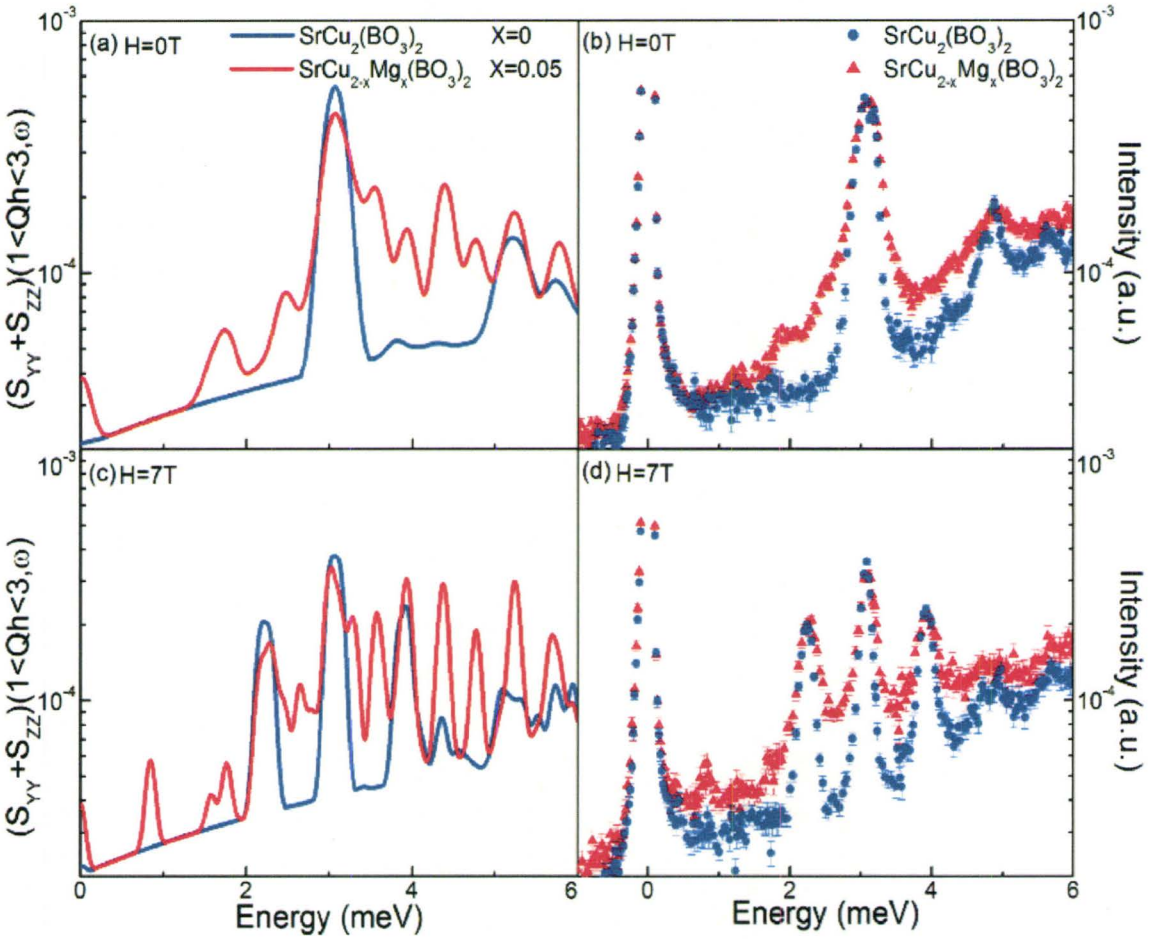

FIG. 2: The right hand panels show inelastic neutron scattering data for both $SrCu_2(BO_3)_2$ and $SrCu_{2-x}Mg_x(BO_3)_2$ in H=0 (b) and H=7 T (d). This data has been integrated in **Q** between H=1 and H=3 and over all L. The intensity is plotted on a logarithmic scale. Clearly the one and two triplet excitations are considerably broader in energy in $SrCu_{2-x}Mg_x(BO_3)_2$ as compared with $SrCu_2(BO_3)_2$, and in-gap states are introduced on doping. The left hand panels show the numerical calculation for $S^{zz}(\mathbf{Q},\omega) + S^{yy}(\mathbf{Q},\omega)$, using J=76.8 K and J'/J=0.62, which accounts for many of the qualitative features observed in $SrCu_{2-x}Mg_x(BO_3)_2$.

Numerical calculations have also been carried out using a new variational approach[23] to solve the model of a single quenched impurity on the two dimensional

Shastry-Sutherland lattice. This method generates a variational space by successively applying the off-diagonal parts of the Hamiltonian, Eq. 1, on the starting approximation for the single impurity ground state, which consists of a free spin 1/2 neighboring the impurity site, embedded within a dimer background. The resulting small spin polaron structure and exponential growth of the variational space with each iteration guarantee good convergence of the spin polaron ground state, as well as for the lowest energy excited states. Full details will be given separately[23]. For energies below ~ 3 meV the method provides accurate and converged results for both the longitudinal, $S^{zz}(\mathbf{Q},\omega)$, as well as the transverse, $S^{yy}(\mathbf{Q},\omega)$ components of the dynamical spin structure factor. These are compared directly to the neutron scattering experiments in Fig. 2.

Figures 2a and 2c show the calculated $S^{zz}(\mathbf{Q},\omega) + S^{yy}(\mathbf{Q},\omega)$, integrated over the same range of wavevectors as the experimental data, and at magnetic fields of 0 (a) and 7T (c). The comparison between theory and experiment is qualitatively good. The numerical results confirm that quenched magnetic vacancies induce in-gap states, substantial spectral weight below the zero field gap energy of ~ 3 meV. A component of these in-gap states show little magnetic field dependence, and appear in the $S^{zz}(\mathbf{Q},\omega)$, longitudinal channel. The calculation also shows the $g\mu_B H$ transverse, $S^{yy}(\mathbf{Q},\omega)$, excitation in finite magnetic field. Furthermore, the calculation[23] allows a determination of the spatial distribution of the spin polaron S=1/2 degree of freedom and its low lying excited states, and these can guide the interpretation of the **Q**-dependence of the field-induced $g\mu_B H$ transverse spin excitation observed in the experiments.

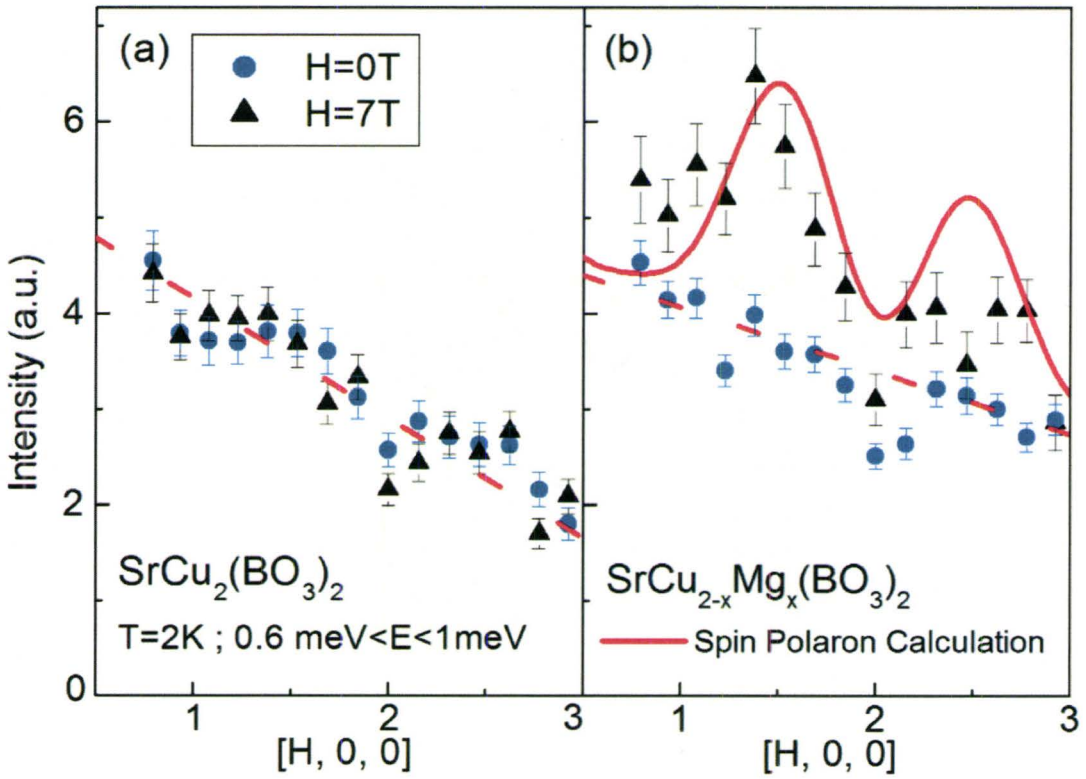

FIG. 3: **Q**-scans are shown at T=2 K for both $SrCu_2(BO_3)_2$ (a) and $SrCu_{2-x}Mg_x(BO_3)_2$ (b) which integrate in energy between 0.6meV and 1meV. This energy range captures the Zeeman energy $g\mu_B H$=0.8 meV appropriate to g=2 and H=7 T. (b) shows a comparison between the experimental **Q**-dependence of this scattering with the calculated form described in the text. The field-induced in-gap state in $SrCu_{2-x}Mg_x(BO_3)_2$ is absent in $SrCu_2(BO_3)_2$.

Figure 3 shows the **Q** dependence of the scattering around $g\mu_B H$=0.8 meV in an applied magnetic field of 7 T in both $SrCu_2(BO_3)_2$ (a) and $SrCu_{2-x}Mg_x(BO_3)_2$ (b). This scattering is integrated in wavevector over L, and in energy between 0.6 meV $< \hbar\omega <$ 1 meV and is shown in a magnetic field of both 0 and 7 T. Figure 3a shows the absence of

a magnetic field induced signal in $SrCu_2(BO_3)_2$ within this energy range. Figure 3b shows a clear field induced signal in $SrCu_{2-x}Mg_x(BO_3)_2$ which peaks at [H~1.4, 0, 0], but extends out to almost [H~3.0, 0, 0]. This field induced scattering is attributed to Zeeman split S=1/2 states associated with the S=1/2 moment in a dimer whose partner site is occupied by a quenched, nonmagnetic Mg^{2+} ion. This field induced inelastic scattering is very similar to that associated with end states in Haldane spin chains, such as occur in $Y_2BaNi_{1-x}Mg_xO_5$ [24]. In this case, quenched, non-magnetic Mg^{2+} ions produce finite S=1 magnetic chains. Spin 1/2 degrees of freedom arise at the end of finite chains of S=1 magnetic moments, as one of the two effective S=1/2 degrees of freedom making up the S=1 moments lacks a partner with which to form a singlet. Such excitations occur at an energy of $g\mu_B H$ in finite field, and display a wavevector dependence which indicates antiferromagnetic correlations into the collective singlet of the chain segment.

The wavevector dependence of the magnetic field-induced spin excitation at 0.8 meV can be attributed to the structure of the spin polaron[23], whose ground state possesses strong antiferromagnetic correlations with neighboring dimers, transverse to the dimer containing the impurity site. To first non-trivial order in J'/J, we obtain an analytical expression for the square of the matrix element for this transition:

$$I^{\pm} \propto \Big| (a_3^2 - a_1^2/2)\, e^{i\eta(\mathrm{H}\pm\mathrm{K})} + 2\sqrt{2}\, a_1 a_2 \times \sin(\eta(\mathrm{H}\mp\mathrm{K}))\sin(\pi(\mathrm{H}\mp\mathrm{K})) - 2\sqrt{2}\, a_2 a_3 \times \cos(\eta(\mathrm{H}\mp\mathrm{K}))\cos(\pi(\mathrm{H}\mp\mathrm{K})) \Big|^2 \qquad (2)$$

where a_1, a_2, and a_3 are the weights of the polaron variational wavefunction computed for $J'/J = 0.62$ [25]. $\eta = 0.72$ accounts for microscopic distances in $SrCu_2(BO_3)_2$.The ± sign in

Eq. (2) distinguishes between the two nonequivalent impurity positions within the unit cell. Random doping therefore implies $I \propto I^{+} + I^{-}$, which we show, multiplied by the square of the magnetic form factor for Cu^{2+}, in Fig. 3b along with measurements on **Q**-dependence of this scattering in $SrCu_{2-x}Mg_x(BO_3)_2$. While the agreement between the calculation and experiment is not perfect, the calculation captures the general **Q**-dependence of the excitation.

Figure 4a shows representative data with accompanying fits used to extract the lifetimes of the one triplet excitations as a function of doping and temperature in a magnetic field of 7 T. This data is integrated in **Q** along L, and over a narrow range in wavevector H around H=1.5, and these cuts approximate constant-**Q** scans. Similar analysis was performed around wavevector H=2.0 and 2.5 to look for variation in the one-triplet lifetimes as a function of **Q** along [H, 0, 0]. The data was fit to the sum of three identical damped harmonic oscillators (DHO):

$$S(\mathbf{Q},\omega,T) = \chi(\mathbf{Q},T)\frac{1}{1-exp\left(-\frac{\omega}{kT}\right)} \times \left[\frac{4\omega\Gamma_{\mathbf{Q},T}/\pi}{\left(\omega^2-\Omega^2_{\mathbf{Q},T}\right)^2+4\omega^2\Gamma^2_{\mathbf{Q},T}}\right] \qquad (3)$$

where $\chi(\mathbf{Q},T)$ is the momentum-dependent susceptibility, while the second term takes into account detailed balance. The renormalized DHO frequency, $\Omega_{\mathbf{Q}}$, has contributions from the oscillation frequency, $\omega_{\mathbf{Q},T}$, and the damping coefficient, $\Gamma_{\mathbf{Q},T}$, and is given by:

$$\Omega^2_{\mathbf{Q},T} = \omega^2_{\mathbf{Q},T} + \Gamma^2_{\mathbf{Q},T}.$$

Equation 3 was convoluted with an appropriate resolution function and fit to the data. The results are shown in Figs. 4b), c), and d), for wavevectors H=1.5, 2.0, and 2.5 respectively. The extracted lifetimes show little or no systematic variation with wavevector H, but a finite one-triplet lifetime is observed in $SrCu_{2-x}Mg_x(BO_3)_2$ at all temperatures, in contrast to $SrCu_2(BO_3)_2$, where the low temperature one-triplet lifetimes are very long, compared with the resolution of the spectrometer. In both $SrCu_{2-x}Mg_x(BO_3)_2$ and $SrCu_2(BO_3)_2$, the thermal destruction of the collective singlet ground state near ~ 10 K is characterized by a rapid decrease in the one triplet lifetime ($1/\Gamma$) on warming, with little or no softening of the one triplet excitation energies.

As mentioned previously, the theoretical results for $S^{zz}(\mathbf{Q},\omega) + S^{yy}(\mathbf{Q},\omega)$ are not well converged for energies of ~ 3 meV and greater. Nonetheless, the additional broad spectral weight around the calculated one and two triplet energies seen in Fig 2a) and c) is consistent with finite triplet lifetimes in the presence of a single quenched magnetic vacancy.

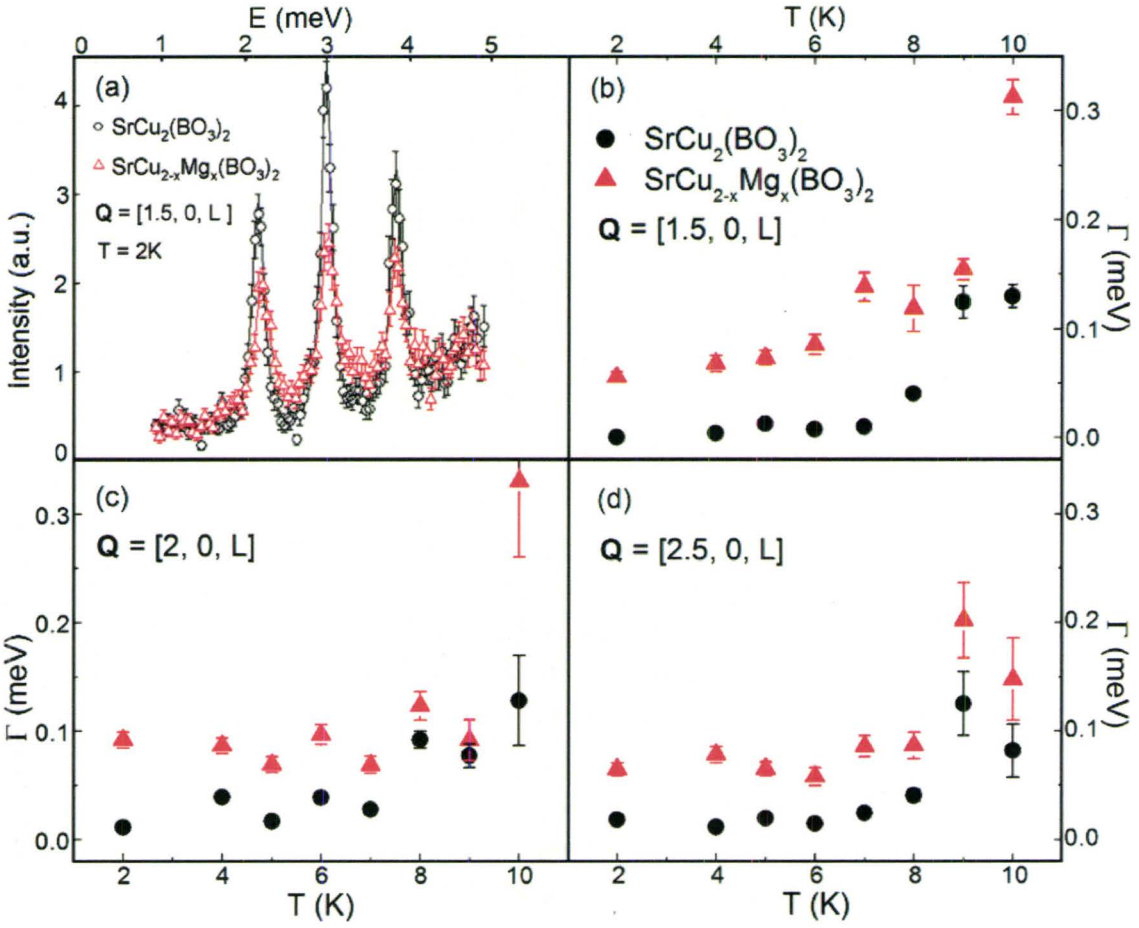

FIG. 4: (a) Cuts of the data simulating constant-Q scans at (1.5,0,L), integrated along L, are shown for $SrCu_2(BO_3)_2$ and $SrCu_{2-x}Mg_x(BO_3)_2$. Resolution convoluted fits to the data are shown as the solid lines and the description of the data is excellent. Such fits allow us to extract the triplet excitation lifetimes (Γ), which are shown in (b), (c), and (d) for wavevectors (1.5, 0, L), (2, 0, L) and (2.5, 0, L) respectively, as a function of temperature. Even at the lowest temperatures, we observe finite triplet lifetimes in $SrCu_{2-x}Mg_x(BO_3)_2$.

To conclude, new inelastic neutron scattering measurements on $SrCu_{2-x}Mg_x(BO_3)_2$ with x~0.05 show relatively broad and field-independent in-gap spin excitations as well

as a magnetic field-induced excitation identified as a Zeeman-split, spin polaron state. The non-magnetic quenched vacancies also give rise to finite and measurable lifetimes in the one and two triplet excitations.

We wish to acknowledge very helpful discussions with T.G. Perring and expert technical support from the ISIS User Group. This work was supported by NSERC of Canada, and the Slovenian Research Agency under contract PI-0044.

References

[1] see, for example: E. Dagotto and T.M. Rice, Science, **271**, 618 (1996); *Dynamical Properties of Unconventional Magnetic Systems*, edited by A.T. Skjeltorp and D. Sherrington, NATO ASI Series, Series E, Applied Sciences **349** (Kluwer Academic Publishers, Boston, 1998).

[2] B.S. Shastry and B. Sutherland, Physica B&C, **108B**, 1069 (1981).

[3] S. Miyahara and K. Ueda, Phys. Rev. Lett., **82**, 3701 (1999).

[4] H. Kageyama et al, Phys. Rev. Lett., **82**, 3168 (1999).

[5] R.W. Smith and D.A. Keszler, J. Solid State Chem. **93**, 430 (1991).

[6] H. Kageyama et al., Phys. Rev. Lett., **84**, 5876 (2000).

[7] O. Cepas et al., Phys. Rev. Lett., **87**, 167205 (2001).

[8] K. Kakurai, in *Quantum Properties of Low Dimensional Antiferromagnets*, edited by A. Ajiro and J.P. Boucher (Kyushu University Press, Fukuoka, 2002).

[9] B.D. Gaulin et al., Phys. Rev. Lett., **93**, 267202 (2004).

[10] A. Zorko, D. Arčon, H. van Tol, L.C. Brunel, and H. Kageyama, Phys. Rev. B, **69**, 174420 (2004).

[11] H. Nojiri, H. Kageyama, Y. Ueda, and M. Motokawa, J. Phys. Soc. Jap., **72**, 3243 (2003).

[12] S. El Shawish, J. Bonča, and I. Sega, Phys. Rev. B, **72**, 184409 (2005).

[13] M. Miyahara and K. Ueda, J. Phys. Condens. Matter, **15**, R327 (2003).

[14] K. Kodama et al., Science, **298**, 395 (2002).

[15] K. Onizuka et al., J. Phys. Soc. Jap., **69**, 1016 (2000).

[16] G.A. Jorge et al., Phys. Rev. B, **71**, 092403 (2005).

[17] See, for example: J. Orenstein and A.J. Millis, Science, **288**, 468 (2000).

[18] B.S. Shastry and B. Kumar, Prog. Theor. Phys. Suppl. **145**, 1 (2002).

[19] T. Kimura, K. Kuroki, R. Arita, and H. Aoki, Phys. Rev. B, **69**, 054501 (2004).

[20] C-H. Chung and Y.B. Kim, Phys. Rev. Lett., **93**, 207004 (2004).

[21] G.T. Liu, J.L. Luo, N.L. Wang, X.N. Jing, D. Jin, T. Xiang, and Z.H. Wu, Phys. Rev. B, **71**, 014441 (2005).

[22] M.T.F. Telling and K.H. Andersen, Phys. Chem. Chem. Phys., **7**, 1255 (2005).

[23] S. El Shawish and J. Bon·ca, Cond-mat/0607753.

[24] M. Kenzelmann, G. Xu, I.A. Zaliznyak, C. Broholm, J.F. DiTusa, G. Aeppli, T. Ito, K. Oka, and H. Takagi, Phys. Rev. Lett., **90**, 087202 (2003).

[25] For $J'/J = 0.62$, we obtain a_1=0.914, a_2=0.234, a_3=0.165.

Chapter 5

Neutron Scattering from $Sr_{(1-x)}La_xCu_2(BO_3)_2$

We had reported the first single crystal neutron scattering measurements of doped $SrCu_2(BO_3)_2$ and compared the results to the pure system which were published in Physical Review Letters (Chapter 5). The dopant introduced into the system was Mg^{2+} substituting onto the Cu^{2+} sites with the aim of introducing disorder without altering the carrier concentration. The measurements showed the existence of in-gap states and the broadening of the singlet-triplet excitation peaks for the Mg doped system in comparison to the pure system. Our interesting results and the corresponding theoretical predictions intrigued us to try to introduce charge carriers into the system. The results of the neutron scattering measurements on this doped sample are incorporated in this chapter and will be submitted for publication to The Journal of Physics: Condensed Matter.

One Triplet Excitation in Pure and Doped $SrCu_2(BO_3)_2$

S. Haravifard,[1] S.R. Dunsiger,[1] B.D. Gaulin,[1,2] H.A. Dabkowska and[1] M.T.F. Telling.[3]

[1] *Department of Physics and Astronomy, McMaster University, Hamilton, Ontario, L8S 4M1, Canada*

[2] *Canadian Institute for Advanced Research, 180 Dundas St. W., Toronto, Ontario, M5G 1Z8, Canada*

[3] *Rutherford Appleton Laboratory, ISIS Pulsed Neutron Facility, Chilton, Didcot, Oxon, OX110QX, UK*

Abstract

We have performed high resolution neutron scattering measurements on single crystals of $SrCu_2(BO_3)_2$, $SrCu_{(2-x)}Mg_x(BO_3)_2$ and $Sr_{(1-x)}La_xCu_2(BO_3)_2$. These experiments revealed the presence of new spin excitations within the gap for the $SrCu_{(2-x)}Mg_x(BO_3)_2$ sample and some spectral weight for the $Sr_{(1-x)}La_xCu_2(BO_3)_2$ sample. The broadening of the one and two triplet excitations in the doped materials was observed and compared to the thermally induced finite lifetime of the pure system. In case of the $Sr_{(1-x)}La_xCu_2(BO_3)_2$ sample the temperature dependence of this broadening demonstrates different behaviour in comparison to that seen in either $SrCu_2(BO_3)_2$ or $SrCu_{(2-x)}Mg_x(BO_3)_2$.

Introduction

For over fifteen years low-dimensional spin systems with spin-singlet ground states have attracted much attention due to their possible relevance to high temperature superconductivity in copper oxides and the existence of novel ground states.[1] Most of the systems studied to date have been limited to quasi-one dimensional structures since there are relatively few quasi two-dimensional quantum magnets which display collective singlet or spin gap behaviour. Crystal growth difficulties have further limited their study in single crystal form. Strontium copper borate, $SrCu_2(BO_3)_2$, is a unique two-

dimensional quantum spin system. $SrCu_2(BO_3)_2$ crystallizes into the tetragonal space group I42*m* with room temperature lattice parameters of a=8.995 Å, c=6.649 Å [2]. In this system the $CuBO_3$ and Sr planes are alternatively stacked along the c-axis. $SrCu_2(BO_3)_2$ has attracted much interest in recent years as the first realization of the two dimensional Shastry-Sutherland model [3] for interacting S=1/2 dimers [4]. It is comprised of well separated layers of Cu^{2+} S=1/2 orthogonal dimers arranged on a square lattice. Its ground state is known to be a non-magnetic collective singlet state with a singlet-triplet gap of ~3meV and a the two-triplet onset of bound state at ~4.8meV [3,5]. The ratio of the intra to inter-dimer exchange in this compound is close to a quantum critical point where the ground state transforms from a gapped, non-magnetic singlet state to a gapless long-range ordered antiferromagnetic state as a function of the ratio between the strength of the inter and intra dimer magnetic interactions [6].

Earlier neutron [7-9] and ESR spectroscopy [10,11] have established the leading terms in its microscopic Hamiltonian:

$$\mathcal{H} = J\sum_{nn}\mathbf{S_i}\cdot\mathbf{S_j} + J'\sum_{nnn}\mathbf{S_i}\cdot\mathbf{S_j} + g\mu_B\mathbf{H}\cdot\sum_{i}\mathbf{S_i}, \quad (1)$$

where J is the intra dimers exchange interaction and J' is the inter dimer exchange interaction. Both J and J' exchange interactions are antiferromagnetic. The estimated values of J and J' have evolved over time as both theory and experiment have improved and their ratio x= J'/J has been estimated between 0.68 and 0.60 with more recent

refinements being smaller. The ratio, x, of inter to intra dimer antiferromagnetic exchange is close to the critical quantum value of $x_c \sim 0.69$ and for $x < x_c$ such a quantum magnet is known to possess a singlet ground state [12]. All of these estimates place $SrCu_2(BO_3)_2$ on the low side of the critical value of x at which a quantum phase transition occurs between a four sublattice antiferromagnetic Neel state and a collective singlet state. Additionally, neutron scattering experiments showed that the singlet-triplet excitations are not purely localized even at zero magnetic field. Cepas *et al.* [8] have argued that corrections to the Hamiltonian, Eq(1) are necessary and subleading Dzyaloshinskii-Moriya interactions in the Hamiltonian, which occur in low-symmetry crystals, must be considered to explain the weakly split nature of the three triplet natural modes, even in zero applied magnetic field [8,9,13,14].

In finite magnetic field, beyond ~ 20 T, much interest has focused on a finite magnetization which develops at high enough fields, wherein the lowest energy of the three triplet states has been driven to zero energy [4,14-16,18]. High magnetic field measurements performed by Jorge *et al.* [17] on pure $SrCu_2(BO_3)_2$ revealed the 1/3, 1/4 and 1/8 plateaus as a function of magnetic field.

$SrCu_2(BO_3)_2$ and other two-dimensional magnetic systems with a singlet-triplet gap are of particular importance because of their relevance to the study of high temperature superconductivity. Recent theoretical work has pursued related possibilities for the Shastry-Sutherland model. Shastry and Kumar [19] have argued that the Mott-Hubbard gap will be suppressed by doping charge carriers into such a Shastry-Sutherland system, and several different superconducting phases are predicted at low temperature as

a function of doping [19-21]. While pure $SrCu_2(BO_3)_2$, a Mott insulator itself, has been well studied, there is little information on this quantum magnet in the presence of dopants. Several doping studies of $SrCu_2(BO_3)_2$ have been reported using polycrystalline samples wherein La, Na, and Y substitute at the Sr site and Mg substitutes at the Cu site [22,23]. Due to the difficulty of growing high quality large single crystals of the doped $SrCu_2(BO_3)_2$ there are not many single crystal measurements on the doped systems. We were able to report the first single crystal neutron scattering measurements of doped system on $SrCu_{(2-x)}Mg_x(BO_3)_2$ and compared the results to the pure system which showed the existence of the in-gap states as well as the broadening of the one-triplet excitation peaks for the Mg doped system in comparison to the pure system [9,23]. Substituting Mg^{2+}onto the Cu^{2+} site was done with the aim of introducing disorder without altering the carrier concentration. These interesting results, as well as the calculated theoretical predictions and the relationship between doping and Shastry-Sutherland system, intrigued us to try introducing charge carriers into the system. We were able to grow single crystals of $Sr_{(1-x)}La_xCu_2(BO_3)_2$. Substitution of La^+ ions onto the Sr^{2+} site has the effect of altering the concentration of charge carriers. We thus began a series of investigations on the effect of electron doping and introducing disorder on this model system. In particular, doping may alleviate the frustration, alter the inter-dimer coupling, or affect the localisation of the triplet excitations. [9,23]

Experimental Details

Single crystals of $SrCu_2(BO_3)_2$, $Sr_{(1-x)}La_xCu_2(BO_3)_2$, and $SrCu_{(2-x)}Mg_x(BO_3)_2$ were grown from a self-flux by optical floating zone image furnace techniques in an O_2 atmosphere at a rate of 0.2 mm/hour as reported previously.[24] These crystals were grown with the isotope of ^{11}B to avoid the high neutron absorption cross section of natural boron. The crystals are of almost identical and cylindrical in shape, with approximate dimensions of 0.6 cm in diameter by 10 cm long.

Small pieces of the crystal were used for bulk characterisation and the characteristic falloff of the dc-susceptibility near 10 K was observed. The pure and Mg-doped single crystals were the same high quality single crystals that were studied previously [9,11,23] . The dc-susceptibility measurements performed on these samples using SQUID magneto-meter at McMaster University are shown in Fig 1. The magnetisation measurements as a function of temperature were performed in a field of 1000 Oe applied parallel to the *ab* plane. The sharp falloff in the susceptibility below ~13 K, provides the evidence of the development of the low-temperature spin singlet ground state. The significant feature of the dc-susceptibility observed in $SrCu_{(2-x)}Mg_x(BO_3)_2$ and $Sr_{(1-x)}La_xCu_2(BO_3)_2$ samples in comparison to the pure system, is the Curie-like upturn seen below 4 K due to the paramagnetic Cu^{2+} spins induced by the dopants in the doped samples. Aczel *et al.* analysed the dc-susceptibility data in order to find the concentration of dopants in the system [25]. They fitted the susceptibility data to the following functional form:

$$\chi = \frac{C}{T} + B \cdot e^{-\Delta/T} + \chi_{\circ} \qquad (2)$$

where the first Curie term represents the contributions of magnetic impurities/dopants, the second term accounts for the spin-gap, and the third temperature-independent term is due to Van-Vleck paramagnetism and core diamagnetism. According to the analysis done by Aczel *et al.* and if we assign the Curie term to free Cu^{2+} spins introduced in the system by doping , then the value of the concentration of dopants in Mg-doped sample would be x~0.05 and in La-doped sample would be x~0.04.

High resolution time-of-flight neutron scattering measurements were performed on $SrCu_2(BO_3)_2$, $SrCu_{(2-x)}Mg_x(BO_3)_2$ and $Sr_{(1-x)}La_xCu_2(BO_3)_2$ single crystals using the OSIRIS spectrometer [26] at ISIS Pulsed Neutron Source of the Rutherford Appleton Laboratory. OSIRIS is an indirect geometry time-of-flight spectrometer which employs an array of pyrolytic graphite monochromators to energy analyse the scattered neutron beam. In these experiments the data was collected with the spectrometer configured to use the 004 analysing reflection afforded by pyrolytic graphite. In this configuration only those neutrons with the scattered energy of 7.375 meV are Bragg reflected towards the detector. All three samples were mounted in a 7 T vertical, [0,K,0], field magnet cryostat while the [H,0,L] plane of them was coincident with the horizontal scattering plane.

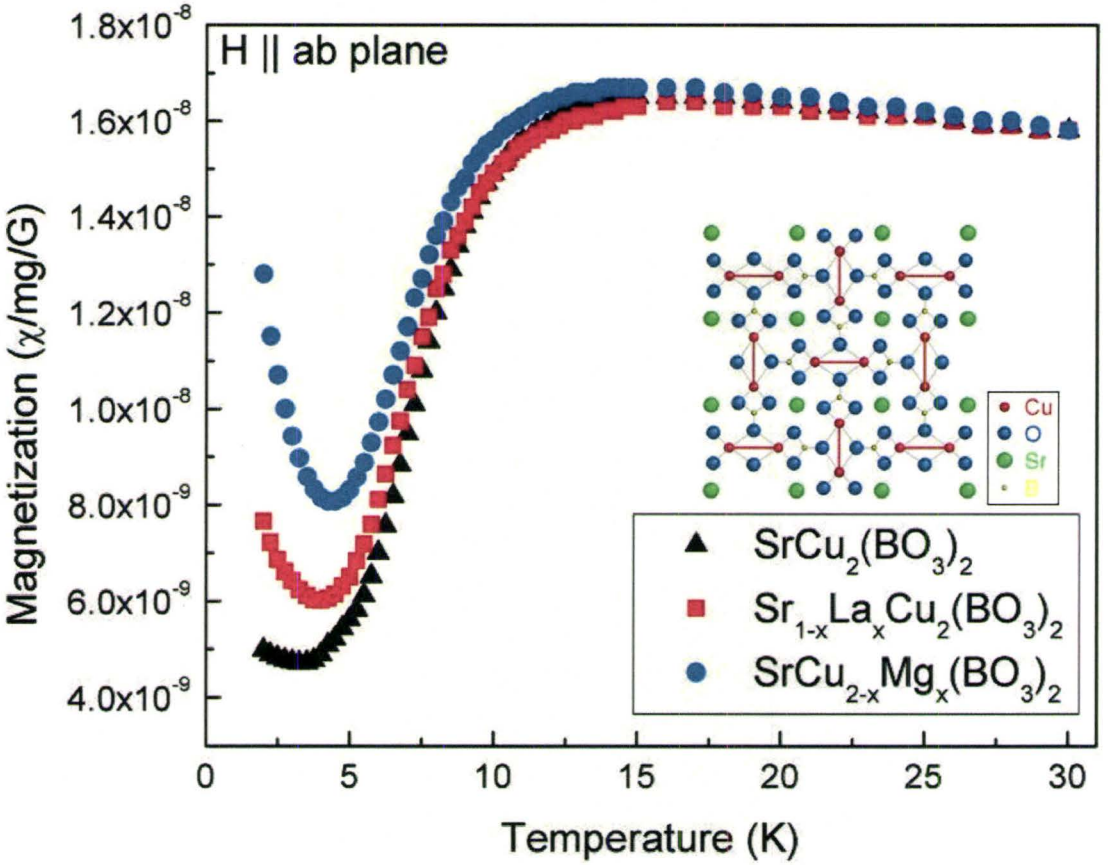

Fig 1: The dc-susceptibility measurements on $SrCu_2(BO_3)_2$, $SrCu_{(2-x)}Mg_x(BO_3)_2$ [x~0.05] and $Sr_{(1-x)}La_xCu_2(BO_3)_2$ [x~0.04] as a function of temperature in an applied magnetic field parallel to the *ab* basal plane (shown in the inset). The sharp falloff in the susceptibility below ~13 K, provides the evidence of the development of the low-temperature spin singlet ground state. The Curie-like upturn seen below 4 K in doped samples is the result of paramagnetic Cu^{2+} spins induced by the dopants in the system.

Inelastic Neutron Scattering Measurements

As was mentioned in the introduction, the relationship between doping in Mott insulators with an energy gap and the possibility of superconductivity has motivated in our part, a series of neutron scattering experiments on $SrCu_2(BO_3)_2$, $SrCu_{(2-x)}Mg_x(BO_3)_2$ and $Sr_{(1-x)}La_xCu_2(BO_3)_2$. As it turns out the single crystal growth of the doped $SrCu_2(BO_3)_2$ has proven very challenging. While there have been some studies on doped polycrystalline systems the only published work on single crystals to date has been that of our group on Mg-doped $SrCu_2(BO_3)_2$.[23] In the case of the Mg-doped system we have substituted Mg^{2+} (non-magnetic) onto the Cu^{2+} (carrying spin ½ and responsible for magnetisation in this system) sites with aim of introducing non-magnetic disorder into the system without altering the carrier concentration. Liu *et al.*[22] studied the doped polycrystalline system wherein La, Na, and Y substituted at the Sr site with the aim of introducing the charge carriers into the system. The published results of these studies, demonstrates that the La-doped samples showed almost two order of magnitude smaller resistivity than samples doped by Al, Na, Y on Sr sites. [22]

Following these results, we performed a series of neutron scattering experiments on single crystals of $SrCu_2(BO_3)_2$, $SrCu_{(2-x)}Mg_x(BO_3)_2$ and $Sr_{(1-x)}La_xCu_2(BO_3)_2$ with the goal of investigating the effect of charge carriers in this system.

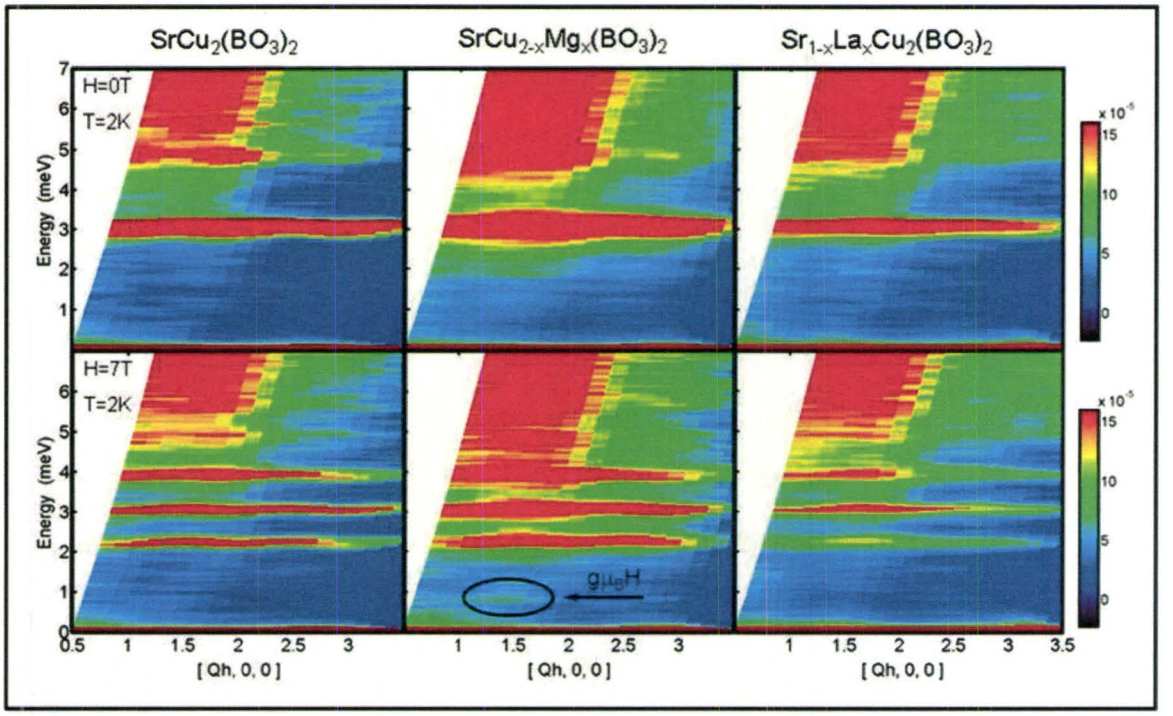

Fig 2: A summary of the time-of-flight neutron scattering data measured with OSIRIS at the ISIS facilities in 0 T and 7 T applied magnetic field for $SrCu_2(BO_3)_2$ (left panel), $SrCu_{(2-x)}Mg_x(BO_3)_2$ x ~ 0.05 (middle panel) and $Sr_{(1-x)}La_xCu_2(BO_3)_2$ x ~ 0.04 (right panel) that are integrated up along L since the spin excitations show little dispersion in that direction. The splitting of the triplet excitations near 3 meV on application of the 7 T magnetic field along (0, K, 0) is clear for all three samples. Application of a magnetic field induces Zeeman-split states in the Mg-doped system ($g\mu_B H$) associated with S=1/2 unpaired spins which is evident in the figure.

Figure 2 shows the representative time-of-flight neutron scattering data, taken at T=2 K and H=0 T and H=7 T for $SrCu_2(BO_3)_2$ (left panel) $SrCu_{(2-x)}Mg_x(BO_3)_2$ x ~ 0.05 (middle panel) and $Sr_{(1-x)}La_xCu_2(BO_3)_2$ x ~ 0.04 (right panel) samples. These results have been integrated along the L direction. Our previous neutron scattering studies on the pure

system revealed that spin excitations have little dispersion along the L direction in this system and therefore the data could be integrated along L.[9]

It is worth mentioning again that these measurements were all done under the same conditions in which the samples were mounted such that the [H, 0, L] plane was coincident with the horizontal scattering plane and while a 7 T magnetic field was applied along the [0, K, 0] direction.

As shown in Fig 2 the splitting of the one triplet excitation into three branches representing S_z = 0, +1 and -1 eigenstates near 3 meV energy transfer in the applied magnetic field of 7 T is clear in all three samples. The weak dispersion observed in finite field as a function of wave vector H in all three samples is due to the subleading terms in the Hamiltonian as was discussed in the introduction.

There are several qualitative features observed in doped samples when compared to the pure system. When comparing $SrCu_{(2-x)}Mg_x(BO_3)_2$ with the pure system, one can see that the one-triplet excitation is significantly broader in energy than what has been observed in the case of $SrCu_2(BO_3)_2$. In addition from Fig 2 one can clearly see that the application of 7T magnetic field gives rise to an inelastic peak at the energy $g\mu_B H$ = 0.8 meV . This field induced peak is attributed to Zeeman-split S=1/2 states associated with the S=1/2 moment in a dimer whose partner site is occupied by the quenched non-magnetic Mg^{2+} ion. These features in the Mg-doped system have been discussed at length in our previous paper [24].

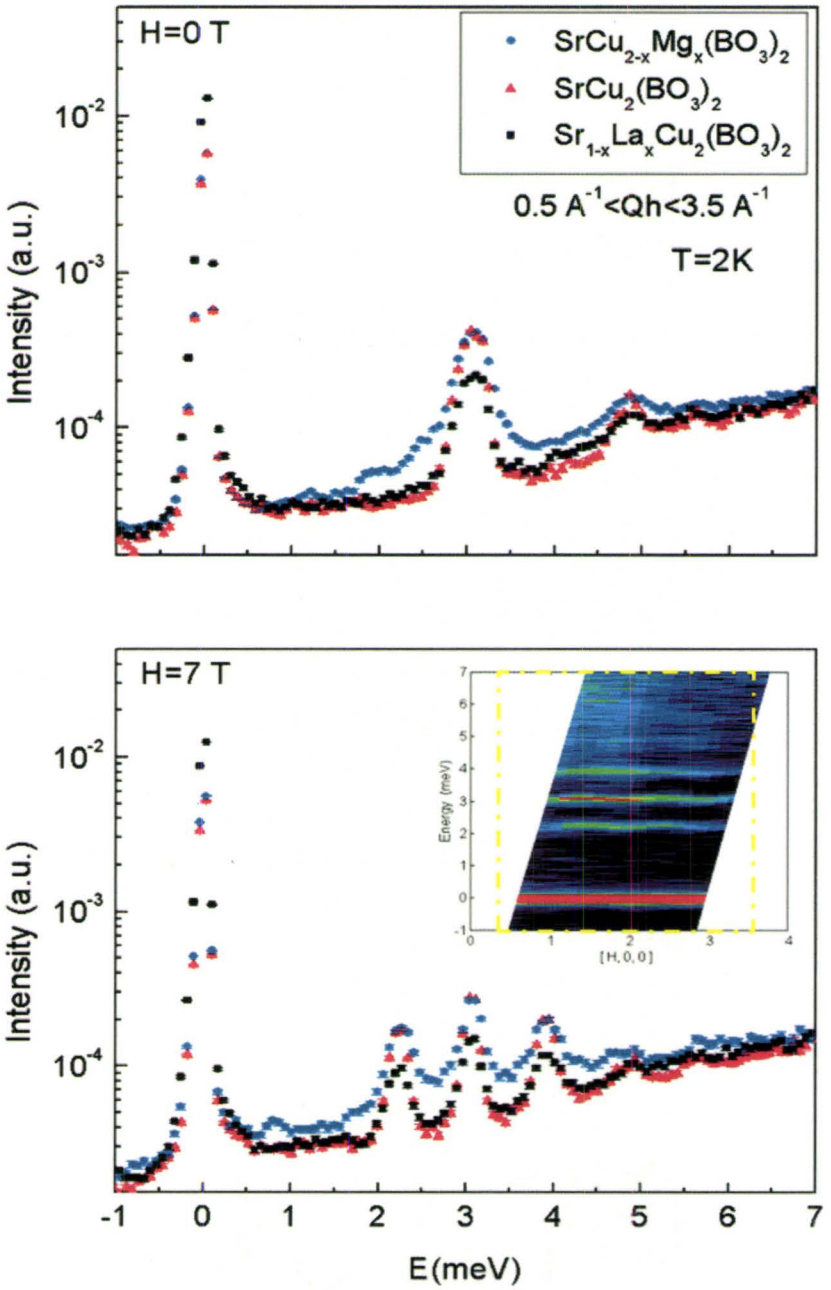

Fig 3: The figure shows subsequent data analysis using scattering integrated up over a wide range in H , from 0.5 to 3.5 , for $SrCu_2(BO_3)_2$, $SrCu_{(2-x)}Mg_x(BO_3)_2$ x ~ 0.05 and $Sr_{(1-x)}La_xCu_2(BO_3)_2$ x ~ 0.04 in 0 T (top) and 7 T (bottom).

The same experimental data shown in Fig 2 that was already integrated in the L direction was integrated along the H direction between H= 0.5 rlu and H=3.5 rlu and plotted as a function of energy in Fig 3. The data in a magnetic field of 0T and 7T is shown in Fig 3a and 3b, respectively. In all three samples the splitting of the single triplet excitation into three branches representing S_z = 0, +1 and –1 in finite applied filed is obvious. The extra breadth in the $SrCu_{(2-x)}Mg_x(BO_3)_2$ sample in comparison to the pure system for both the single triplet excitation and the two triplet bound state is clear.

As shown in Fig 2 and Fig 3, the main features seen in the $Sr_{(1-x)}La_xCu_2(BO_3)_2$ data in comparison to the $SrCu_2(BO_3)_2$ and $SrCu_{(2-x)}Mg_x(BO_3)_2$ data is the lower excitation intensity and the higher incoherent quasi-elastic scattering intensity at zero energy transfer. Further analysis shows that similar to the Mg-doped system, the La-doped system has rather broader one triplet excitation peaks in comparison to the pure system. A broadening of the excitation peak in the La-doped system in comparison to pure system was also observed.

Additionally the excitation width in the La-doped sample demonstrates a different behaviour as a function of temperature when compared to either the Mg-doped or pure system.

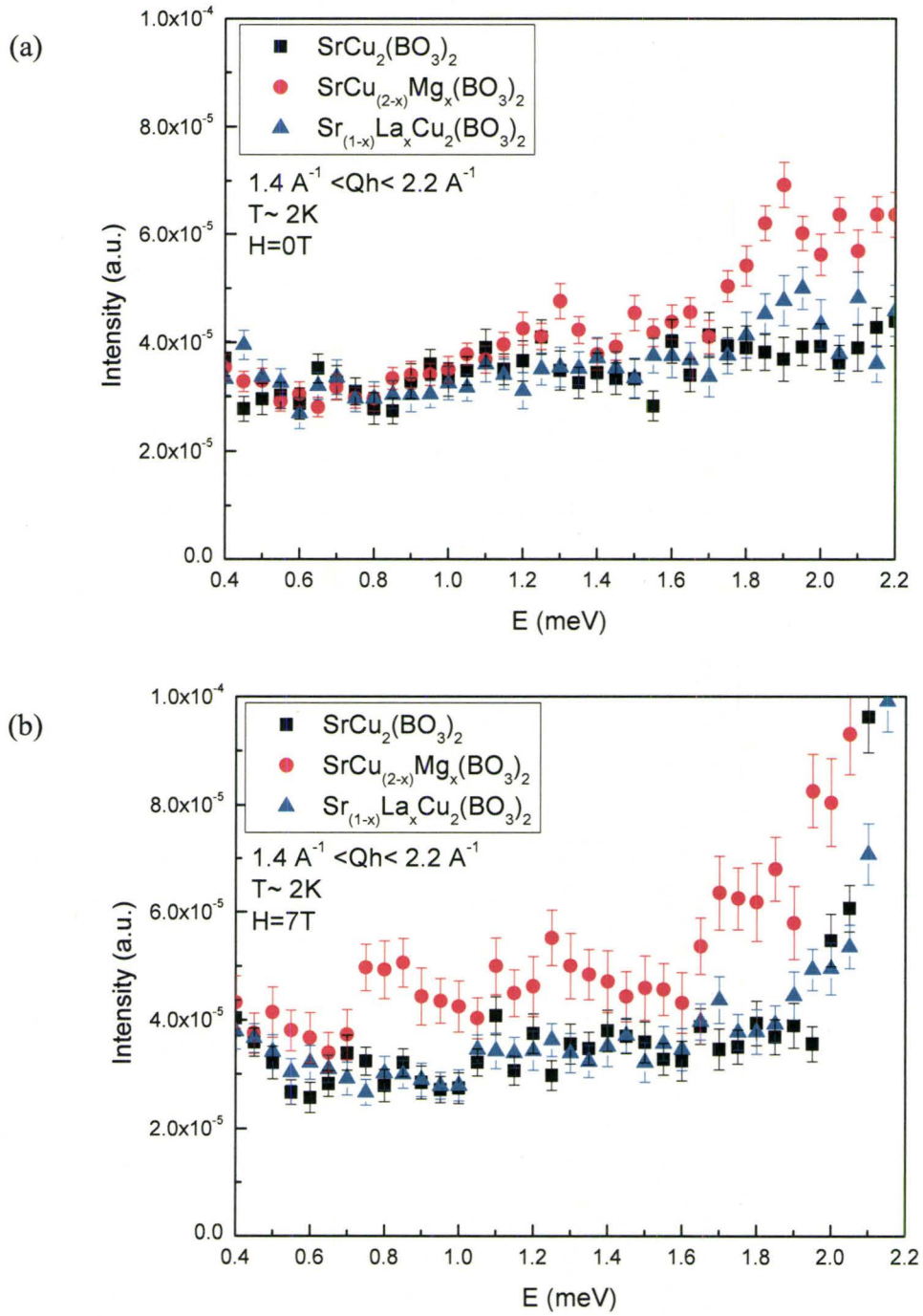

Fig 4: The scattering data integrated up in the H direction which clearly shows additional spectral magnetic weight within the singlet-triplet energy gap for the $SrCu_{(2-x)}Mg_x(BO_3)_2$ in 0 T (a) and 7 T (b) and some additional spectral weight for the $Sr_{(1-x)}La_xCu_2(BO_3)_2$ at zero magnetic field.

Figure 4 clearly shows broad inelastic feature which appears within the gap for $SrCu_{(2-x)}Mg_x(BO_3)_2$ in comparison to the pure system. These features possess little magnetic field dependence indicating a longitudinal nature. Additionally sharp, field-induced inelastic scattering peak due to the Zeeman-split of the free spin (S = ½) at E ~ 0.8 meV is also evident at 7 T. In the case of $Sr_{(1-x)}La_xCu_2(BO_3)_2$ data, it is harder to reliably identify any in-gap states. As shown in Fig 4 one could argue that there is some extra spectral weight at energies within the gap. This could be due to the fact that there might be dispersive excitations within the gap so it is possible that they are washed out by integrating over some range of wavevectors, especially if they are weak. Therefore further experiments would be required in order to reach a definite characteristic of a gap state in the Sr-doped system. It would also be helpful to have more theoretical studies done relevant to the doped system in order to help identify any possible in-gap states.

Figure 5 shows the comparison between the incoherent quasi-elastic scattering for $SrCu_2(BO_3)_2$, $SrCu_{(2-x)}Mg_x(BO_3)_2$ and $Sr_{(1-x)}La_xCu_2(BO_3)_2$. This data is integrated over all L and in the H direction between H= 1.4 rlu and H=2.2 rlu. As it is obvious from the Fig. 5, the intensity of the quasi-elastic incoherent peak at zero energy transfer for La-doped sample is almost twice the intensity of the quasi-elastic incoherent peaks of the either pure or Mg-doped samples. An interesting point is that the main factor determining the intensity of the quasi-elastic incoherent scattering is the volume of sample and ironically in this case while all three sets of data have been normalised to the same experimental conditions, the volume of the La-doped sample was about 75% of the size of either the pure or Mg-doped samples. This makes the comparison between the La-doped and the

pure systems even more pronounced and could be an indication that there is a possibility of magnetic scattering near zero energy transfer that is contributing to this higher intensity of the incoherent quasi-elastic peak in La-doped system given that the La-doped sample was even smaller than the pure and Mg-doped samples.

Figure 6 shows representative cuts of the data with the accompanying resolution convoluted fits which were used to extract the lifetime of the one-triplet excitation as a function of doping and temperature in 7 T applied magnetic field. These cuts simulate constant-**Q** scans. That is, these data are integrated in **Q** along all possible L and over a narrow range in wavevector H around H=2. Similar analysis was performed around wave vectors H=1.5 and H=2.5 to investigate the variation of the one-triplet excitation as a function of **Q** along [H, 0, 0] in the pure and doped systems.

The data shown in Fig 6 were fit to the three identical damped harmonic oscillators (DHOs):

$$S(\mathbf{Q},\omega,T) = \chi(\mathbf{Q},T)\frac{1}{1-exp\left(-\frac{\omega}{kT}\right)} \times \left[\frac{4\omega\Gamma_{\mathbf{Q},T}/\pi}{\left(\omega^2-\Omega^2_{\mathbf{Q},T}\right)^2+4\omega^2\Gamma^2_{\mathbf{Q},T}}\right] \qquad (3)$$

where $\chi(\mathbf{Q}, T)$ is the momentum-dependent susceptibility. The renormalized DHO frequency, $\Omega_{\mathbf{Q}}$, has contributions from the oscillation frequency, $\omega_{\mathbf{Q},T}$, and the damping coefficient, $\Gamma_{\mathbf{Q},T}$, and is given by $\Omega^2_{\mathbf{Q},T} = \omega^2_{\mathbf{Q},T} + \Gamma^2_{\mathbf{Q},T}$.

(a)

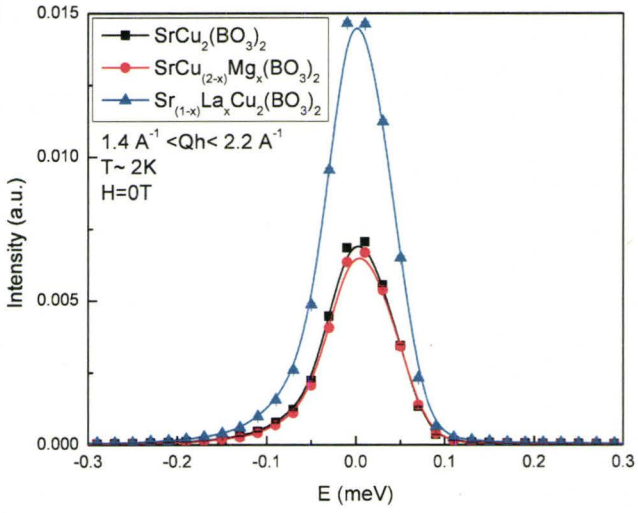

(b)

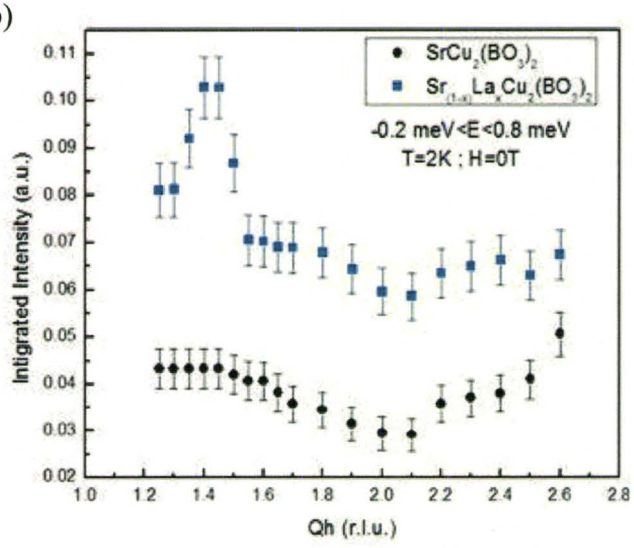

Fig 5: (a) Comparison of the incoherent quasi-elastic peak around zero energy transfer for $SrCu_2(BO_3)_2$, $SrCu_{(2-x)}Mg_x(BO_3)_2$ and $Sr_{(1-x)}La_x\ Cu_2\ (BO_3)_2$. It was observed that the quasi-elastic scattering in $Sr_{(1-x)}La_xCu_2(BO_3)_2$ is larger than that in either $SrCu_2(BO_3)_2$ or $SrCu_{(2-x)}Mg_x(BO_3)_2$ (even though the La-doped sample was smaller than the pure and Mg-doped samples), and in contrast the one-triplet scattering is weaker. This could indicate that there is magnetic scattering contribution at energies near zero causing the higher intensity in the incoherent quasi-elastic peak.(b) Q-dependence of the integrated intensity of the incoherent quasi-elastic peak at zero energy transfer. It is shown that the incoherent quasi-elastic intensity peaks up at Qh ~ 1.4 $Å^{-1}$ for the La-doped sample in comparison to the pure sample.

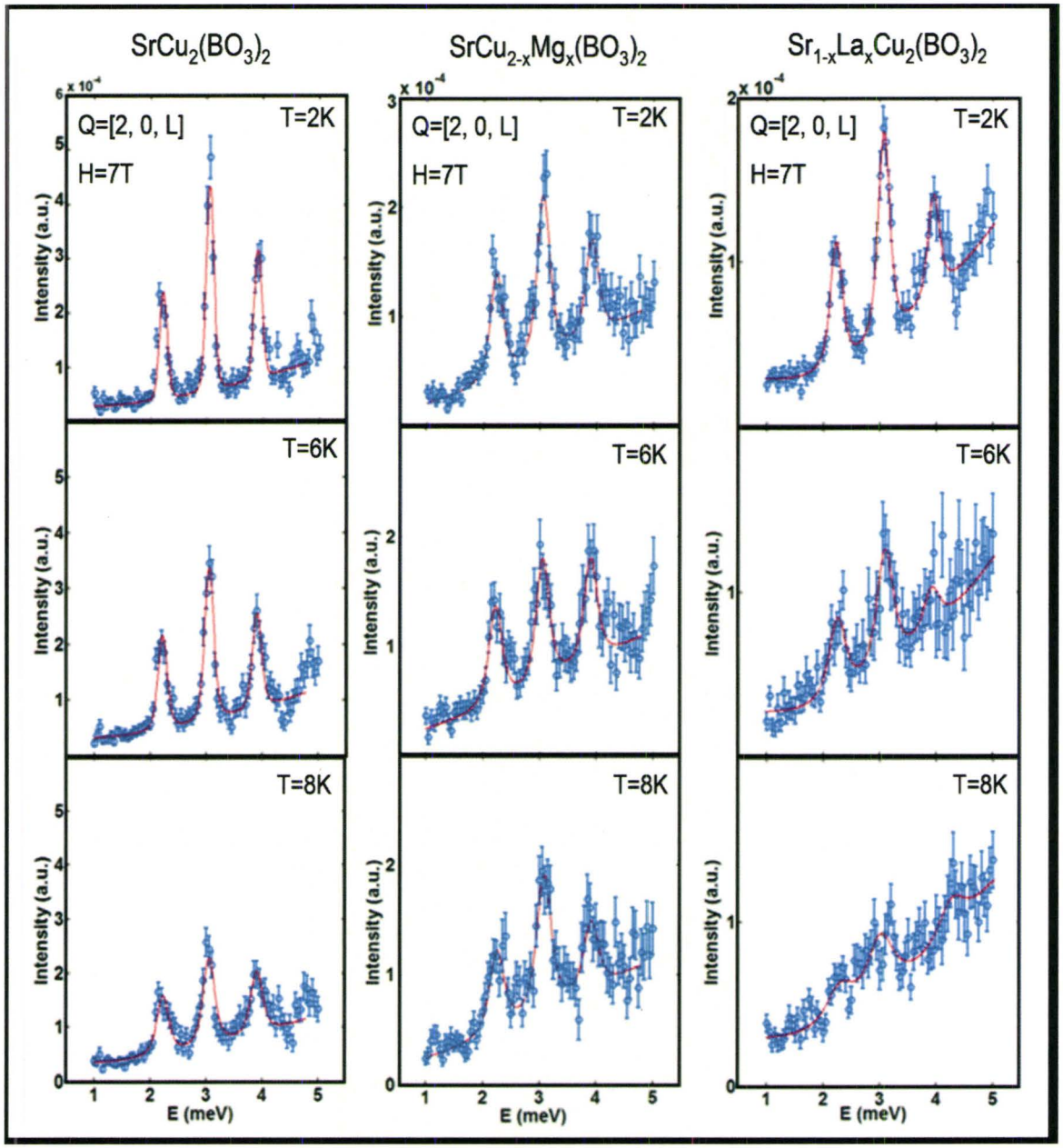

Fig 6: Representative cuts of the data simulating constant-**Q** scans at (2, 0) and integrating along L are shown for $SrCu_2(BO_3)_2$, $SrCu_{(2-x)}Mg_x(BO_3)_2$ and $Sr_{(1-x)}La_xCu_2(BO_3)_2$ samples as a function of temperature. Resolution convoluted fits to data (shown as solid lines) were performed using a Damped Harmonic Oscillator model.

Equation (3) was convoluted with an appropriate resolution function and fit to the data. The fits shown in Fig 6 are good descriptions of the data. Figures 6 (a), (b) and (c) show the constant-**Q** scans at (2, 0), integrating along L, for the pure, the Mg-doped and the La-doped data, respectively. The main feature observed in Fig 6 is a difference between the temperature dependence of the one-triplet excitation in La-doped sample in comparison to the pure and Mg-doped data. We analysed these data further in order to investigate the effect of doping on the lifetime of the excitations for the singlet-triplet excitation as well as the temperature dependence of it. The results of the resolution convoluted fits are shown in Fig 7. The figure shows the extracted widths of the triplet-excitation, Γ, as a function of temperature for wave vectors H=1.5, 2.0 and 2.5, respectively. The results show that the extracted width of the one-triplet excitation, which is inversely proportional to the lifetime of the triplet excitation, has little or no systematic variation with wave-vector H. However, a finite one-triplet lifetime is observed in both $SrCu_{(2-x)}Mg_x(BO_3)_2$ and $Sr_{(1-x)}La_xCu_2(BO_3)_2$ at all temperatures in contrast to $SrCu_2(BO_3)_2$, where the low temperature one-triplet lifetimes are very long compared with the resolution of the spectrometer.

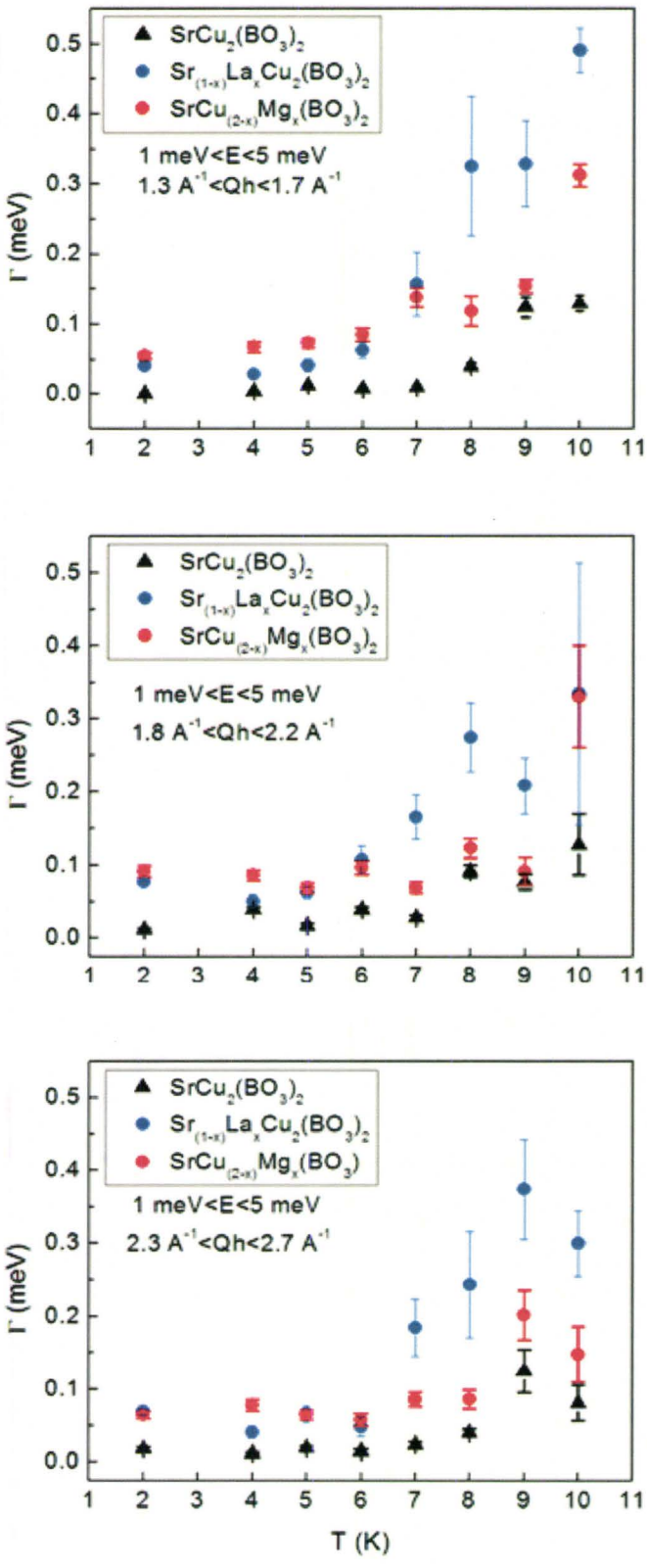

Fig 7: The one triplet energy widths as a function of temperature for the wave-vectors (1.5,0), (2,0) and (2.5,0) within the Shastry - Sutherland plane and integrated in L for $SrCu_2(BO_3)_2$, $SrCu_{(2-x)}Mg_x(BO_3)_2$ and $Sr_{(1-x)}La_xCu_2(BO_3)_2$. Even at the lowest temperature we observe finite triplet lifetimes in the doped systems. We also observed that the one-triplet excitation lifetime in the La-doped system becomes shorter at temperatures above 7K.

The main feature observed in these neutron scattering results was that the temperature dependence of the lifetime excitation in the La-doped sample displays different thermal behavior when compared to the pure and Mg-doped systems. As it is shown in Fig 7, while the rapid decrease in the lifetime of the one triplet excitation on warming is observed at temperatures ~ 10 K for $SrCu_2(BO_3)_2$ and $SrCu_{(2-x)}Mg_x(BO_3)_2$ but in case of $Sr_{(1-x)}La_xCu_2(BO_3)_2$ this rapid decrease in the lifetime of the one triplet excitation happens at lower temperatures ~ 7 K. This appears to be the main influence of the La in the system. Further studies and theoretical work is required in order to fully understand this feature as well as the effect of the La-doping in the system. Probably this would be easier by having a successful growth of the higher concentrations of La in the system.

Conclusion

We successfully grew single crystals of $SrCu_2(BO_3)_2$, $SrCu_{(2-x)}Mg_x(BO_3)_2$ and $Sr_{(1-x)}La_xCu_2(BO_3)_2$ using optical floating zone techniques. Neutron scattering measurements were performed on the pure, Mg-doped and La-doped samples under same experimental conditions. The one-triplet excitation spectrum in all materials were modeled on the basis of Damped Harmonic Oscillator model. The results of these fits revealed the finite measurable lifetime for the doped samples at low temperatures when compared to the long lifetime of the one-triplet excitation in the pure system.

The main feature observed from these neutron scattering results was a different behaviour of the lifetime of the excitation in the La-doped sample as a function of temperature in comparison to the pure and the Mg-doped samples. In the La-doped sample the lifetime of the one-triplet excitation decreases rapidly at ~ 7 K.

Although the volume of the La-doped sample was smaller than the volume of the pure and Mg-doped samples, these neutron scattering data revealed that the incoherent quasi-elastic scattering in $Sr_{(1-x)}La_xCu_2(BO_3)_2$ was substantially stronger compared to $SrCu_2(BO_3)_2$ and $SrCu_{(2-x)}Mg_x(BO_3)_2$ systems, while the one triplet excitation peak was weaker. This could indicate that there are magnetic scattering contributions at energies near zero energy transfer in the La-doped system that could be reflected in the stronger incoherent quasi-elastic scattering.

Acknowledgments

We wish to acknowledge expert technical support from the ISIS User Group, as well as from CNBC Chalk River. This work was supported by NSERC of Canada.

References

[1] see, for example: E. Dagotto and T.M. Rice, Science, **271**, 618 (1996); *Dynamical Properties of Unconventional Magnetic Systems*, edited by A.T. Skjeltorp and D. Sherrington, NATO ASI Series, Series E, Applied Sciences, **349** (Kluwer Academic Publishers, Boston, 1998).

[2] R.W. Smith and D.A. Keszler, J. Solid State Chem., **93**, 430 (1991).

[3] B.S. Shastry and B. Sutherland, Physica B&C, **108B**, 1069 (1981).

[4] S. Miyahara and K. Ueda, Phys. Rev. Lett., **82**, 3701 (1999).

[5] H. Kageyama, K. Yoshimura, R. Stern, N. Mushnikov, K. Onizuka, M. Kato, K. Kosuge, C. Slichter, T. Goto and Y. Ueda, Phys. Rev. Lett., **82**, 3168 (1999).

[6] Z. Weihong, C.J. Hamer, and J. Oitmaa, Phys. Rev. B, **60**, 6608 (1999).

[7] H. Kageyama, M. Nishi, N. Aso, K. Onizuka, T. Yosihama, K. Nukui, K. Kodama, K. Kakurai and Y. Ueda, Phys. Rev. Lett., **84**, 5876 (2000).

[8] O. Cépas, K. Kakurai, L.P. Regnault, J.P.B.T. Ziman, N. Aso, M. Nishi, H. Kageyama and Y. Ueda, Phys. Rev. Lett., **87**, 167205 (2001).

[9] B.D. Gaulin, S.H. Lee, S. Haravifard, J.P. Castellan, A.J. Berlinsky, H.A. Dabkowska, Y. Qiu and J.R.D. Copley, Phys. Rev. Lett., **93**, 267202 (2004).

[10] A. Zorko, D. Arčon, H. van Tol, L.C. Brunel, and H. Kageyama, Phys. Rev. B, **69**, 174420 (2004).

[11] H. Nojiri, H. Kageyama, Y. Ueda, and M. Motokawa, J. Phys. Soc. Jap., **72**, 3243 (2003).

[12] M. Miyahara and K. Ueda, J. Phys. Condens. Matter, **15**, R327 (2003).

[13] K. Kakurai, in *Quantum Properties of Low Dimensional Antiferromagnets*, edited by A. Ajiro and J.P. Boucher (Kyushu University Press, Fukuoka 2002).

[14] S. El Shawish, J. Bonča, and I. Sega, Phys. Rev. B, **72**, 184409 (2005).

[15] K. Kodama, M. Takigawa, M. Horvatić, C. Berthier, H. Kageyama, Y.Ueda, S. Miyahara, F. Becca and F. Mila, Science, **298**, 395 (2002).

[16] K. Onizuka, H. Kageyama, Y. Narumi, K. Kindo, Y. Ueda and T. Goto, J. Phys. Soc. Jap., **69**, 1016 (2000).

[17] G.A. Jorge, R. Stren, M. Jaime, N. Harrison, J. Bonča, S. El Shawish, C.D. Baista, D.A. Dabkowska, and B.D. Gaulin, Phys. Rev. B, **71**, 092403 (2005).

[18] B.S. Shastry and B. Kumar, Prog. Theor. Phys. Suppl. **145**, 1 (2002).

[19] S.E. Sebastian, N. Harrison, P. Sengupta, C.D. Batista, S. Francoual, E. Palm, T. Murphy, N. Marcano, H.A. Dabkowska, and B.D. Gaulin, PNAS **105**, 20157 (2008).

[20] T. Kimura, K. Kuroki, R. Arita, and H. Aoki, Phys. Rev. B, **69**, 054501 (2004).

[21] C-H. Chung and Y.B. Kim, Phys. Rev. Lett., **93**, 207004 (2004).

[22] G.T. Liu, J.L. Luo, N.L. Wang, X.N. Jing, D. Jin, T. Xiang and Z.H. Wu., Phys. Rev. B, **71**, 014441 (2005).

[23] S. Haravifard, S.R. Dunsiger, S. El Shawish, B.D. Gaulin, H.A. Dabkowska, M.T.F. Telling, T.G. Perring and J. Bonča, Phys. Rev. Lett., **97**, 247206 (2006).

[24] H.A. Dabkowska, A.B. Dabkowski, G.M. Luke, S.R. Dunsiger, S. Haravifard, M. Cecchinel and B.D. Gaulin, J. Cryst. Growth, **306**, 123, (2007).

[25] A.A. Aczel, G.J. MacDougall, J.A. Rodriguez, G.M. Luke, P.L. Russo, A.T. Savici, Y.J. Uemura, H.A. Dabkowska, C.R. Wiebe, J.A. Janik and H. Kageyama, Phys. Rev. B, **76**, 214427 (2007).

[26] M.T.F. Telling and K.H. Andersen, Phys. Chem. Chem. Phys., **7**, 1255 (2005).

Chapter 6

Neutron Scattering from the Static and Dynamic Lattice of $SrCu_2(BO_3)_2$

Recently there has been increased interest in the study of the crystalline structure and vibrational modes of $SrCu_2(BO_3)_2$. Recent infrared spectroscopy measurements with polarized light on $SrCu_2(BO_3)_2$ have shown an optic phonon excitation in the *a-b* plane whose temperature dependence indicates possible significant spin-lattice coupling within the singlet ground state of $SrCu_2(BO_3)_2$. We performed a series of inelastic neutron scattering measurements to study both the crystalline structure as well as the normal modes of the vibration of the lattice, acoustic and optical phonons, in $SrCu_2(BO_3)_2$, in order to investigate the role of the lattice in the formation of its singlet ground state. The results will be submitted for publication to Physical Review B.

Neutron Scattering from the Static and Dynamic Lattice of $SrCu_2(BO_3)_2$ in its Shastry-Sutherland Singlet Ground State

S. Haravifard,[1] B.D. Gaulin,[1,2] Z. Yamani,[3] T.G. Perring,[4] S.R. Dunsiger,[1] H.A. Dabkowska,[1]

[1]*Department of Physics and Astronomy, McMaster University, Hamilton, Ontario, L8S 4M1, Canada*

[2]*Canadian Institute for Advanced Research, 180 Dundas St. W., Toronto, Ontario, M5G 1Z8, Canada*

[3]*Canadian Neutron Beam Centre, NRC, Chalk River Laboratories, Chalk River, Ontario, K0J 1J0, Canada*

[4]*Rutherford Appleton Laboratory, ISIS Pulsed Neutron Facility, Chilton, Didcot, Oxon, OX110QX, UK*

ABSTRACT

Elastic and inelastic neutron scattering results show that $SrCu_2(BO_3)_2$ enters its low temperature singlet ground state below 10 K without an obvious accompanying structural phase transition, despite what had been suggested to explain earlier heat capacity measurements. However, evidence for significant spin-phonon coupling is evident in the energy widths, and the corresponding lifetimes, of transverse acoustic phonons propagating in the (H00) direction of the Shastry-Sutherland plane. Transverse acoustic phonons with energies comparable to and higher than the onset of the two-triplet continuum show substantially increased lifetimes on entering the singlet ground state below ~ 10 K. This is qualitatively consistent with the removal of a decay channel for the phonons due to the gapping of the spin excitation spectrum in $SrCu_2(BO_3)_2$ at low temperatures. High energy inelastic scattering observes broadening of optic phonons in the ~ 52 to 65 meV region on entering the low temperature singlet ground state.

I. INTRODUCTION

The novelty of the ground states of quasi-two dimensional quantum magnets displaying collective singlet or spin gap behavior and the relation of these materials to high temperature superconductivity in the copper oxides have been cause for great interest[1]. There are, however, relatively few examples of such materials, and the

difficulties in crystal growth have further added to the challenges for the study of these systems.

$SrCu_2(BO_3)_2$ as a realization of the two dimensional Shastry-Sutherland model[2] for interacting S=1/2 dimers[3,4] has been well studied and has been shown to possess a non-magnetic ground state. $SrCu_2(BO_3)_2$ is comprised of well separated layers of Cu^{2+}, S=1/2 orthogonal dimers on a square lattice and crystallizes into the tetragonal space group I42*m* with lattice parameters a= 8.995 Å, c= 6.649 Å at room temperature[5].

Earlier neutron[6-9] and ESR spectroscopy[10,11] studies have established the leading terms in $SrCu_2(BO_3)_2$ microscopic Hamiltonian as:

$$\mathcal{H} = J\sum_{nn} \mathbf{S_i}\cdot\mathbf{S_j} + J'\sum_{nnn} \mathbf{S_i}\cdot\mathbf{S_j} \qquad (1)$$

where J and J' are the exchange interactions within the dimers and between S=1/2 spins on neighboring dimers, respectively. Both the exchange interactions J and J' are antiferromagnetic. It has been shown that subleading Dzyaloshinskii-Moriya interactions weakly split the three one-triplet modes excited out of the singlet ground states, even at zero applied magnetic field[7-9,12].

Theoretically, a small enough value for the ratio of $x= J'/J$ would mean that such a quantum magnet possesses a singlet ground state[13]. The ratio, x, has been estimated to be between 0.68 and 0.60, which place $SrCu_2(BO_3)_2$ on the low side of the critical value of x at which a quantum phase transition occurs between a four sublattice Neel state and a collective singlet state at low x.

In finite magnetic field, much interest has focused on a finite magnetization which develops at high enough fields, wherein the lowest energy of the three triplet states has been driven to zero energy. [4,14-17]

The study of this material has been mostly focused on the magnetic properties of this system. However, recently there has been increasing interest in the possible role of the spin-lattice effects in $SrCu_2(BO_3)_2$. It has been suggested that there is a relation between the spin-lattice interaction in $SrCu_2(BO_3)_2$ and its magnetic dynamics at low temperatures and high magnetic fields.[3] Such a strong interplay between crystal and magnetic properties is well known and a characteristic aspect of low dimensional spin systems, especially quasi-one-dimensional spin Peierls systems. In $SrCu_2(BO_3)_2$ a lattice distortion has been suggested to stabilize the spin superstructure associated with the 1/8 magnetization plateau, for example, the first observation of such a magnetization plateau in a quasi 2D material.[1,5] In general, lattice distortions in $SrCu_2(BO_3)_2$ have the potential to allow magnetic interactions which are otherwise forbidden in a more symmetric environment by lowering the crystal symmetry.[7] For example, buckling of the $CuBO_3$ planes allows certain components of Dzyaloshinskii-Moriya interactions to be non-zero. As previously mentioned, these subleading Dzyaloshinskii-Moriya interactions weakly split the three triplet modes even in zero applied magnetic field.[7-9] For these and related reasons a careful study of the crystalline structure and vibrational modes of $SrCu_2(BO_3)_2$ is of interest. Recent infrared spectroscopy measurements with polarized light on $SrCu_2(BO_3)_2$ have revealed an optic phonon excitation in the *a-b* plane at ~ 55meV which splits below 15 K [10,11] This indicates that significant spin-lattice coupling may be

manifest within the singlet ground state of $SrCu_2(BO_3)_2$.[10,11] These results motivated us to use inelastic neutron scattering techniques to study both the crystal structure as well as the normal modes of vibration of this structure, acoustic and optical phonons, in a single crystal of $SrCu_2(BO_3)_2$ as the sample was cooled from a paramagnetic state into its singlet ground state below ~ 10 K.

II. EXPERIMENTAL DETAILS

The $SrCu_2(^{11}BO_3)_2$ single crystal studied was the same high quality single crystal employed in the previous magnetic neutron scattering experiments.[9] It was grown by floating zone image furnace techniques at a rate of 0.2 mm/hour in flowing O_2. The crystal was approximately cylindrical in shape, with approximate dimensions of 4.5 cm in length by 0.6 cm in diameter. The sample was grown using ^{11}B, to avoid the high neutron absorption cross section of natural boron. Powder neutron diffraction measurements were performed on a fine powder sample of $SrCu_2(^{11}BO_3)_2$ using 2.37 Å and 1.3 Å neutrons at the C2 diffractrometer of the Canadian Neutron Beam Laboratory (CNBC), Chalk River Laboratories. The sample (4.5 cm in length and 0.6 cm in diameter) was loaded in an Al sample cell in the presence of a He exchange gas and mounted in a pumped ^4He cryostat. Measurements were preformed as a function of temperature from 3 K to 20 K. Relatively high and low resolution measurements were performed over the range of scattering angles using neutrons of wavelength λ = 2.37 Å and λ = 1.3 Å, respectively. Low energy

inelastic neutron scattering measurements were performed on the single crystal of $SrCu_2(^{11}BO_3)_2$ using the C5 triple axis spectrometer at CNBC, Chalk River. The crystal was mounted in a He cryostat with its (H,K,0) plane coincident with the horizontal plane, such that wave-vectors near the **Q** = (4,0,0) zone centre could be accessed. These measurements employed pyrolitic graphite (PG) as both monochromator and analyser crystals, and used a fixed final neutron energy of 14.7 meV. A PG filter was placed in the scattered beam to reduce higher order contamination. High energy time-of-flight neutron scattering measurements were performed using the MAPS spectrometer at the ISIS Pulsed Neutron Source of the Rutherford Appleton Laboratory. MAPS is a direct geometry time-of-flight spectrometer with a 6m sample-to-detector distance, affording relatively high energy resolution at high energy transfers. The same single crystal sample of $SrCu_2(^{11}BO_3)_2$ was employed in these measurements as had been employed at Chalk River, again with the [H,K,0] plane of crystal coincident with the horizontal plane.

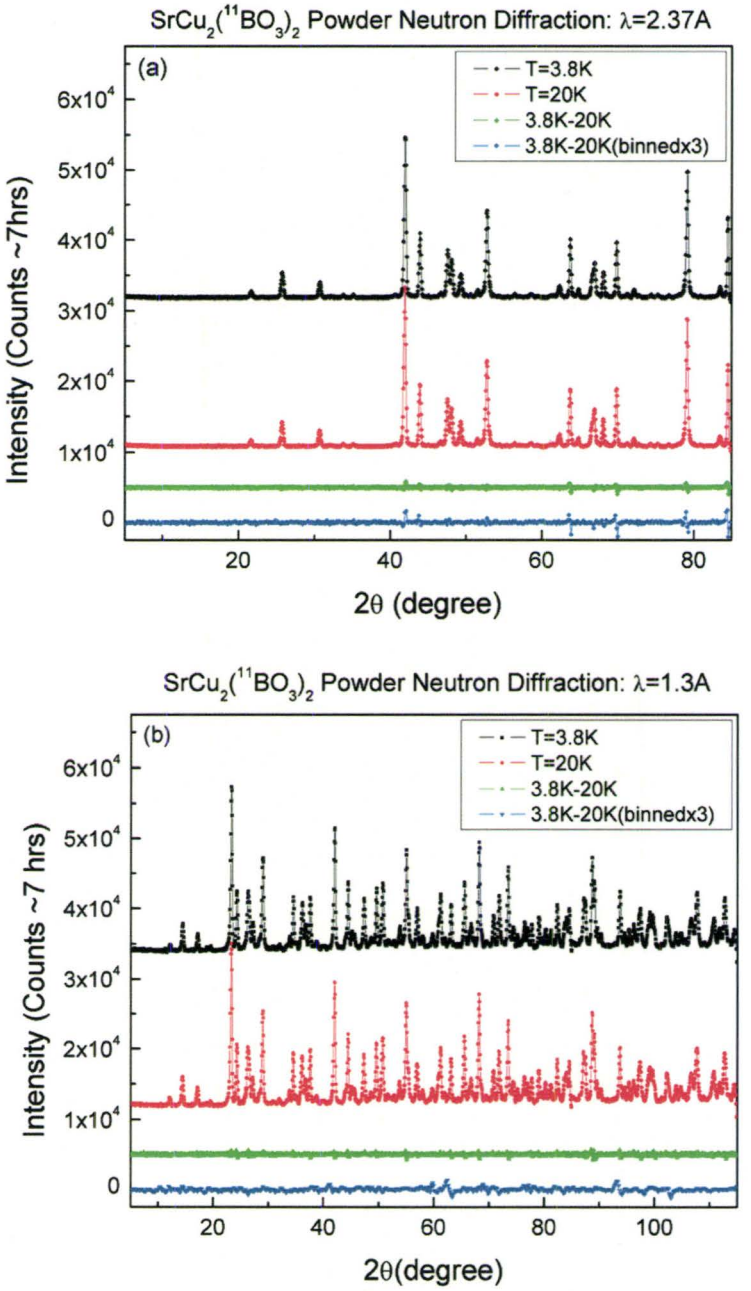

FIG. 1: Powder neutron diffraction from $SrCu_2(BO_3)_2$ taken at T=3.8 K and T=20 K is shown using neutrons of wavelength λ =2.37 Å (top) and λ =1.3 Å (bottom). Also plotted in both panels is the subtracted data sets from the two temperatures which show no evidence for a structural distortion on cooling $SrCu_2(BO_3)_2$ into the singlet ground state below ~ 10 K.

III. POWDER NEUTRON DIFFRACTION MEASUREMENTS

$SrCu_2(BO_3)_2$ displays a tetragonal crystal structure characterized by stackings of $CuBO_3$ and Sr planes along the c-direction [5,18,19]. Within the $CuBO_3$ layer, BO_3 molecules form a triangle and the Cu^{2+} ions are connected through the BO_3 molecules. All the Cu^{2+} ions are located at crystallographically equivalent sites and have a spin S = 1/2 magnetic moment associated with them. Each Cu^{2+} ion has one nearest-neighbour Cu^{2+} ion and four next-nearest-neighbour Cu^{2+} ions in the plane. A pair of nearest-neighbour Cu^{2+} ions are connected through O sites, which are vertices of BO_3 triangles, and form a dimer unit. The dimer units are connected orthogonally through BO_3 molecules. The distance between the nearest-neighbour Cu^{2+} ions is 2.905 Å, and that between the next nearest-neighbour Cu^{2+} ions is 5.132 Å at room temperature. Sparta *et al.* were the first to report that a structural phase transition occurs in $SrCu_2(BO_3)_2$ at T_s = 395 K, from the space group I 4 2 to I 4/m cm (both tetragonal) by X-ray diffraction [19]. Below T_s there is a buckling in the $CuBO_3$ plane, while above T_s the dimers within a unit cell lie in the same plane and there is no buckling, making the $CuBO_3$ plane a mirror plane. The existence of a mirror plane is important for possible Dzyaloshinsky-Moriya interactions. Above T_s, the DM interactions may exist only for the next-nearest neighbor pairs and do not exist for the nearest-neighbor pairs, since the middle of a nearest-neighbor bond possesses an inversion centre. However, below T_s, the mirror plane is lost; therefore, Dzyaloshinsky-Moriya interactions can exist for both next-nearest-neighbor pairs and nearest-neighbor pairs.

Jorge *et al.* performed specific heat measurements on $SrCu_2(BO_3)_2$ in a continuous magnetic field H up to 33T.[16] They argued that an intra-dimer Dzyaloshinsky-Moriya (DM) interaction, which violates the observed crystal symmetry at temperatures below T_s = 395K is required to explain the low temperature specific heat of $SrCu_2(BO_3)_2$ in magnetic fields H ~ 18T. [7,11] The components of the *nn* DM interaction are constrained by the crystal symmetry [7,19]. Jorge *et al.* proposed a possible structural phase transition at low temperatures that lowers the crystal symmetry allowing a non-zero value for the z-component of the nearest neighbor DM interaction [16]. The crystal symmetry of the system affects the Dzyaloshinsky-Moriya interactions and consequently may modify the thermal and magnetic properties of the material. The proper inclusion of such small, subleading terms in the spin Hamiltonian would allow, in principle, for an improved theoretical understanding of $SrCu_2(BO_3)_2$ and better accounting for the experimental results.

Motivated by the arguments made by Jorge *et al.*, neutron diffraction measurements were performed in order to investigate any possible structural phase transition in $SrCu_2(BO_3)_2$ at low temperatures. Figure 1 shows the results of the neutron diffraction measurements performed on $SrCu_2(BO_3)_2$. Figure 1(a) shows the results for λ = 1.3Å at 3.8K and 20K temperatures while Fig. 1(b) shows the results for λ = 2.37Å at 3.8K and 20K temperatures. In both figures, black squares and red circles represent the data collected at 3.8K and 20K, respectively. The difference between the measurements at these two temperatures was calculated and the green upward triangles represent the subtracted values. The blue downward triangles show the subtracted values binned to help visualize any weak variation between the two data sets well within and well above

the singlet ground state. No such temperature dependent behavior is observed, implying that any possible structural phase transition involves changes in Bragg intensity at the 1 part in 10^3 level or lower.

IV. NEUTRON SCATTERING MEASUREMENTS OF ACOUSTIC PHONONS

Measurements of the spectrum of transverse and longitudinal acoustic phonons propagating in the (H00) direction of $SrCu_2(BO_3)_2$ were performed using triple axis neutron spectrometry and the C5 spectrometer at the CNBC, Chalk River. Constant-**Q** measurements were performed along (4,K,0) to preferentially measure transverse acoustic phonons, and along (4+H, 0, 0) to preferentially measure longitudinal acoustic phonons. These measurements employed pyrolitic graphite (PG) as both vertically-focused monochromator and analyser. Measurements were performed in constant-E_f mode using E_f =14.7 meV and two PG filters were placed in the scattered beam to remove harmonic contamination. Collimation between the components of the instrument was [none, 0.48, 0.55, 1.2], using the convention [source-monochromator, monochromator-sample, sample-analyzer, analyzer-detector], resulting in an approximate energy resolution of ~ 1 meV. The single crystal sample was mounted in a closed cycle refrigerator in the presence of a He exchange gas allowing us to access temperatures as low as 3 K with a temperature stability of ~ 0.05 K.

We were particularly interested in potential phonon-magnon coupling associated with the formation of the singlet spin state in $SrCu_2(BO_3)_2$ below ~ 10 K. The gapping of the magnetic spectrum at low energies and formation of one and two-triplet excitation bands at low temperature has the potential to couple strongly to the low lying phonons, as the gapped magnetic excitation spectrum may eliminate a decay channel for low lying phonons. This would result in longer phonon lifetimes within the singlet ground state. The relevant constant-**Q** measurements were performed with tighter collimation [none, 0.273, 0447, 1.2] than those employed for the T=150 K survey shown in Fig. 2, achieving an energy resolution of 0.5meV. This was done as the anticipated effects on phonon lifetimes were relatively small, and thus higher energy resolution was desirable. Although measurements were performed on both longitudinal and transverse acoustic phonons, focusing effects led to better resolution and intensity associated with the low energy transverse acoustic phonons, and we will restrict our discussion to constant-**Q** measurements of the form (4, K, 0) which probe these.

Our (4, K, 0) constant-**Q** measurements were performed at temperatures of 3, 9, 15, 30 and 100 K, spanning a range from well below to well above the onset of the singlet ground state as identified by the rollover in the low temperature susceptibility near 10 K,[20] signifying entrance into the non-magnetic ground state. We chose to study **Q**'s of the form (4, K, 0) with K ranging from 0.1 to 0.275, such that the corresponding energies of the transverse acoustic phonons we were studied varied from ~ 2 meV to 6.5 meV. This range of energies spans the one-triplet bandwidth between 2.8 and 3.2 meV as well as the onset of the two-triplet continuum, above ~ 4.7 meV. At low temperatures, below ~10 K,

the magnetic excitation spectrum is gapped below the one triplet excitation, ~ 2.8 meV, and also between the one and two triplet bands, from ~ 3.2 meV to ~ 4.7 meV. If appreciable interaction or hybridization occurred between the low lying acoustic phonons and the low lying spin excitations, the gapped structure of the magnetic excitation spectrum below 10 K would be expected to manifest itself in the phonons. One natural manifestation of such an interaction could be the removal of a decay channel for the phonons, were their lifetimes influenced by the decay of the phonon into a combination of lower energy phonon plus magnetic excitation. Indeed, as described below, this is consistent with what we observe.

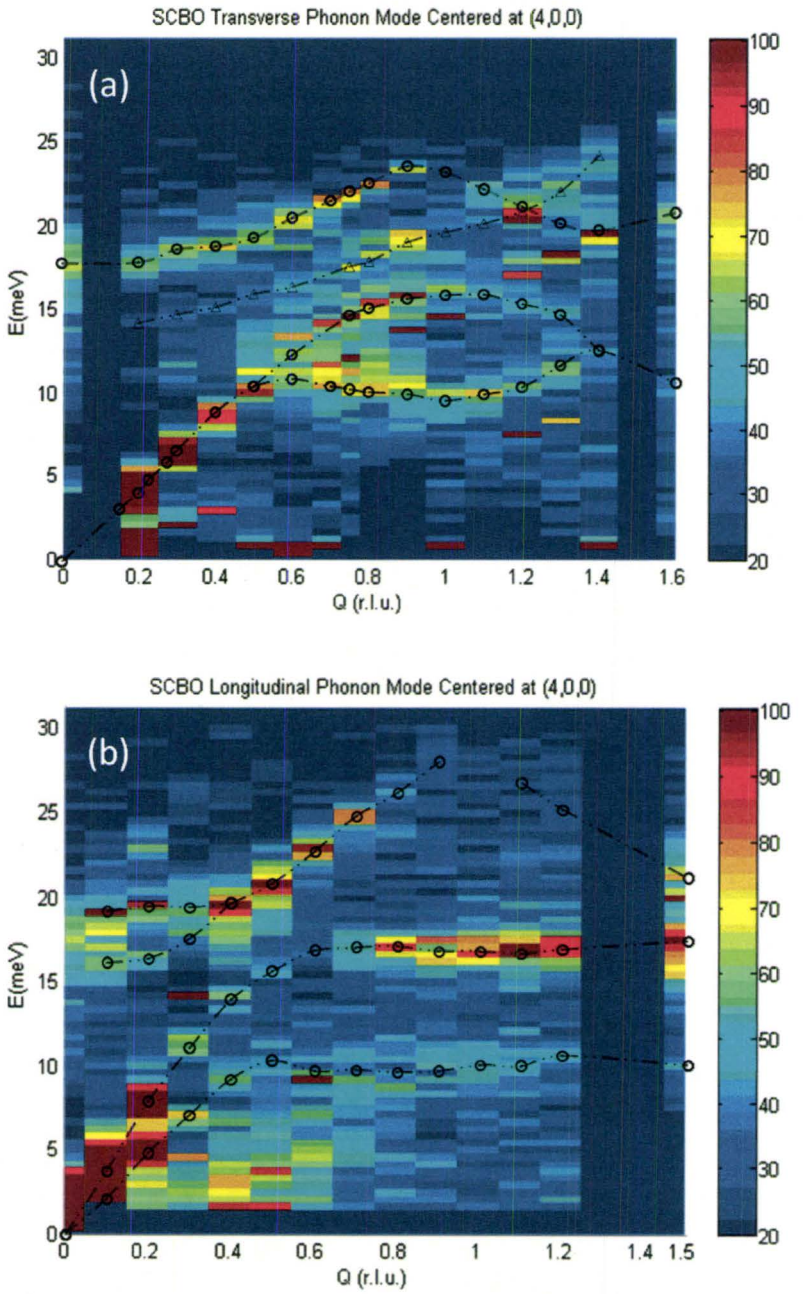

FIG. 2: Color contour maps summarizing neutron scattering primarily from transverse acoustic (top) and longitudinal acoustic (bottom) phonons in single crystal $SrCu_2(BO_3)_2$. Constant-**Q** measurements at (4, K, 0) (top) and (4+H, 0, 0) (bottom) measure primarily transverse and longitudinal phonon modes, respectively. All data was taken at T=150 K. Typical (4, K, 0) constant-**Q** scans at lower temperatures are shown in the left hand panels of Fig. 3. The dispersion of the excitations is summarized by the dashed lines which are guide to the eye.

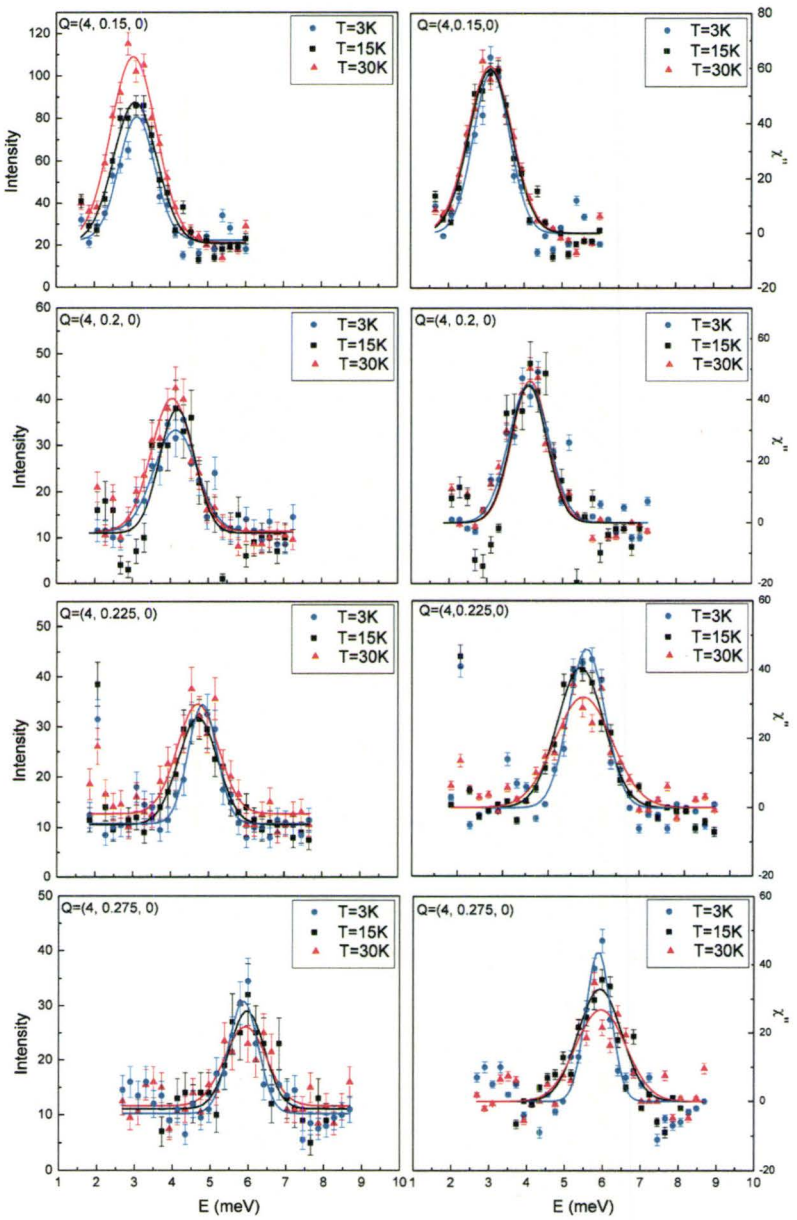

FIG. 3: Constant-**Q** neutron scans (left hand panels) are shown for **Q** = (4, 0.15, 0), (4, 0.2, 0), (4, 0.225, 0) and (4, 0.275, 0), from top to bottom. The corresponding energies of these transverse acoustic phonons range from ~ 3 to 6 meV, spanning the region from near the one-triplet energy to within the two-triplet continuum. The right hand panels show the resulting χ'', which is related to the measured scattering, $S(\mathbf{Q}, \omega)$ through Eq. 2. The three data sets shown in each panel are at T = 3 K (well within the singlet ground state), 15 K and 30 K (well within the paramagnetic state). The solid lines shown are resolution-convoluted fits of the data to appropriate damped harmonic oscillator lineshapes (Eq. 2).

The constant-**Q** measurements at representative temperatures of 3 K, 15 K and 30 K are shown in the left hand panels of Fig. 3. These data sets have been fit to an appropriate resolution-convolution of a Bose temperature factor × a damped harmonic oscillator form for $\chi''(\mathbf{Q}, \omega)$, Eq. 2. The right hand panel of Fig. 3 shows the same data, but with an energy-independent background removed and the result has been multiplied through by the Bose factor, thereby isolating $\chi''(\mathbf{Q}, \omega)$ as a function of $\hbar\omega$. This clearly shows that $\chi''(\mathbf{Q}, \omega)$ is temperature independent between 3 K and 30 K for low energy transverse acoustic phonons below ~ 4.5 meV, but not for the higher energy transverse acoustic phonons, which become qualitatively sharper in energy at the lowest temperatures, within the singlet ground state. The solid lines in all the Fig. 3 panels are the results of fitting a resolution-convolution of Eq. 2 to the data, and clearly this provides a good description to the data at all **Q**'s and temperatures measured.

$$S(\mathbf{Q},\omega,T) = \chi(\mathbf{Q},T)\frac{1}{1-exp\left(-\frac{\omega}{kT}\right)} \times \left[\frac{4\omega\Gamma_{\mathbf{Q},T}/\pi}{\left(\omega^2-\Omega^2_{\mathbf{Q},T}\right)^2+4\omega^2\Gamma^2_{\mathbf{Q},T}}\right] \qquad (2)$$

where $\chi(\mathbf{Q}, T)$ is the momentum-dependent susceptibility, while the second term takes into account detailed balance. The renormalized DHO frequency, $\Omega_{\mathbf{Q}}$, has contributions from the oscillation frequency, $\omega_{\mathbf{Q},T}$, and the damping coefficient, $\Gamma_{\mathbf{Q},T}$, and is given by:

$$\Omega^2_{\mathbf{Q},T} = \omega^2_{\mathbf{Q},T} + \Gamma^2_{\mathbf{Q},T}.$$

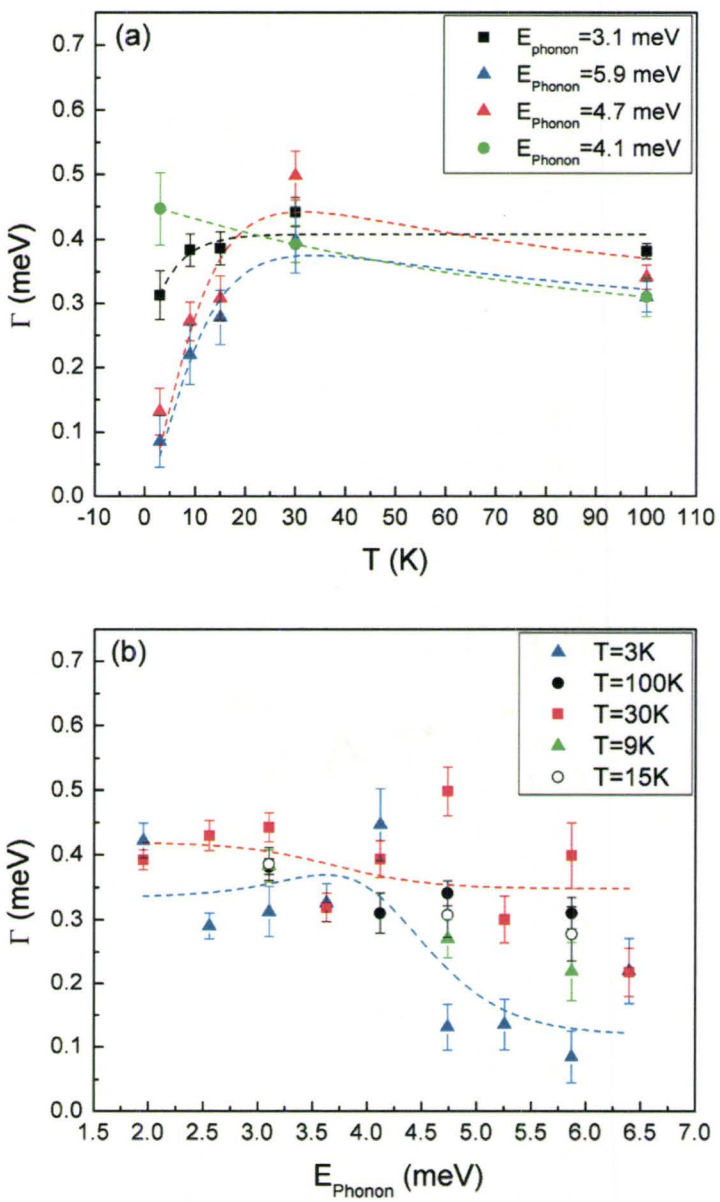

FIG. 4: The inverse lifetimes (Γ) of the transverse acoustic phonons as function of temperature for different energies ((a) top panel) and as a function of energy for different temperatures ((b) bottom panel) are shown. These values were extracted from fits of the data in Fig. 3 to a resolution-convolution of Eq. 2, in which the transverse acoustic lineshape is treated as a damped harmonic oscillator. It is clear that only the higher energy, low temperature transverse acoustic phonons show resolution-limited behavior, and hence long lifetimes.

The damping coefficient $\Gamma_{\mathbf{Q},T}$, which is inversely proportional to the lifetime of the appropriate transverse acoustic phonon at wavevector $\mathbf{Q}$ and temperature T, was extracted from this fitting and it is plotted as a function of temperature for different phonon energies in Fig. 4 (a) and as a function of energy for different temperatures in Fig. 4 (b). The trend in Fig. 4 is clear: transverse acoustic phonons propagating along (H00) have long lifetimes for energies above the approximate onset of the two-triplet continuum and for temperatures less than 10 K, the onset of the singlet ground state. These higher energy transverse acoustic phonons have lifetimes which can benefit the most by the gapping of the magnetic excitation spectrum below ~ 4.7 meV. Lower energy phonons cannot decay into a combination of excitations at least one of which is a spin excitation whose energy is higher than that of the original phonon. Removal of this density of one or two two-triplet states would be expected to make less of a difference for such low energy phonons.

These results also show that the low energy transverse acoustic phonons possess finite and largely temperature-independent lifetimes for all temperatures below ~ 100 K. It appears that some interaction with other degrees of freedom maintain a finite lifetime even in the absence of thermal fluctuations at low temperatures.

V. NEUTRON SCATTERING MEASUREMENTS OF OPTIC PHONONS

Previous infrared spectroscopy of $SrCu_2(BO_3)_2$ had thoroughly investigated the zone center optic phonons in $SrCu_2(BO_3)_2$. This work had identified a particular mode near ~ 55 meV which split on entering the singlet ground state at low temperatures. The overall energy scale of the optic phonon appears too high to influence or be influenced by the singlet ground state, which can be characterized by an energy scale which is either ~ 1 meV = 11 K, the temperature at which the susceptibility rolls over, or ~ 3 meV = 33 K, which is the energy of the one-triplet excitation of the singlet ground state. However, the relevant splitting of the optic phonon mode is of the order of 3 meV, so there can be relevance to such an effect even in a high energy optic phonon.

We performed high energy inelastic neutron spectroscopy of the optic phonons in the 35 meV to 65 meV range to explore possible optic phonon splitting on entering the singlet ground state. These measurements, taken on the direct geometry chopper spectrometer MAPS at the ISIS pulsed neutron facility, are shown in Fig. 5. Top panels of Figure 5 show color contour maps of inelastic scattering in the (H,K,0) Shastry-Sutherland plane at 1.5 K and 30 K, respectively. The energy transfer of the scattering correlates with the **Q** in this plot, such that the middle of the map corresponds to 52 meV energy transfer, while the highest **Q**'s (such as [5,5,0]) correspond to 65 meV energy transfer.

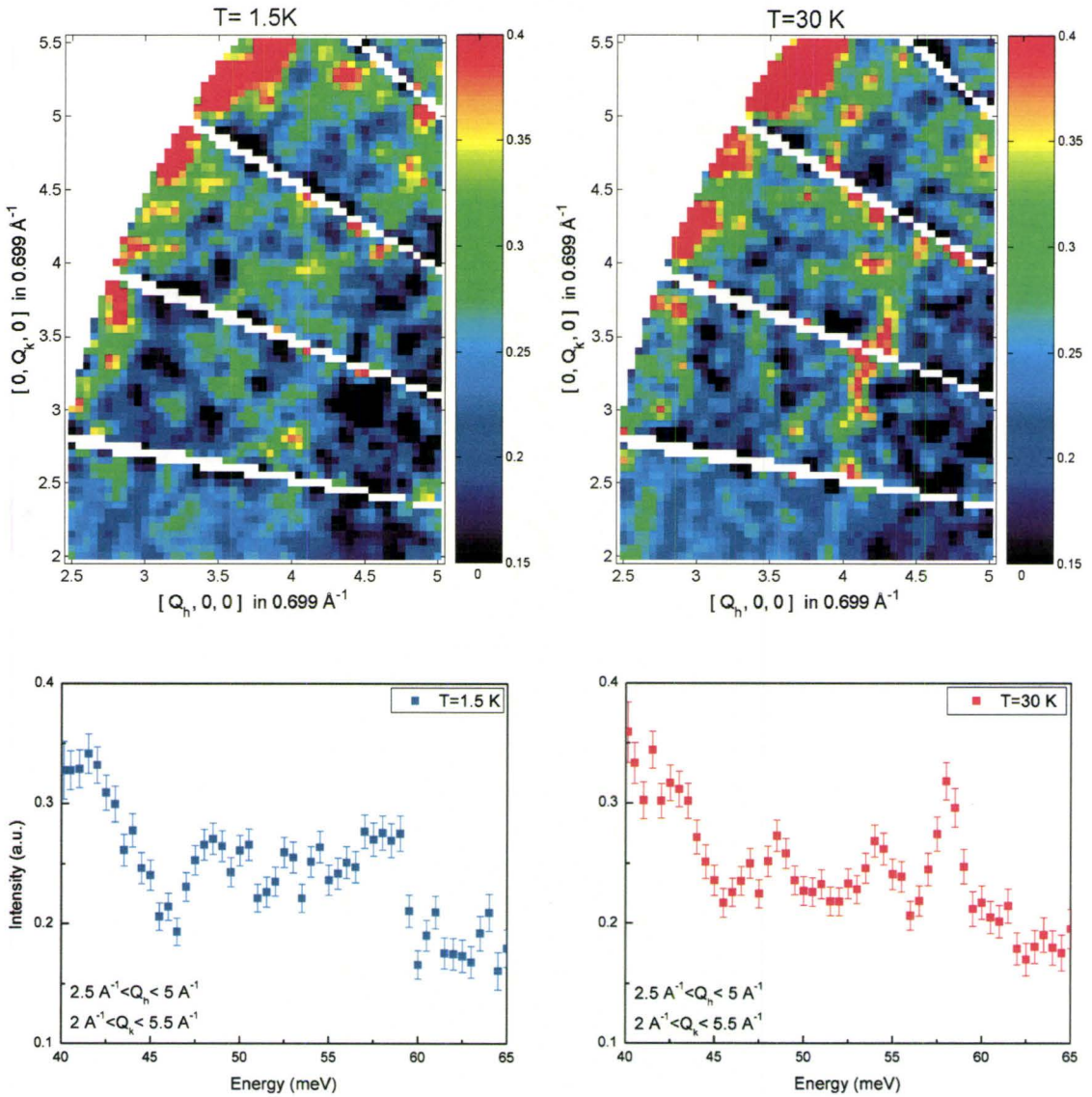

FIG. 5: Colour contour maps of the relatively high energy inelastic scattering from $SrCu_2(BO_3)_2$ taken at T=1.5 K (top left) and T=30 K (top right). These maps show scattering in the (H,K,0) plane where higher $\|\mathbf{Q}\|$ positions corresponds to higher energies in the range from ~ 40 meV < E < ~ 65 meV. Bottom panels show **Q**-integrated spectra plotted as a function of energy for T=1.5 K (bottom left) and (bottom right) T=30 K. The broadening of the optic phonons near ~ 52-60 meV is consistent with a splitting of **Q**=0 optic phonons observed with infrared spectroscopy. [10,11]

Bottom panels of Figure 5 show **Q**-integrated spectra plotted as a function of energy transfer for T = 1.5 K and 30 K, respectively. It is clear from this comparison that three neutron groups in the energy range from 53 meV to 60 meV broaden appreciably on cooling the sample from 30 K in the paramagnetic phase to 1.5 K in the singlet ground state of $SrCu_2(BO_3)_2$. While not in complete agreement with the observation of a splitting of a single optic phonon mode, it is qualitatively consistent, demonstrating that certain optic phonon modes are also influenced by the formation of the collective singlet.

VI. CONCLUSION

In conclusion, we have investigated the role of the lattice in the formation of the singlet ground state of the quasi-two-dimensional Shastry-Sutherland quantum magnet $SrCu_2(BO_3)_2$. A neutron powder diffraction study failed to detect any evidence for a structural phase transition on entering the low temperature singlet ground state below ~10 K. Such a possibility had been raised by earlier heat capacity measurements. We carried out extensive inelastic neutron scattering studies of the transverse and longitudinal acoustic phonons propagating in the (H00) direction within the Shastry-Sutherland plane. A survey of these acoustic phonons shows the zone boundary acoustic phonons at ~ 16 meV. Higher resolution triple axis measurements investigated the temperature dependence of the low lying transverse acoustic phonons. Interestingly, transverse acoustic phonons with energies greater than or equal to the onset of the two-triplet

continuum at ~ 4.7 meV display significantly enhanced lifetimes on entering the low temperature singlet ground state. This is attributed to removal of a decay mechanism for these phonons in which the phonons decay into a combination of excitations involving low energy spin excitations. The spin excitation spectrum is gapped within the singlet ground state such that little or no density of spin excitation states exist below ~ 2.8 meV or between ~ 3.2 and 4.7 meV. Finally, high energy inelastic scattering showed a broadening of optic phonon modes in the energy range from ~ 52 to 65 meV. This is qualitatively consistent with earlier infrared measurements showing a splitting of an optic mode near 55 meV on entering the singlet ground state below 10 K. Taken together these measurements demonstrate an intriguing coupling between spin and lattice degrees of freedom, but not one which obviously manifests itself in a structural phase transition on entering the singlet ground state, as occurs in spin-Peierls-like materials. We hope this work motivates further theoretical and experimental studies of such subtle effects on the intriguing quantum ground state in $SrCu_2(BO_3)_2$.

Acknowledgments

We wish to acknowledge expert technical support from CNBC, Chalk River as well as from the ISIS User Group. This work benefited from discussions with T. Ziman. This work was supported by NSERC of Canada.

References

[1] see, for example: E. Dagotto and T.M. Rice, Science, **271**, 618 (1996); *Dynamical Properties of Unconventional Magnetic Systems*, edited by A.T. Skjeltorp and D. Sherrington, NATO ASI Series, Series E, Applied Sciences, **349** (Kluwer Academic Publishers, Boston, 1998).

[2] B.S. Shastry and B. Sutherland, Physica B&C, **108B**, 1069 (1981).

[3] S. Miyahara and K. Ueda, Phys. Rev. Lett., **82**, 3701 (1999).

[4] H. Kageyama, K. Yoshimura, R. Stern, N. Mushnikov, K. Onizuka, M. Kato, K. Kosuge, C. Slichter, T. Goto and Y. Ueda, Phys. Rev. Lett., **82**, 3168 (1999).

[5] R.W. Smith and D.A. Keszler, J. Solid State Chem., **93**, 430 (1991).

[6] H. Kageyama, M. Nishi, N. Aso, K. Onizuka, T. Yosihama, K. Nukui, K. Kodama, K. Kakurai and Y. Ueda, Phys. Rev. Lett., **84**, 5876 (2000).

[7] O. Cépas, K. Kakurai, L.P. Regnault, J.P.B.T. Ziman, N. Aso, M. Nishi, H. Kageyama and Y. Ueda, Phys. Rev. Lett., **87**, 167205 (2001).

[8] K. Kakurai, in *Quantum Properties of Low Dimensional Antiferromagnets*, edited by A. Ajiro and J.P. Boucher (Kyushu University Press, Fukuoka, (2002).

[9] B.D. Gaulin, S.H. Lee, S. Haravifard, J.P. Castellan, A.J. Berlinsky, H.A. Dabkowska, Y. Qiu and J.R.D. Copley, Phys. Rev. Lett., **93**, 267202 (2004).

[10] A. Zorko, D. Arčon, H. van Tol, L.C. Brunel, and H. Kageyama, Phys. Rev. B, **69**, 174420 (2004).

[11] H. Nojiri, H. Kageyama, Y. Ueda, and M. Motokawa, J. Phys. Soc. Jap., **72**, 3243 (2003).

[12] S. El Shawish, J. Bonča, and I. Sega, Phys. Rev. B, **72**, 184409 (2005).

[13] M. Miyahara and K. Ueda, J. Phys. Condens. Matter, **15**, R327 (2003).

[14] K. Kodama, M. Takigawa, M. Horvatić, C. Berthier, H. Kageyama, Y.Ueda, S. Miyahara, F. Becca and F. Mila, Science, **298**, 395 (2002).

[15] K. Onizuka, H. Kageyama, Y. Narumi, K. Kindo, Y. Ueda and T. Goto, J. Phys. Soc. Jap., **69**, 1016 (2000).

[16] G.A. Jorge, R. Stren, M. Jaime, N. Harrison, J. Bonča, S. El Shawish, C.D. Baista, D.A. Dabkowska, and B.D. Gaulin, Phys. Rev. B, **71**, 092403 (2005).

[17] S.E. Sebastian, N. Harrison, P. Sengupta, C.D. Batista, S. Francoual, E. Palm, T. Murphy, N. Marcano, H.A. Dabkowska, and B.D. Gaulin, PNAS, **105**, 20157 (2008).

[18] H. Kageyama, K. Onizuka, T. Yamauchi, Y. Ueda, S. Hane, H. Mitamura, T. Goto, K. Yoshimura, and K. Kosuge, J. Phys. Soc. Japan, **68**, 1821 (1999).

[19] K. Sparta, G.J. Redhammer, P. Roussel, G. Heeger, G. Roth, P. Lemmens, A. Ionescu, M. Grove, G. Güntherodt, F. Hüning, H. Lueken, H. Kageyama, K. Onizuka, Y. Ueda, Eur. Phys. J., **19**, 507 (2001).

[20] A.A. Aczel, G.J. MacDougall, J.A. Rodriguez, G.M. Luke, P.L. Russo, A.T. Savici, Y.J. Uemura, H.A. Dabkowska, C.R. Wiebe, J.A. Janik and H. Kageyama, Phys. Rev. B, **76**, 214427 (2007).

Chapter 7

Neutron Scattering from $CuMoO_4$

$CuMoO_4$, Copper Molybdate, is a triclinic quantum magnet based on S=1/2 moments at the Cu^{2+} site. Recently it has attracted interest due to its remarkable change in its chromic, volumetric, and magnetic properties near a first-order structural phase transition. We are primary interested in the low temperature magnetic properties of this system where it exhibits magnetic phase transition at ~1.75 K in zero applied magnetic field. Taka Asano, our collaborator in Japan, carried out heat capacity and magnetization measurements and we carried out elastic and inelastic neutron scattering measurements at low temperatures. The results presented in this chapter will be submitted for publication to the Physical Review B.

Neutron Scattering Studies of the Quantum Magnet $CuMoO_4$

S. Haravifard and B.D. Gaulin

Department of Physics and Astronomy, McMaster University, Hamilton, Ontario, L8S 4M1, Canada

T. Asano

Department of Physics, Kyushu University, Fukuoka 812-8581, Japan

Z. Yamani and I. Swainson

Canadian Neutron Beam Centre, NRC, Chalk River Laboratories, Chalk River, Ontario, K0J 1J0, Canada

Abstract

$CuMoO_4$, Copper Molybdate, is a triclinic quantum magnet based on S=1/2 moments at the Cu^{2+} site. Recently it has attracted interest due to the remarkable changes in its chromic, volumetric, and magnetic properties. This material exhibits a first order structural phase transition at ~ 190 K as well as a magnetic phase transition at ~ 1.75 K. The structural phase transition of this material is accompanied by a 13% volume change as well as a change in color of the material. We are primarily interested in this material for its low temperature magnetic properties. In this paper we report the magnetization and heat capacity measurements as well as elastic and inelastic neutron scattering measurements within the low temperature magnetically ordered phase. We discuss a possible model for the spin state based on magnetization measurements as well as the neutron scattering data.

Introduction

$CuMoO_4$ is a triclinic magnetic insulator made up of a network of quantum S=1/2 magnetic moments residing at the Cu^{2+} site [1,3]. The Mo^{6+} site is non-magnetic. This material exhibits two triclinic phases known as α and γ $CuMoO_4$. At ambient pressure, there is a strong 1st order structural phase transition between these two structures at T_c ~

200 - 250 K [3-5]. While both the α (high-T) and γ phases (low-T) phases are triclinic, the structural phase transition between the two shows a remarkable 13% volume change that occurs in the unit cell between the phases above and below this transition. This phase change is accompanied by a change in color of the material from green (α) to red-ish brown (γ). For this reason, this material is referred to as displaying piezo or thermal chromism, and is of considerable current interest. Figure 1 shows the crystal structure of $CuMoO_4$ in both high-temperature and low-temperature phases.

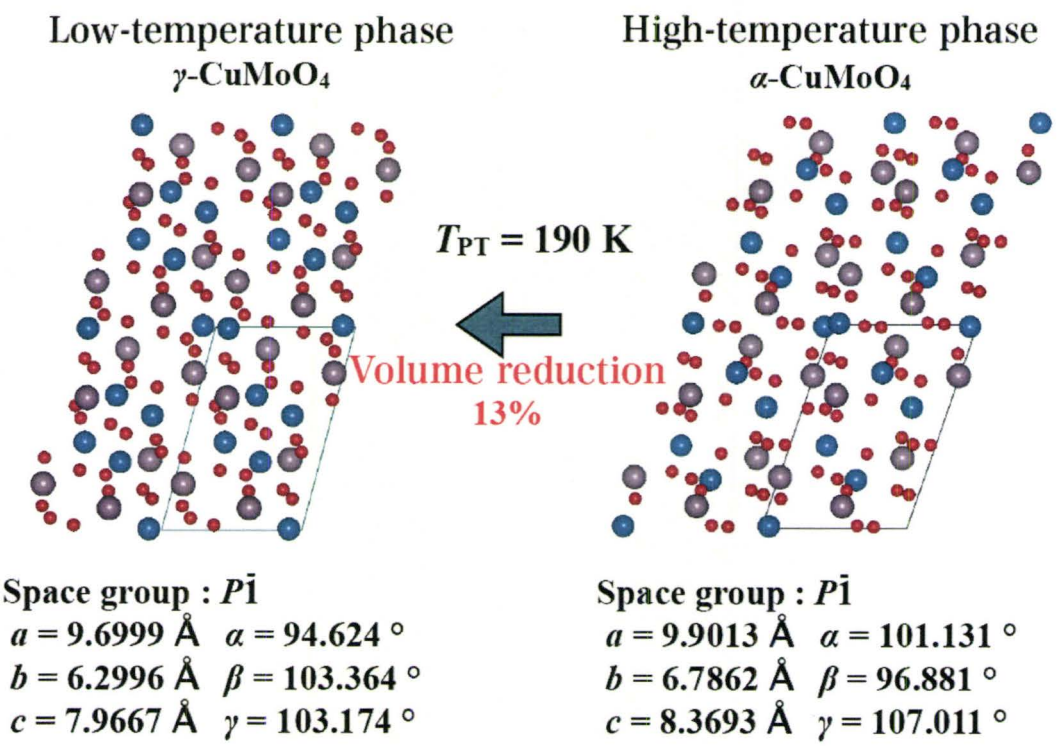

Fig 1: Crystal structure of $CuMoO_4$ in its low-temperature and high-temperature phase. Red, Purple and Blue circles represent Oxygen, Molybdenum and Copper atoms respectively. (Figure courtesy of Asano *et al.*) [6]

In addition to a volume reduction of 13% on cooling through the structural phase transition from α to γ phase, the lattice constant shrinks up to ~7% (the largest change is along the b axis)[3-5].

The color of this material changes from above to below the structural phase transition as there is a change in the crystalline environment surrounding the copper cations charges [3,4]. The large reduction of lattice constants in the γ phase could be due to the fact that, in the α phase, the system consists of relatively isolated clusters of six Cu-O polyhedral connected to each other. In the γ phase the Cu-O polyhedral possess a one dimensional connectivity that is also observed in the polymerization of molecules.

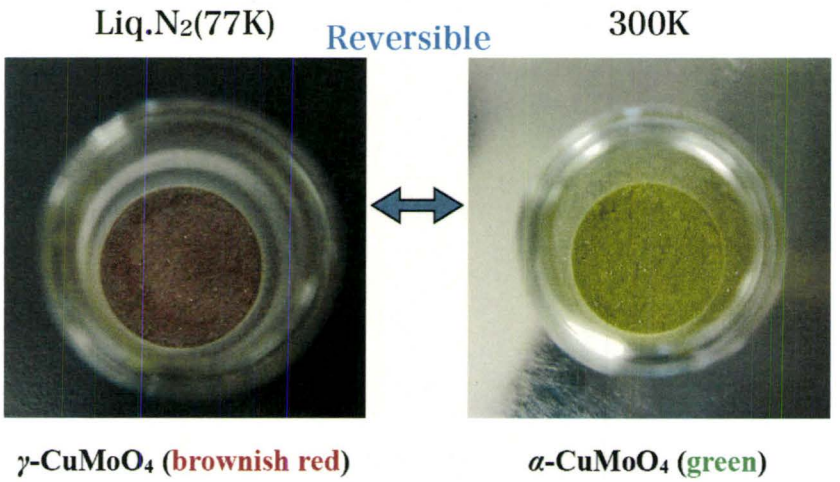

Fig 2: The phases above and below the transition temperature are called α and γ phases and are yellow-green and red-brown, respectively. (Figure courtesy of Asano *et al.*) [6]

Magnetic Properties

We are primarily interested in this material for its low temperature magnetic properties, related to networks of interacting S=1/2 Cu^{2+} moments. Asano *et al.* conducted high field magnetization studies on this material at low temperatures and observed an interesting 1/3 magnetization plateaus occurring at ~ 9 T. However the variation in the form of the M vs H curves as a function of temperature suggest that at least a subset of the networks of free S=1/2 moments may enter a magnetically ordered state below T~ 4 K. The data is shown in Fig. 3a. This low temperature, high field magnetization behavior can also be modeled based on networks of six S=1/2 moments, which arrange to form two dimers and two free spins in the low temperature γ phase. Such a model can explain the low temperature magnetization data in terms of two singlets, and two free spins as shown in Fig 3b. [1]

Asano *et al.* proposed an explanation for the relationship between the observed magnetic properties from the magnetization measurements and the magnetic interactions that can be expected according to the crystal structure of this material below and above the structural phase transition temperature (T_c ~ 190 K).[1] Within the α phase, all the polyhedras are edge sharing so the magnetic interactions between the Cu ions are expected to be weaker, and therefore, the spins are more likely to fluctuate freely.

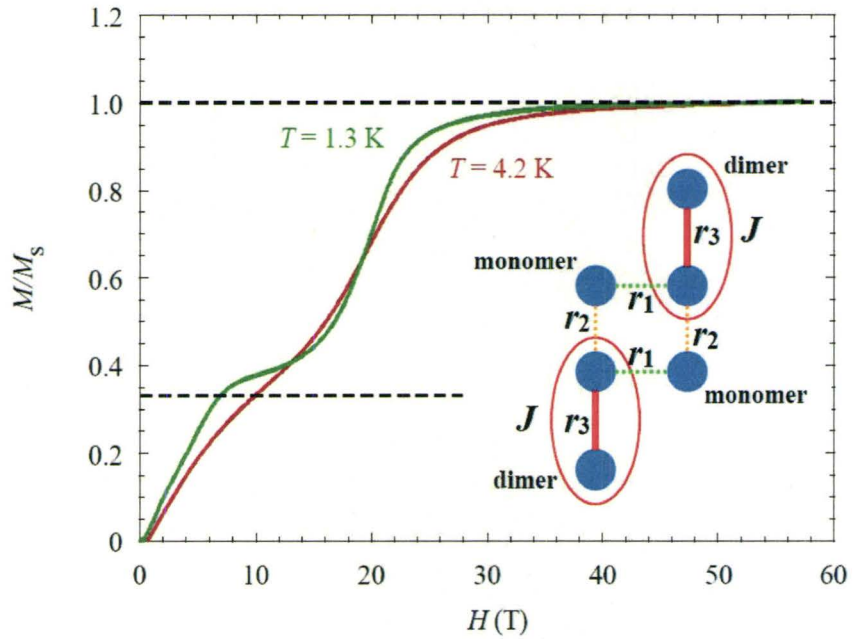

(a)

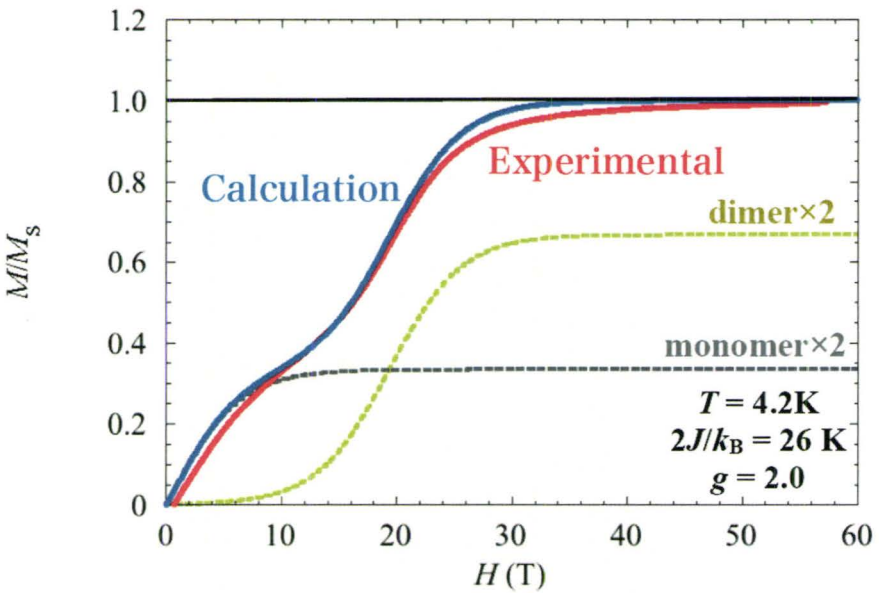

(b)

Fig 3: (a) Magnetization plateaus at 1/3 of the saturation magnetization observed in $CuMoO_4$ by high field magnetometry. (b) The plateaus can be modeled on the basis of a network of six spin-½ moments, organized into two dimers and two free spins shown in the inset of (a).

Figure 4 shows the arrangements of Cu-O polyhedra in $CuMoO_4$ for (a) α- and (b) γ-phases. In the γ-phase, the magnetic interaction of the Cu ions in the corner sharing polyhedra is stronger than those that have edge sharing polyhedra, so one can suggest that the spins on the Cu sites in the corner sharing Cu-O polyhedras are connected by strong antiferromagnetic interactions. Therefore one can suggest that these Cu sites dimerize and form a singlet with the remaining two spins left nearly free and isolated. This model is schematically shown in Fig 4a for α phase and Fig 4b for γ phase. Similar spin dimer analysis has also been proposed by Thiry *et al.* as well.[7]

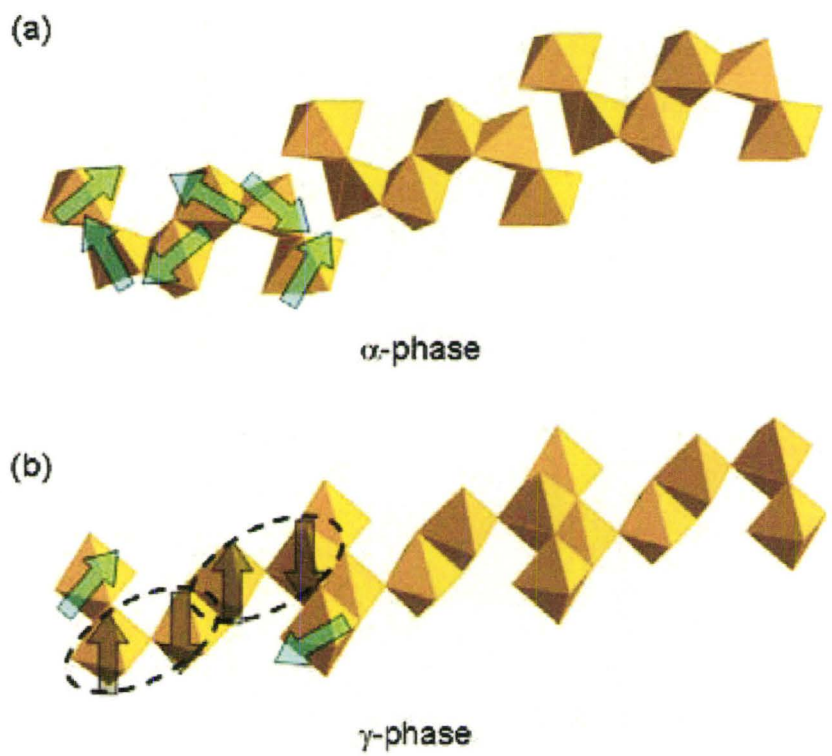

Fig 4: Arrangements of Cu-O polyhedra in $CuMoO_4$ for (a) α- and (b) γ-phases. Cu^{2+} S=1/2 spins are shown schematically by arrows; green arrow depicts free spin and a pair of gray ones dimerized to form spin singlet.[1]

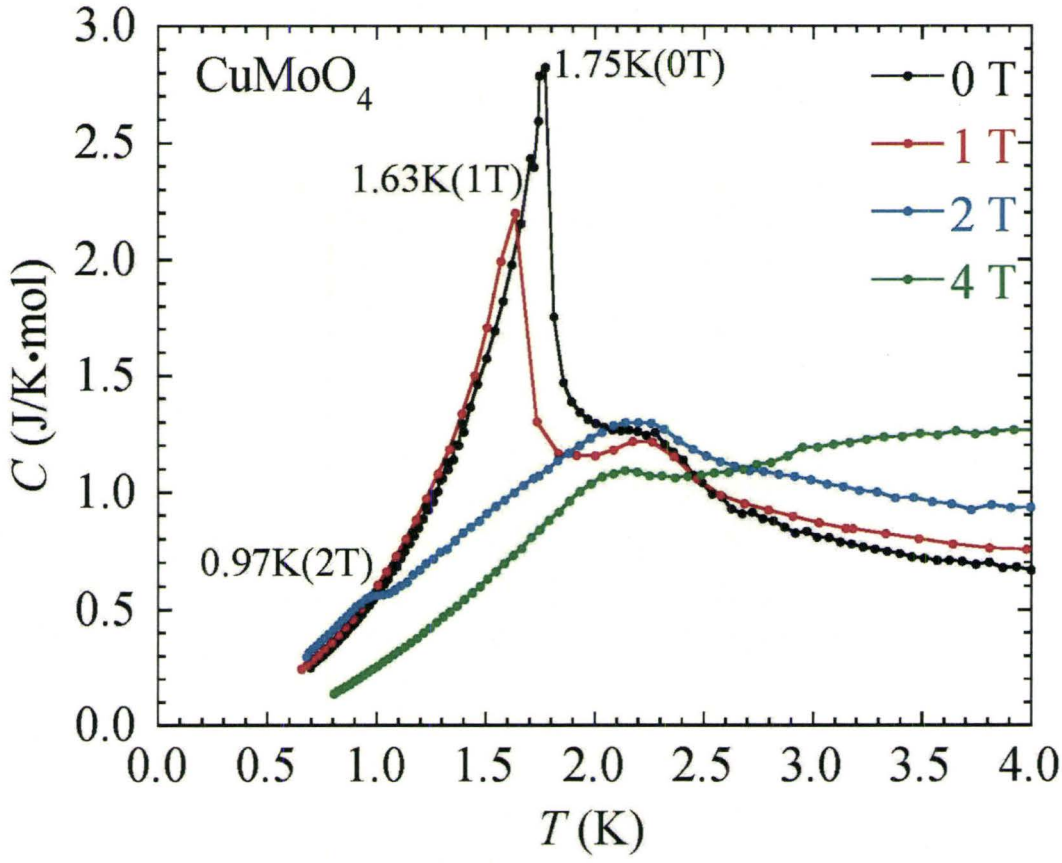

Fig 5:The temperature dependence of the specific heat observed in zero-field as well as in magnetic fields up to 4 T as shown.

Asano *et al.* conducted heat capacity measurements at low temperatures to investigate the magnetic nature of this system further. Figure 5 shows the results of the heat capacity measurements as a function of temperature and magnetic field. The heat capacity measurements at H=0 T reveal a magnetic phase transition at T~1.75 K. As shown in Fig. 5, the temperature and the field dependence of the heat capacity results indicate that the magnetic phase transition occurs from a disordered state to a long-range

ordered state on cooling. These results motivated us to study the low temperature magnetic properties of this system using neutron scattering techniques.

Experiment Details

Polycrystalline samples were prepared for neutron scattering measurements. The powders were mixed in stoichiometric proportions:

$$MoO_3 + CuO \rightarrow CuMoO_4$$

The material was loaded into a rubber tube and pressed hydrostatically at 65 MPa to produce rods for a better chemical reaction. The rods were annealed in air at 700 °C for 72 hours. Powder X-day diffraction measurements of the final powder sample showed a high quality compound with very little residue of CuO. The powder was loaded in a sealable Al can in He exchange gas in order to make sure the sample would reach the very low temperatures required to access the magnetically ordered state, and mounted in a pumped ^{4}He cryostat.

In order to investigate the magnetic behavior of the low temperature ground state of $CuMoO_4$, we carried out elastic and inelastic neutron scattering measurements on polycrystalline samples as a function of temperature and magnetic field on the C2 and C5 spectrometers at the Canadian Neutron Beam Centre Laboratory (CNBC), Chalk River.

We used a vertically focusing PG-002 monochro-mator and a flat PG-002 analyzer with a fixed final energy of E_f = 2.37 Å. Two PG filters were used in the scattered side to eliminate higher order wavelength neutrons from the beam. A nitrogen cooled sapphire filter was used in the main beam to minimize the fast neutron background. For both experiments we used a collimation setting of [none, 0.48°, 0.56°, 1.2°] achieving an energy resolution of ~ 1 meV.

Results and Discussions

Our high resolution powder neutron diffraction measurements collected using C2 spectrometer clearly show that a peak at the scattering angle of $2\theta \sim 7.4°$ appears below ~ 1.7 K on cooling (see Fig 6a). From the observed scattering angle (2θ value) of this magnetic Bragg peak and the incident neutron wavelength (λ = 2.37 Å) and using Bragg formula of $2\ d \sin\theta = \lambda$ we can calculate that the d spacing associated with the observed 2θ of the magnetic peak at 7.4° is ~ 18.362 Å. When comparing the experimental value of d to the calculated one based on the proposed model shown in Fig 6b, one can conclude that the free spins of neighboring sites along *a* direction order antiferromagnetically with the wavevector **Q** ~ 0.342 $Å^{-1}$ .This models is simply characterized by a doubling of the unit cell along the *a* axis. The proposed model matches well with the measured neutron scattering data. Based on these results and in agreement to the models suggested by the magnetization measurements [1,7], we propose that the low

temperature ground state of this quantum magnet is indeed magnetically ordered with the two free spins in the unit cell ferromagnetically coupled to each other while antiferromagnetically coupled to the ones in the neighboring sites, as schematically shown in Fig 6b.

Fig 7a shows the order parameter (integrated intensity of the magnetic Bragg scattering observed at $6.6° < 2\theta < 7.8°$) as a function of temperature, while Fig 7b shows the order parameter as a function of magnetic field for the same integrated intensity range in 2θ. Our study of the field dependence of this peak (see Fig 7b) is in full agreement with the observed field dependence of the specific heat across the transition as shown in Fig 5. In addition, the temperature dependence of the peak shown in Fig 7a clearly resembles the magnetic phase transition that was observed with specific heat measurements represented by the zero-field curve in Fig 5.

(a)

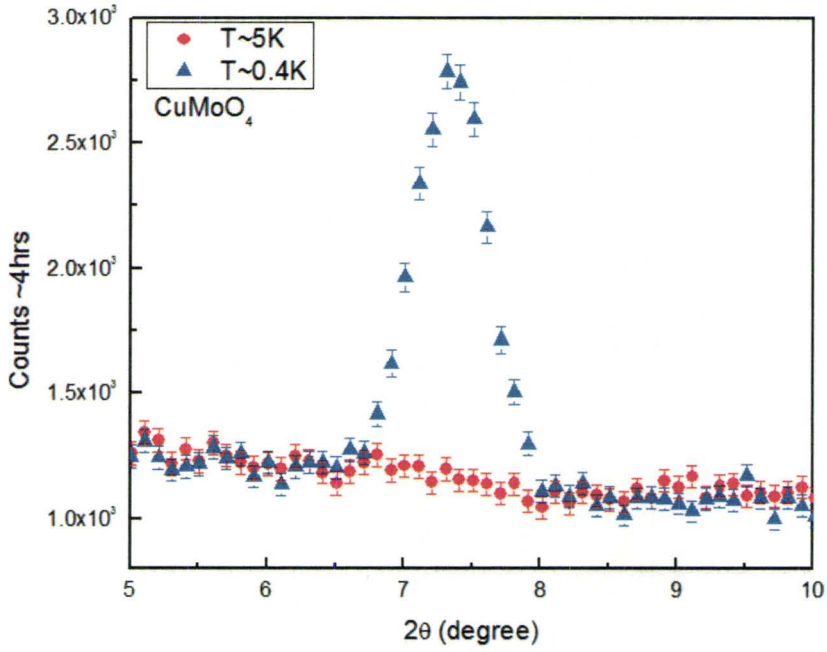

(b)

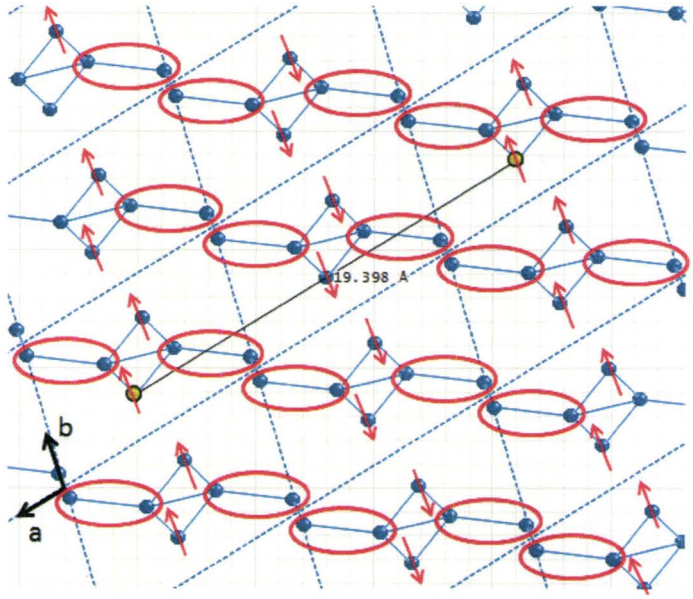

Fig 6: Elastic neutron scattering measurements carried out using C2 neutron powder diffraction at Chalk River laboratories. The results show that the low temperature ground state of this quantum magnet is magnetically ordered. (a) The magnetic Bragg peak at ~ 7.4° and ~0.4 K. (b) The proposed spin configuration model based on the experimental and calculated d-spacing value. The ellipses surround S=1/2 moments which pair to form singlets.

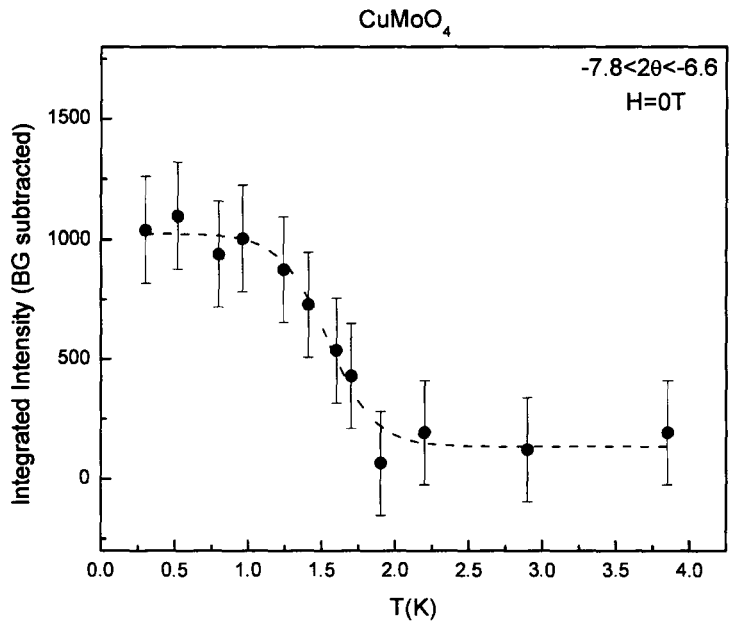

(a)

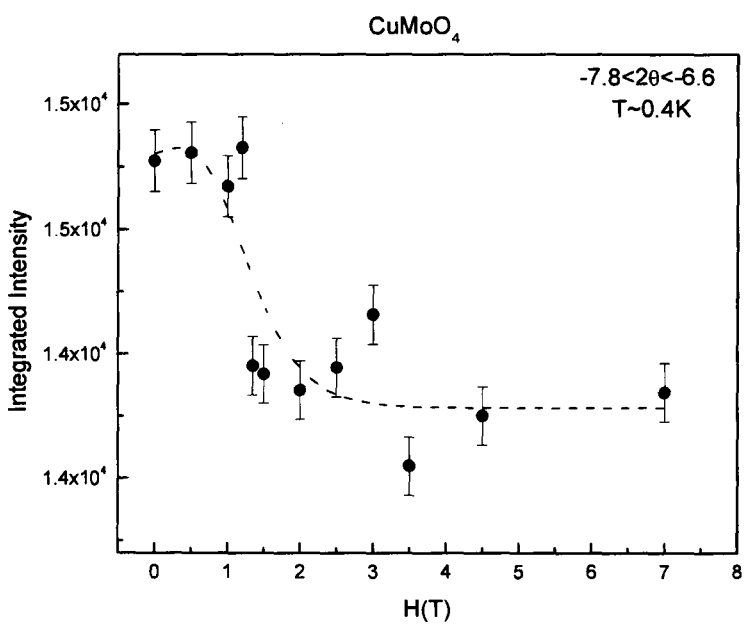

(b)

Fig 7: (a) The order parameter (integrated intensity of the magnetic Bragg peak observed at $6.6° < 2\theta < 7.8°$) as a function of temperature. (b) The order parameter (integrated intensity of the magnetic Bragg peak observed at $6.6° < 2\theta < 7.8°$) as a function of magnetic field at T ~ 0.4 K, within the magnetically ordered state.

In order to study the spin excitation spectrum associated with the S = 1/2 moments, we also carried out inelastic neutron scattering measurements on this polycrystalline material at the C5 triple-axis spectrometer in Chalk River Laboratories. The results of these measurements as a function of temperature and magnetic field are shown in Fig 8-10.

Figure 8 shows the results of the constant |Q| neutron scattering measurements on polycrystalline sample as a function of temperature in H=0 T (Fig 8a) and H=7.5 T (Fig 8b). As shown in Fig 8a, two broad peaks are observed in the ordered state (T~ 1.5 K) and in zero magnetic field. According to the magnetization results and the elastic neutron scattering measurements the proposed model describing this systems is that 4 out of 6 Cu^{2+} sites that carry the S=1/2 moments would form two dimers (See Fig 6b), when the other two free spins will magnetically order below the critical temperature of ~1.7 K. As shown in Fig 8a broad peaks appear at ~ 2.5 meV and ~4 meV energy transfers at zero field and T ~ 1.5 K at |Q| = 1.1 $Å^{-1}$.

Since the resolution of this experiment was ~ 1 meV, the separation between these two inelastic peaks is not resolution limited and one could speculate that these peaks correspond to the singlet-triplet excitations of the two different dimers in the unit cell. It is also possible that since these neutron powder scattering measurements were performed at constant |Q|=1.1 $Å^{-1}$, there might be dispersion related to the triplet excitations and the peaks observed at ~ 2.5meV and ~4meV could be representative of the bottom and top of the bands of the one triplet excitation peak, where their density of states would be higher.

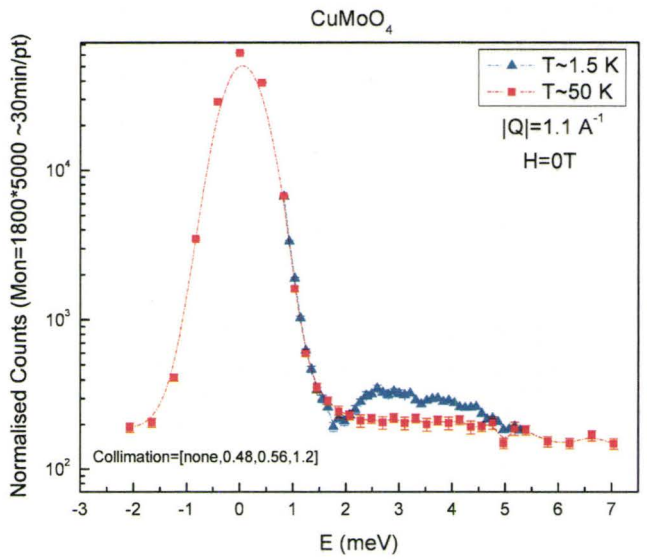

a)

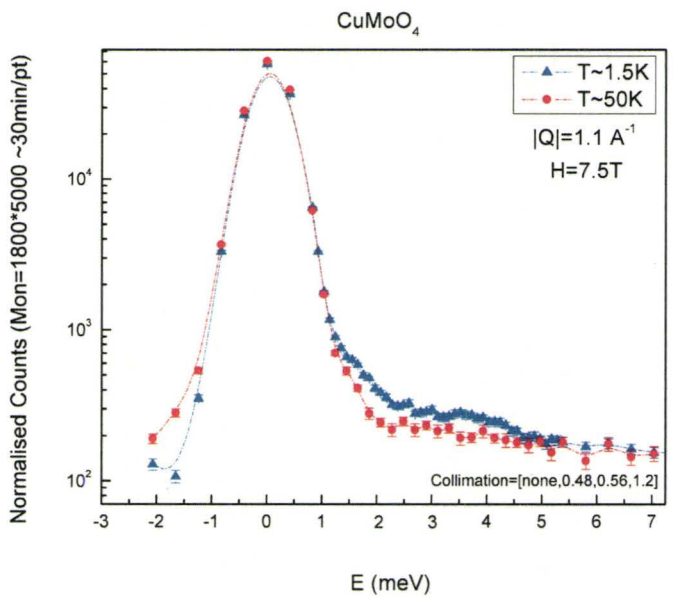

(b)

Fig 8: Inelastic neutron scattering measurements carried out at the C5 triple-axis spectrometer at Chalk River laboratories to study the spin excitation spectrum. (a) In the ordered state and in zero magnetic field, we observe two broad peaks at an energy transfer of ~ 2.5 meV and ~ 4 meV. (b) At the largest applied field of 7.5 T, we observe a substantial broadening of the excitation peaks. Better Q-coverage would be needed to further resolve the structure in the excitation peaks both in the presence and absence of the magnetic field.

Figure 9 shows the constant-**Q** neutron scattering results at T~ 1.5K and as a function of magnetic field. As shown in Fig 9, with the application of a magnetic field in the range of zero to 7.5 T, the inelastic peaks broaden and an additional field-dependent feature develops at a lower energy of ~ 1.75 meV. This broadening of the inelastic peaks could be associated with the Zeeman-split of the triplet excitation for the three eigenstates of $S_z = 0, -1$ and $+1$. Additionally one could speculate that the spectral weight observed at lower energy transfers as a function of magnetic field could be due to magnetic contributions from quasi-elastic incoherent scattering at energies close to zero.

Figure 9b shows the background subtracted scattering data at zero and 7.5 T applied magnetic field for $|Q| = 1.1$ Å^{-1} wavevector. This is also qualitatively in agreement with the expected Zeeman splitting at 7.5 T magnetic field as the $g\mu_B H$ for H=7.5 T is ~ 0.85 meV and the observed separating between the excitation peaks in zero and 7.5 T is also ~ 1meV. Additionally the magnetic contributions at quasi-elastic energies close to zero could also have an effect as they would be raised from zero energy to $g\mu_B H = 0.85$ meV.

Figure 10 shows the magnetic field dependence of the spectral weight observed at ~ 1.75 meV and $|Q| = 1.1$ Å^{-1}. As shown in Fig 10, clear but complicated field dependence of this feature is observed as a function of magnetic field. According to the proposed model for the ground state of this system (see Fig 5) the magnetic contributions from the two free S=1/2 moments could also have an effect on the field dependence of the observed spectral weight at ~ 1.75 meV.

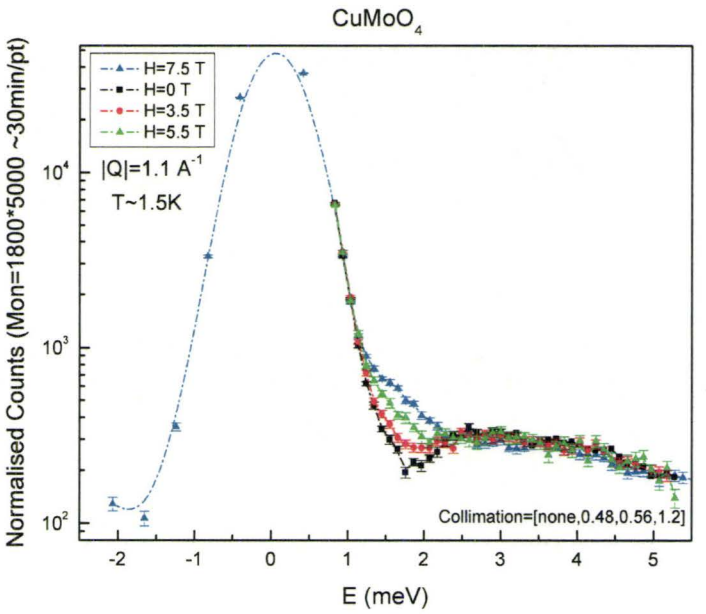

a)

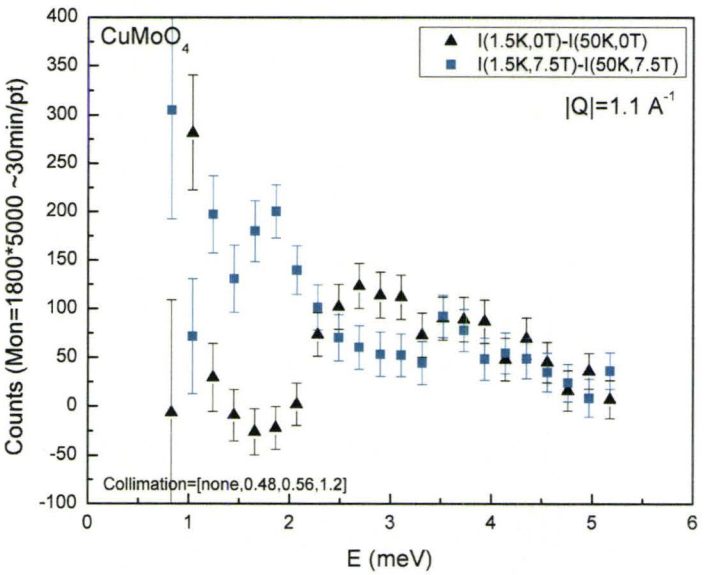

(b)

Fig 9: (a) The effect of the application of a magnetic field in the range of 0 T to 7.5 T on the magnetic excitation spectrum is shown in $CuMoO_4$. (b) High temperature background-subtracted inelastic intensity at zero field and at an applied field of 7.5 T is shown.

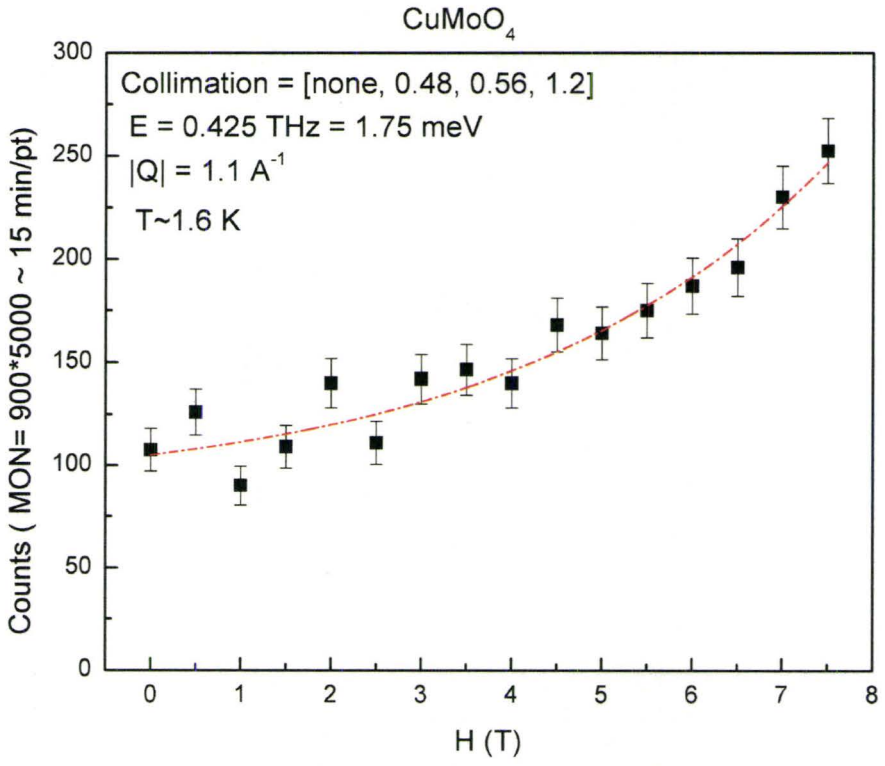

Fig 10: The inelastic scattering at an energy transfer of 1.75 meV as a function of magnetic field is shown.

Conclusions

Our study confirms that the system undergoes a magnetic phase transition to an ordered low temperature ground state below 1.7 K.

We have observed resolution limited magnetic Bragg peak which appears below $T_N \sim 1.7$ K and found that consistent with a magnetically ordered state characterized by a doubling of the *a* axis.

In addition our study confirmed the presence of the spin excitations in the system. However the magnetic field dependence of the spin excitations appears to be complex. This could be due to the fact that based on the proposed model, describing the configuration of the spins within the magnetically ordered state, in addition to the magnetic dimers, there are also two free spins in the unit cell. Further inelastic neutron scattering experiments with better Q-coverage as well as additional related theoretical work would be needed to better understand this system.

References

[1] T. Ito, H. Takagi and T. Asano, Chem. Mater., **21**, 3376 (2009).

[2] M. Gaudon, P. Deniard, A. Demourgues, A-E. Thiry, C. Carbonera, A. Le Nestour, A. Largeteau, J-F. Létard and S. Jobic, Adv. Mater., **20**, 3517 (2007).

[3] M. Wiesmann, H. Ehrenberg, G. Miehe, T. Peun, H. Weitzel and H. Fuess, J. Solid State Chem., **132**, 88 (1997).

[4] H. Ehrenberg, H. Weitzel, H. Paulus, M. Wiesmann, G. Wltschek, M. Geselle and H. Fuess, J. Phys. Chem. Solids, **58**, 153 (1997).

[5] F. Rodríguez, D. Hernández, J. Garcia-Jaca, H. Ehrenberg and H. Weitzel, Phys. Rev. B, **61**, 16497 (2000).

[6] Private communication with Taka Asano.

[7] A-E. Thiry, M. Gaudon, C. Payen, N. Daro, J-F. Létard, S. Gorsse, P. Deniard, X. Rocquefelte, A. Demourgues, M-H. Whangbo and S. Jobic, Chem. Mater., **20**, 2075 (2008).

Chapter 8

Summary and Conclusion

Quantum magnets, particularly those that display collective singlet ground state or spin gap behaviour have been receiving much interest recently due to the novelty of their ground state and their relevance to high temperature superconductivity. Neutron scattering techniques are powerful probes for the study of magnetic properties of these exotic systems.

$SrCu_2(BO_3)_2$ is a unique two-dimensional spin singlet ground state system. It has attracted much attention recently as the first realization of the two dimensional Shastry-Sutherland model for interacting S=1/2 dimers. $SrCu_2(BO_3)_2$ has been well studied using different experimental techniques, which confirm that it possesses a non-magnetic singlet ground state. While pure $SrCu_2(BO_3)_2$ is well studied, there is little information on this

quantum magnet in the presence of dopants. For this reason, a series of neutron scattering studies on doped $SrCu_2(BO_3)_2$ were initiated.

Initially single crystals of $SrCu_{(2-x)}Mg_x(BO_3)_2$ x ~ 0.05 were successfully grown with the aim of introducing disorder without altering the carrier concentration. High resolution neutron scattering studies on $SrCu_{(2-x)}Mg_x(BO_3)_2$ revealed the presence of new relatively broad and field-independent in-gap spin excitations. Application of a magnetic field induces excitations identified as Zeeman-split S=1/2 unpaired spins which are antiferromagnetically correlated within the bulk singlet, spin polaron state. The non-magnetic quenched vacancies also give rise to finite and measurable lifetimes in the one and two triplet excitations. Theoretical calculations using a variational algorithm and single quenched magnetic vacancy on an infinite lattice qualitatively account for these effects.

A single crystal of $Sr_{(1-x)}La_xCu_2(BO_3)_2$ x ~ 0.04 was also successfully grown with the aim of introducing charge carries to the system. Neutron scattering measurements were performed on $Sr_{(1-x)}La_xCu_2(BO_3)_2$. The broadening of the one and two triplet excitations was observed in the La-doped system, as compared to the pure system. The main feature observed with these neutron scattering results was a different temperature dependence of the excitation lifetime in the La-doped sample in comparison to the pure and the Mg-doped samples. Additionally it was observed that although the volume of the La-doped sample was smaller than the volume of the pure and the Mg-doped samples, the incoherent quasi-elastic scattering in $Sr_{(1-x)}La_xCu_2(BO_3)_2$ was substantially stronger as compared to $SrCu_2(BO_3)_2$ and $SrCu_{(2-x)}Mg_x(BO_3)_2$, while the one triplet excitation peak

was weaker. This could indicate a shift in magnetic spectral weight in the presence of the La-induced doping from the one triplet excitations to a quasi-elastic spin spectrum at low energies compared with the one triplet spin gap.

In order to investigate the role of the lattice in the formation of the singlet ground state in $SrCu_2(BO_3)_2$, a series of low and high energy neutron scattering measurements were carried on this system. A neutron powder diffraction study failed to detect any evidence for a structural phase transition on entering the low temperature singlet ground state below ~10 K. Low energy inelastic neutron scattering measurements revealed the temperature dependence of the low lying transverse acoustic phonons. Interestingly, transverse acoustic phonons with energies greater than or equal to the onset of the two-triplet continuum at ~ 4.7 meV display significantly enhanced lifetimes on entering the low temperature singlet ground state. This could be due to the removal of a decay mechanism for these phonons in which the phonons decay into a combination of excitations involving low energy spin excitations. High energy inelastic neutron scattering showed a broadening of optic phonon modes in the energy range from ~ 52 to 65 meV. This is qualitatively consistent with earlier infrared measurements showing a splitting of an optic mode near 55 meV on entering the singlet ground state below 10 K. These measurements demonstrate an intriguing coupling between spin and lattice degrees of freedom.

$CuMoO_4$ is a triclinic quantum magnet system based on S=1/2 moments at the Cu^{2+} site. We have studied the low temperature magnetic properties of this material through magnetization measurements, heat capacity measurements as well as elastic and

inelastic neutron scattering experiments. This material exhibits a first order structural phase transition at ~ 190 K. $CuMoO_4$ also undergoes a magnetic phase transition at ~ 1.75 K which has been confirmed by heat capacity results as well as neutron powder diffraction measurements. Elastic neutron scattering results indicate that this magnetically ordered phase is characterized by a doubling of the *a* axis. Additionally, inelastic scattering is consistent with a gapped spin excitation spectrum in zero applied field, which substantially fills in on application of a magnetic field of up to 7 T. The field dependence of these magnetic excitations appears to be complex. Further experimental and theoretical studies are required to fully understand the low temperature magnetic properties of this system.

Bibliography

Aczel, A. A., MacDougall, G. J., Rodriguez, J. A., Luke, G. M., Russo, P. L., Savici, A. T., Uemura, Y. J., Dabkowska, H. A., Wiebe, C. R., Janik, J. A. & Kageyama, H. *Phys. Rev. B* **76**, 214427 (2007).

Ashcroft, N. W. & Mermin, N. D. *Solid State Physics,* Toronto: Sauders College Publishing, (1976).

Cépas, O., Kakurai, K., Regnault, L. P., Ziman, J. P. B. T., Aso, N., Nishi, M., Kageyama, H. & Ueda, Y. *Phys. Rev. Lett.* **87,** 167205, (2001).

Chung, C-H. & Kim, Y.B. *Phys. Rev. Lett.* **93**, 207004 (2004).

Chung, C-H., Marston, J. B. & Sachdev, S. *Phys. Rev. B* **64,** 134407 (2001).

Collins, M.F. *Magnetic Critical Scattering*, Oxford, New York (1989).

Copley, J. & Terrence, U. *J. Res. Natl. Inst. Stand. Technol.* **98**, 71-87 (1993).

Dabkowska, H. A., Dabkowski, A. B., Luke, G. M., Dunsiger, S. R., Haravifard, S., Cecchinel, M. & Gaulin, B. D. *J. Cryst. Growth* **306**, 123, (2007).

Dagotto, E. & Rice, T.M. *Science* **271**, 618 (1996).

Ehrenberg, H., Weitzel, H., Paulus, H., Wiesmann, M., Wltschek, G., Geselle, M. & Fuess, H. *J. Phys. Chem. Solids* **58**, 153 (1997).

El Shawish, S. & Bonča, J. *Phys. Rev. B* **74**, 174420 (2006).

El Shawish, S., Bonča, J. & Sega, I. *Phys. Rev. B* **72**, 184409 (2005).

Furrer, A. *Magnetic Neutron Scattering*, Vol. 1st, World Scientific, Singapore (1995).

Gaudon, M., Deniard, P., Demourgues, A., Thiry, A - E., Carbonera, C., Le Nestour, A., Largeteau, A., Létard, J - F. & Jobic, S., *Adv. Mater.* **20**, 3517 (2007).

Gaulin, B. D., Lee, S. H., Haravifard, S., Castellan, J. P., Berlinsky, A. J., Dabkowska, H. A., Qiu, Y. & Copley, J. R. D. *Phys. Rev. Lett.* **93**, 267202 (2004).

Haravifard, S., Dunsiger, S. R., El Shawish, S., Gaulin, B. D., Dabkowska, H. A., Telling, M. T. F., Perring, T. G. & Bonča, J. *Phys. Rev. Lett.* **97**, 247206 (2006).

Ito, T., Takagi, H. & Asano, T., *Chem. Mater.* **21**, 3376 (2009).

Jorge, G. A., Stren, R., Jaime, M., Harrison, N., Bonča, J., El Shawish, S., Baista, C. D. , Dabkowska, D. A. & Gaulin, B. D. *Phys. Rev. B* **71**, 092403 (2005).

Kadanof, L. P. *Phase Transition and Critical Phenomena*, Academic Press (1976).

Kageyama, H., Nishi, M., Aso, N., Onizuka, K., Yosihama, T., Nukui, K., Kodama, K., Kakurai, K. & Ueda, Y. *Phys. Rev. Lett.* **84**, 5876 (2000).

Kageyama, H., Onizuka, K., Yamauchi, T., Ueda, Y., Hane, S., Mitamura, H., Goto, T., Yoshimura, K. & Kosuge, K. *J. Phys. Soc. Japan* **68**, 1821 (1999).

Kageyama, H., Yoshimura, K., Stern, R., Mushnikov, N., Onizuka, K., Kato, M., Kosuge, K., Slichter, C., Goto, T. & Ueda, Y. *Phys. Rev. Lett.* **82**, 3168 (1999).

Kakurai, K. *Quantum Properties of Low Dimensional Antiferromagnets*, Fukuoka: Kyushu University Press (2002).

Kenzelmann, M., Xu, G., Zaliznyak, I.A., Broholm, C., DiTusa, J. F., Aeppli, G., Ito, T., Oka, K. & Takagi, H. *Phys. Rev. Lett.* **90**, 087202 (2003).

Kimura, T., Kuroki, K., Arita, R. & Aoki, H. *Phys. Rev. B* **69**, 054501 (2004).

Knetter, C. & Uhrig, G. S. *Phys. Rev. Lett.* **92**, 027204 (2004).

Knetter, C., Bühler, A., Müller-Hartmann, E. & Uhrig, G. S. *Phys. Rev. Lett.* **85** 3958 (2000).

Knetter, C., Müller-Hartmann, E. & Uhrig, G. S. *J. Phys.: Condens. Matter* **12** 9069 (2000).

Kodama, K., Takigawa, M., Horvatić, M., Berthier, C., Kageyama, H., Ueda, Y., Miyahara, S., Becca, F. & Mila, F. *Science* **298**, 395 (2002).

Kodama, K., Yamazaki, J., Takigawa, M., Kageyama, H., Onizuka, K. & Ueda, Y. *J. Phys.: Condens. Matter* **14**, L319 (2002).

Koga, A. & Kawakami, N. *Phys. Rev. Lett.* **84**, 4461 (2000).

Läuchli, A., Wessel, S., & Sigrist, M. *Phys. Rev. B* **66**, 014401 (2002).

Lemmens, P., Grove, M., Fischer, M., Guntherodt, G., Kotov, V. N., Kageyama, H., Onizuka, K. & Ueda, Y. *Phys. Rev. Lett.* **85**, 2605 (2000).

Liu, G. T., Luo, J. L., Wang, N.L., Jing, X. N., Jin, D., Xiang, T. & Wu, Z. H. *Phys. Rev. B* **71**, 014441 (2005).

Manousakis, E. *Rev. Mod. Phys.* **63,** 1 (1991).

Miyahara S. & Ueda K. *Phys. Rev. Lett.* **82**, 3701 (1999).

Miyahara, S. & Ueda, K. *J. Phys. Condens. Matter* **15**, R327 (2003).

Miyahara, S. & Ueda, K. *Phys. Rev. Lett.* **82**, 3701 (1999).

Nojiri, H., Kageyama, H., Onizuka, K., Ueda, Y. & Motokawa, M. *J. Phys. Soc. Japan* **68**, 2906 (1999).

Nojiri, H., Kageyama, H., Ueda, Y. & Motokawa, M. *J. Phys. Soc. Japan* **72**, 3243 (2003).

Onizuka, K., Kageyama, H., Narumi, Y., Kindo, K., Ueda Y. & Goto T. *J. Phys. Soc. Jap.* **69**, 1016 (2000).

Orenstein, J. & Millis, A. J. *Science* **288**, 468 (2000).

Rodríguez, F., Hernández, D., Garcia-Jaca, J., Ehrenberg, H. & Weitzel, H. *Phys. Rev. B* **61**, 16497 (2000).

Rõõm, T., Nagel, U., Lippmaa, E., Kageyama, H., Onizuka, K. & Ueda, Y. *Phys. Rev. B* **61**, 14342 (2000).

Sakurai, J. J. *Modern Quantum Mechanics*, Addison-Wesley Publishing Company Inc. (1985).

Sebastian, S. E., Harrison, N., Sengupta, P., Batista, C. D., Francoual, S., Palm, E., Murphy, T., Marcano, N., Dabkowska, H. A. & Gaulin, B. D. *PNAS* **105**, 20157 (2008).

Shastry, B. S. & Kumar, B. *Prog. Theor. Phys. Suppl.* **145**, 1 (2002).

Shastry, B. S. & Sutherland B. *Physica B&C* **108B**, 1069 (1981).

Skjeltorp, A. T. & Sherrington, D. *Dynamical Properties of Unconventional Magnetic Systems*, NATO ASI Series, Series E, Applied Sciences. Boston: Kluwer Academic Publishers, 349 (1998).

Smith R. W. & Keszler D. A. *J. Solid State Chem.* **93**, 430 (1991).

Sparta, K., Redhammer, G. J., Roussel, P., Heeger, G., Roth, G., Lemmens, P., Ionescu, A., Grove, M., Güntherodt, G., Hüning, F., Lueken, H., Kageyama, H., Onizuka, K., Ueda,Y. *Eur. Phys. J.* **19**, 507 (2001).

Squires, G. L. *Introduction to the Theory of Thermal Neutron Scattering*, Dover, Mineola (1996).

Stanley, H. E., *Introduction to Phase Transition and Critical Phenomena*, Clarendon Press, Oxford (1971).

Takushima, Y., Koga, A. & Kawakami, N. *J. Phys. Soc. Japan* **70**, 1369 (2001).

Telling, M. T. F. & Andersen, K. H. *Phys. Chem. Chem. Phys.* **7**, 1255 (2005).

Thiry, A - E., Gaudon, M., Payen, C., Daro, N., Létard, J - F., Gorsse, S., Deniard, P., Rocquefelte, X., Demourgues, A., Whangbo, M - H. & Jobic, S. *Chem. Mater.* **20**, 2075 (2008).

Totsuka, K., Miyahara, S. & Ueda, K. *Phys. Rev. Lett.* **86**, 520 (2001).

Weihong, Z., Hamer, C. J. & Oitmaa, J. *Phys. Rev. B* **60**, 6608 (1999).

Wiesmann, M., Ehrenberg, H., Miehe, G., Peun, T., Weitzel, H. & Fuess, H. *J. Solid State Chem.* **132**, 88 (1997).

Zheng, W., Hamer, C. & Oitmaa, J. *Phys. Rev. B* **60**, 6608 (1999).

Zorko, A., Arčon, D., van Tol, H., Brunel, L. C. & Kageyama, H. *Phys. Rev. B* **69**, 174420 (2004).